Investigating the Role of DLK Signaling in Synapse Loss Inflammation and Cell Death

by

Elham Asghari Adib

A dissertation submitted in partial fulfillment
of the requirements for the degree of
Doctor of Philosophy
(Molecular, Cellular, and Developmental Biology)
in the University of Michigan
2022

Doctoral Committee:

Associate Professor Catherine Collins, Chair
Professor Mohammed Akaaboune
Associate Professor Sami Barmada
Professor Roman Giger
Professor Richard Hume
Professor Emeritus John Kuwada
Associate Professor Ryan Mills

Elham Asghari Adib

adibe@umich.edu

ORCID iD: 0000-0002-3205-1609

Dedication

To my parents and my brother

Acknowledgments

This thesis work could not have been completed without the support and help of many people. First and foremost, I would like to thank my advisor, Dr. Catherine Collins, for providing me with ample opportunities to learn and grow as a scientist. Knowing that I would like to acquire as many skills as possible in my Ph.D., she encouraged me to conduct new experiments and formed great collaborations. I appreciate her trust in me to introduce the mammalian system to her lab, providing me with so much experience on how one can set up mouse protocols and all the different decisions and plannings that are required. Given that the Ph.D. path is very difficult where successes are rare and far in between, having Dr. Collins as my mentor was an absolute privilege. I cannot thank her enough for all the scientifically stimulating discussion and her support.

I want to thank Dr. Ryan Insolera, for being the most amazing colleague and friend. His kindness, patience, and encouraging words have saved me from despair many times. I would like to thank my other wonderful lab mate, Dr. Laura Smithson, for all the great discussion and her unending support. I would also like to acknowledge my good friend and scientific partner in crime, Abigail Rogers who has been an asset to the progress of this work and has been a great emotional support. I would like to thank Chris Jasinski for all the genotyping he has done over the years for me, and Hari and Varsha for their all-time kindness and support. I am grateful to all the Collins past and present lab members such as TJ, Shameena, Jiaxing, and Lucas.

I want to thank my committee members Dr. John Kuwada, Dr. Richard Hume, Dr. Mohammed Akaaboune, and Dr. Sami Barmada for their insightful feedback and support along the way. I am truly thankful to Dr. Roman Giger and Dr. Brian Pierchala, for teaching me many

mice-related skills, for great joint lab meetings and stimulating discussions, and for cheering me on along the way. I would like to mention Dr. Jen Shadrach for all she taught me about mice and RNA isolation in my first years of Ph.D. and Dr. Ashley Kalinski for all the beautiful science we got to do together and for encouraging me to explore and for her helpful feedback along the way. I would like to give thanks to my friends Roop, Petra, Hana, Negin, and Maria for being the best friends and support system, a girl could ask for and for all the adventures we had together.

My deepest gratitude goes to my family. My mother showered me with so much love and kindness and taught me how to be brave, strong, and proud. My father for teaching me how to be independent and for his undivided devotion to his family. And finally, my one and only brother, who has been my source of inspiration, and solace. He has had my back all these years and there will never be any fitting word to describe the depth of my love and gratitude toward him.

In the end, I want to mention my friend and partner, Amir, for providing a haven for me in the past year. His unwavering support and generous heart have been my source of happiness and peace.

Preface

The content in Chapter 1 is adapted from a manuscript that is published in Current Opinion in Neurobiology, 2018, **53**:110–119. The content in Chapters 2 and 3 is prepared from a manuscript ready for submission. The content in Chapters 4 and 5 may be used for a future manuscript.

Table of Contents

List of Tables

List of Figures

List of Appendices

Abstract

Continued neuronal function throughout the aging brain requires the maintenance of synaptic connections between neurons that form functional circuits. We hypothesize that neurons are equipped with stress response pathways that enable them to sense and respond to defects in their axons, and that important elements of the stress response are controlled by the evolutionarily conserved dileucine zipper kinase (DLK). Signaling downstream of DLK becomes activated in a range of cellular conditions that impair axons and is required for a range of neuronal responses, including the ability to initiate axonal regeneration following peripheral nerve injury (PNI), and neuronal death.

The goal of my thesis work has been to understand the effect(s) DLK signaling has on neurons on a cellular level. I focused on two *in vivo* paradigms of DLK signaling activation: (1) peripheral nerve injury (PNI) in the mouse sciatic nerve, which is expected to induce survival and a regenerative response within injured motoneurons (MNs), and (2) ectopic activation of the *Drosophila* homolog of DLK in the adult fly brain, which leads to neurodegeneration and early lethality.

Chapters 2-4 describe the work and new insights learned from the PNI paradigm. I used a RiboTag approach to profile ribosome-associated transcript changes within motoneurons (MNs) regulated by DLK following PNI (Chapter 2). The distinct subset of DLK-gated genes includes secreted peptides, immune components, and cytokines, but not regeneration-associated genes (RAGs) required for axonal regeneration. I then confirmed that DLK is not required for axonal

regeneration and NMJ reinnervation in mouse motoneurons, which contrasts with its essential role in *C. elegans*.

To further understand DLK's function in MNs, in Chapter 3, I examined the inflammatory response in the spinal cord following PNI, which is associated with a loss of upstream presynaptic inputs from the axotomized MNs. Strikingly, I found that DLK is required for this synaptic loss and for aspects of the microglial response. Following clues from the profiling data, I found that DLK activation in MNs promotes the activation of complement, which is required for synaptic loss. These findings implicated a new function for DLK in stimulating innate immunity and synaptic remodeling. To consider whether this function may be shared in other paradigms of injury and neuronal stress, I compared genomic datasets of DLK-regulated genes across paradigms with my own data in mouse and *Drosophila* MNs (Chapter 4). These comparisons revealed neuropeptide secretion and signaling as shared targets of DLK regulation. To study the functional relevance and mechanism of new DLK targets, Chapter 5 describes a new paradigm in the adult *Drosophila* nervous system, which will enable future studies that take advantage of the powerful genetic tools in *Drosophila*.

While DLK was previously known for the cell-autonomous phenotypes it confers upon injured neurons, the cumulative findings from my thesis work have turned our attention to the non-cell-autonomous responses that DLK signaling may trigger following axonal damage. Inflammation and loss of upstream synapses are new roles for DLK, however, shared with previously known roles (axon regeneration and neuron death) an overarching theme of neuronal plasticity. The various forms of structural plasticity gated by DLK may enable a broad range of mechanisms for the nervous system to adapt to damage.

Chapter 1 - An Axonal Stress Response Pathway: Degenerative and Regenerative Signaling by DLK

Signaling through the dual leucine zipper-bearing kinase (DLK) is required for injured neurons to initiate new axonal growth; however, activation of this kinase also leads to neuronal degeneration and death in multiple models of injury and neurodegenerative diseases. This has spurred current consideration of DLK as a candidate therapeutic target, and raises a vital question: in what context is DLK a friend or foe to neurons? Here, we review our current understanding of DLK's function and mechanisms in regulating both regenerative and degenerative responses to axonal damage and stress in the nervous system.

1.1 Introduction

An overarching question is whether mechanisms that are required for the wiring of neuronal circuits during development can be reutilized to stimulate repair after damage or to restore function after loss in disease. In contrast to development, the capacity to repair mature neuronal circuits following damage, and, in many circumstances, the inability to repair, is linked to the activation of the damage response pathways in the nervous system. Injury response signaling mediated by the dual leucine zipper-bearing kinase (DLK) is critical for neurons to initiate new axonal growth in the peripheral nervous system (PNS). However, this same kinase enhances neuronal death and degeneration in a growing number of models for neuronal injury, stress, and neurodegenerative diseases. These dichotomous responses, along with other recent observations discussed in this review, can be reconciled into a unified view in which DLK regulates and coordinates stress response signaling in neurons (Farley and Watkins 2018).

In particular, DLK signaling appears specifically tuned to stressors that impair or damage axons (Figure 1-1, 1-2 and Table 1-1). These stressors include mechanical transection (Figure 1-1), which leads to activation of DLK signaling in all neurons and model organisms examined thus far (Watkins et al. 2013; Welsbie et al. 2013; Shin et al. 2012; Xiong et al. 2010; Yan et al. 2009; Hammarlund et al. 2009). They also include more chronic forms of stress associated with genetic mutations and drugs that hinder the microtubule cytoskeleton and axonal transport within neurons (Table 1-1 and Figure 1-2). Since axons often extend over great distances, reaching lengths of over 1000 times the diameter of the neuron's cell body (Matsuda et al. 2009), the integrity of the axon and the ability to transport organelles and proteins within it is a point of vulnerability for neurons. Such impairments within an axon can effectively silence a neuron from communicating with its post-synaptic targets, so, logically, neurons should have mechanisms to monitor the state of their axon. In this review, we will discuss how DLK's signaling mechanisms and functions appear to be intimately linked to the process of axonal transport.

As a mitogen-activated protein kinase kinase kinase (MAP3K), DLK functions as an upstream regulator of MAP Kinase signaling by activating the MAP2Ks MKK7 and MKK4, and the stress activated kinases JNK and p38 (Nihalani, Merritt, and Holzman 2000; Fan et al. 1996) (Figure 1-1). In mammals, DLK (MAP3K12) has a sister kinase, MAP3K13 (LZK), which has some partially overlapping biochemical activities and roles (Welsbie et al. 2017; Nihalani, Merritt, and Holzman 2000). Worms (*Caenorhabditis elegans*) and flies (*Drosophila melanogaster*) each have a single orthologue of equivalent homology to both DLK and LZK, named DLK-1 and Wallenda. Since these kinases share similar functions with DLK in the nervous system, we refer to all of these related kinases as 'DLK' in this review.

1.2 Developmental roles versus stress response

Some roles in nervous system development, including developmental neuronal cell death in sensory and motor neurons, neuronal migration, axon formation, and axon outgrowth have been documented for DLK and LZK (M. Chen et al. 2016; Ghosh et al. 2011; Hirai et al. 2011; Eto et al. 2010; Hirai et al. 2006), particularly when disrupted in combination with other components of JNK signaling (Hirai et al. 2011) (Table 1-1). More dramatic defects in developmental wiring of the nervous system have been linked to lost regulation of DLK: DLK protein is held in check by a highly conserved ubiquitin ligase, Pam/Highwire/Rpm-1 (PHR) (Babetto et al. 2013; Lewcock et al. 2007; Collins et al. 2006; Nakata et al. 2005). This restraint appears to be important for some axon guidance decisions (Shin and DiAntonio 2011; Lewcock et al. 2007), axon termination at correct locations (M. Borgen et al. 2017; Feoktistov and Herman 2016), assembly of presynaptic machinery (J. Li et al. 2017; Collins et al. 2006; Nakata et al. 2005), and elaboration of dendrite branches (Wang et al. 2013). Hence restraint versus activity of DLK appears to be important at specific time points in nervous system development.

In contrast to development, in which only mild axon outgrowth defects have been noted for loss of *Dlk* function in sensory and motor axons (M. Chen et al. 2016; Ghosh et al. 2011; Eto et al. 2010; Hirai et al. 2006; Bloom et al. 2007), DLK becomes activated in all types of neurons and axonal damage paradigms examined thus far in multiple model organisms (Watkins et al. 2013; Welsbie et al. 2013; Shin et al. 2012; Xiong et al. 2010; Yan et al. 2009; Hammarlund et al. 2009) and are required for both regenerative and degenerative responses to axonal damage (Table 1-1). Many of the developmental defects associated with unrestrained DLK regulation may actually mimic responses made by neurons to axonal injury. For instance, recent studies using the

Drosophila larval neuromuscular junction (NMJ) suggest that activation of DLK signaling promotes synaptic decline (Asghari Adib, Smithson, and Collins 2018; Goel and Dickman 2018), which also occurs at disconnected synapses following injury (Mishra et al. 2013). Another well-known response to axonal injury is a reduction in the injured neuron's dendritic tree and in the synaptic inputs received by the injured neuron (Navarro, Vivó and Valero-Cabré 2007; Purves 1975). Whether DLK promotes post-developmental changes in dendrite architecture remains to be examined, however recent findings that DLK mediates a reduction in synaptic spines in a mouse model of Alzheimer's Disease (Le Pichon et al. 2017) suggest this possibility.

Considering DLK's major role in damage responses, and that its most striking requirement during development is for programmed neuron cell death (Ghosh et al. 2011), one may speculate that DLK's function and restraint are relevant for developmental transitions in which neurons inherently experience conditions of cellular stress. For instance, limited levels of neurotrophic factors, or major rearrangements in neuronal cytoskeleton required for neuronal migration, may be considered 'stressful' for neurons. Also, Li *et al.* found that DLK signaling restrains the expression levels of presynaptic proteins to match the timing of synaptic maturation and growth (J. Li et al. 2017). Premature expression of these abundant structural components of the synapse fully ready to transport and implement these molecules may also result in cellular stress.

1.3 DLK regulates retrograde responses to axonal damage and trophic factor withdrawal

A large body of work supports a unified view that DLK regulates an axon-to-nucleus signaling cascade that monitors the state of the axon and becomes activated in response to axonal damage. Endogenous DLK associates with vesicles (Xiong et al. 2010), and live imaging studies of GFP-DLK transgenes suggest these vesicles are transported both anterogradely and retrogradely in axons (Holland et al. 2016; Xiong et al. 2010). DLK function is required cell-autonomously for

nuclear responses induced by axonal injury, including the activation of specific transcription factors (Larhammar, Huntwork-Rodriguez, Jiang, et al. 2017; Welsbie et al. 2017, 2013; Watkins et al. 2013; Ghosh et al. 2011; Shin et al. 2012; Yan et al. 2009). These include phosphorylated STAT3, which is thought to be retrogradely transported in peripheral nerves from axons to the nucleus (Shin et al. 2012), and also transcriptional reporters for JNK signaling (Xiong et al. 2010). Mutations that disrupt retrograde axonal transport, including mutations in dynein and dynactin (Xiong et al. 2010) and a known cargo for retrograde transport, JNK interacting protein JIP3, inhibit cell body responses downstream of DLK (Klinedinst et al. 2013; Ghosh et al. 2011). Importantly, DLK's actions and signaling mechanisms appear specifically tuned to axonal damage and not dendrite damage: in contrast to axonal regeneration, DLK is not required for the regrowth of dendrites following injury (Chung et al. 2016; Stone et al. 2014). In addition, certain cell body responses to axonal injury induced by DLK are not induced by dendritic injury (Hao and Collins 2017; Li Chen et al. 2012; Stone et al. 2010).

DLK was first discovered to play an essential role in the ability of axons to initiate new axonal growth following injury in the PNS (Shin et al. 2012; Xiong et al. 2010; Hammarlund et al. 2009; Itoh et al. 2009; Yan et al. 2009). However, following CNS injury in the optic nerve, DLK signaling initiates a cell death program (Watkins et al. 2013; Welsbie et al. 2013). Death downstream of DLK can be induced by other signals, including trophic factor withdrawal (Ghosh et al. 2011), which is known to rely upon retrograde transport and whose response can be probed specifically in axons using compartmentalized cultures (Campenot 2009; Mok, Lund, and Campenot 2009). Strikingly, DLK is essential for this classic form of developmental apoptosis in embryonic dorsal root ganglion (eDRG) neurons (Ghosh et al. 2011). Moreover, DLK signaling can originate from the axonal compartment following NGF withdrawal: biochemical indications

of DLK and JNK activation can be detected in extracts isolated from axons (Larhammar, Huntwork-Rodriguez, Rudhard, et al. 2017), and inhibition of DLK and/or JNK solely in the axonal compartment can inhibit the appearance of downstream signaling markers in the cell body (Larhammar, Huntwork-Rodriguez, Rudhard, et al. 2017; Ghosh et al. 2011). These studies demonstrate compellingly DLK's ability to initiate compartmentalized signaling within axons.

1.4 Links between DLK signaling, cytoskeleton, and axonal transport

Intracellular transport within axons becomes acutely blocked at sites of axonal damage, and it can also become impaired or diminished in the presence of cellular stressors (Figure 1-2), such as chemotherapeutic agents that disrupt the cytoskeleton (Nicolini, Monfrini, and Scuteri 2015) or accumulations of misfolded proteins in neurodegenerative disease models (Millecamps and Julien 2013). There is a striking correlation between conditions that impair axonal transport and conditions that activate DLK signaling: DLK signaling becomes activated in invertebrate and vertebrate PNS neurons that are treated with cytoskeletal destabilizing agents (Valakh et al. 2015, 2013; Bounoutas et al. 2011; Massaro, Pielage, and Davis 2009), or with genetic mutations in the cytoskeletal components spectroplakin, TCP1, Tau, or spectrin (Voelzmann et al. 2016; Valakh et al. 2013; Hammarlund et al. 2009). Activation also occurs in mutations that impair the kinesin Unc-104 (homologous to Kif1A), which is a major carrier of synaptic vesicle precursors in axons (J. Li et al. 2017). Mutations that inhibit DLK signaling rescue the synaptic defects associated with mutations in the kinesin *unc-104* (J. Li et al. 2017). Other genetic interaction studies in invertebrate peripheral neurons suggest that DLK mediates changes in neuronal morphology caused by mutations that impair cytoskeletal structure (Kurup et al. 2015; C.-H. Chen et al. 2014; Marcette, Chen, and Nonet 2014; Richardson et al. 2014; Valakh et al. 2013). Hence DLK signaling appears

responsible for both neuronal plasticity and for major pathologies associated with defects in the cytoskeleton and axonal transport.

Many previous studies have suggested that JNK signaling may directly regulate kinesin and dynein motors and their cargos (Verhey 2007; J. Liu 2017). However, Li *et al.* found that DLK signaling tunes the expression levels of presynaptic proteins, which are major cargoes for transport in axons by the Unc-104 kinesin (J. Li et al. 2017). The restraint of presynaptic protein levels by DLK signaling when axonal transport is impaired may function as a negative feedback loop to reduce stress by decreasing the amount of cargo for transport, thereby minimizing build-up. These findings suggest that DLK can function as both a sensor and effector to regulate intracellular transport within axons.

1.5 DLK signaling contributes to neurodegenerative disease

The degenerative responses induced by DLK are gaining increased attention for their roles in a growing number of neurodegenerative diseases. These include glaucoma, where functional genomic screens have identified DLK and LZK as key mediators of retinal ganglion cell (RGC) death (Welsbie et al. 2017, 2013). In addition, recent studies have suggested that DLK knockout or inhibition can delay pathology in multiple models of Amyotrophic Lateral Sclerosis (ALS) and Alzheimer's disease (AD) (Le Pichon et al. 2017; Patel et al. 2017). DLK inhibition is also protective in other models of neuronal death, including models of subarachnoid hemorrhage (Yin et al. 2017), 6-OHDA-induced dopaminergic cell death (X. Chen et al. 2008), and excitotoxicity (Pozniak et al. 2013), further increasing interest in DLK as a potential therapeutic target.

These findings imply that DLK signaling can be activated in contexts beyond simple axonal injury. It is also now apparent that the fundamental role of DLK signaling is not simply to increase axonal regeneration, despite its importance in regeneration paradigms. The dichotomous roles in

regeneration and degeneration may be unified into an underlying biological function to stimulate pathways that allow the nervous system to react to axonal damage and cellular stress. Similar to other stress pathways (including ER stress and DNA damage) transient activation of stress pathways enables recovery, however, chronic activation leads to cell death (Pakos-Zebrucka et al. 2016; Fribley, Zhang, and Kaufman 2009).

1.6 DLK signaling influences axonal integrity

An overarching theme for DLK signaling roles relates to the integrity of axons and trafficking within axons. It is striking that the multiple scenarios of DLK signaling summarized in Figure 1-1 and 1-2 also share a common resulting phenotype of axonal degeneration. Disruption of DLK together with other components of MAPK signaling leads to strong inhibition of axonal degeneration following axotomy (Yang et al. 2015; Miller et al. 2009), trophic factor withdrawal (Simon et al. 2016; Huntwork-Rodriguez et al. 2013; Ghosh et al. 2011) and chemotherapy-induced axon degeneration (Bhattacharya et al. 2012; Miller et al. 2009). We, therefore, consider here our current understanding of the mechanistic relationships between DLK signaling and axonal degeneration.

Since DLK signaling may be initiated locally in axons and can regulate global (transcriptional/translational) responses in neurons, its influence upon axonal integrity and degeneration is likely multi-pronged, involving both local mechanisms in axons and global mechanisms downstream of retrograde signaling (Geden and Deshmukh 2016). The ‘global’ responses downstream of retrograde signaling are the simplest to consider first. Following trophic factor withdrawal in mouse DRGs, DLK and downstream MAPK signaling induce the expression of pro-apoptotic proteins Bax, Puma, and caspases, some of which stimulate axonal degeneration following their induction in the cell body (Simon et al. 2016). A strikingly opposite protective

response has been observed in fly motoneurons, where activation of DLK, either by ectopic expression or axonal injury, leads to a global response that increases the resiliency of both axons and dendrites to degenerate in subsequent injuries (Li Chen et al. 2012; Xiong and Collins 2012). These responses may serve a biological purpose for neurons that have been injured to have increased resiliency to subsequent damage. In contrast, the pro-degenerative actions downstream of trophic factor deprivation may allow for pruning of axonal branches.

Together with downstream MAPK signaling effectors, DLK signaling also acts locally in distal axons to influence axonal degeneration. This may be most clearly considered for Wallerian degeneration of distal axons that become separated from cell bodies following acute axonal injury (pictured in Figure 1-1). Wallerian degeneration involves cell-autonomous 'self-destruction' events that occur locally in axons independent of classical cell death machinery (Gerdts et al. 2016; Conforti, Gilley, and Coleman 2014). Acute inhibition of JNK in axotomized axons is sufficient to delay axonal degeneration (Miller et al. 2009), suggesting a local role for DLK/JNK signaling in promoting axon destruction.

What is this local role in axons? A key driver of Wallerian degeneration is the TIR-domain protein Sarm1, which functions as a NADase enzyme, degrading the essential metabolite NAD+ (Essuman et al. 2017; Gerdts et al. 2015). Sarm1 function is antagonized by the NAD+ biosynthetic enzyme NMNAT2 (Walker et al. 2017; Gilley et al. 2015), which, due to its short half-life in axons, must be continuously transported in axons from the cell body (Milde, Gilley, and Coleman 2013). Yang *et al.* observed that genetic inhibition of MAPK signaling could blunt degeneration induced by ectopic activation of Sarm1 in DRG explants and proposed a role for MAPK in promoting degeneration downstream of Sarm1 (Yang et al. 2015). However, Walker *et al.* more firmly identified an upstream role with the finding that MAPK signaling enhances the

stability/turnover of NMNAT2 in both mouse DRG and fly motoneurons (Walker et al. 2017). Connections between DLK and NMNAT2 are also noted via their shared regulation by the PHR ubiquitin ligase (Babetto et al. 2013; Xiong and Collins 2012; Collins et al. 2006; Nakata et al. 2005), which is discussed further below in section 8. We acknowledge inherent challenges to distinguishing local from global effects of DLK signaling, which likely intersect to influence axonal integrity.

1.7 Stress responses regulated by DLK

Given the many cellular responses to DLK activation discussed above, surprisingly little is currently documented about the cellular pathways controlled by DLK. The known pathways thus far all share features of roles in stress response. Studies in worms have suggested that DLK signaling leads to increased mitochondrial transport and density in axons after injury (Han, Baig, and Hammarlund 2016) and that DLK signaling stimulates the expression of poly (ADP-ribose) glycohydrolases (PARGs) (Byrne et al. 2016), which are linked to a growing number of genotoxic and metabolic stress signaling pathways (Luo and Kraus 2012). A recent study using mouse models of axonal stress in both the PNS and CNS found that DLK is a critical regulator of the Integrated Stress Response (ISR) pathway (Larhammar, Huntwork-Rodriguez, Jiang, et al. 2017). ISR appears to influence translational responses in cells: while global translation is inhibited, genes with upstream Open Reading Frames such as ATF4 can be selectively induced. These findings are interesting in light of other data linking ISR to neuronal loss in models of neurodegenerative diseases (Moreno et al. 2012; Page et al. 2006), as well as studies linking DLK to translational mechanisms of the regulation (J. H. Kim et al. 2013; Yan et al. 2009).

In addition to cell-autonomous stress responses, DLK signaling may also promote responses by non-neuronal cell types. A recent study in flies suggested that signaling downstream

of DLK (via p38) may increase neuroinflammation in a TDP-43 overexpression model of neurodegenerative disease (Zhan, Xie, and Tibbetts 2015), while conditional knockout of DLK in an ALS mouse model reduced the appearance of activated microglia (Le Pichon et al. 2017). A recent study found that DLK controls the expression of neuroinflammatory chemokines and is required for microgliosis and neuropathic pain (Wlaschin et al. 2018). Future studies are needed to determine whether these pathways are controlled by DLK in different cell types and model organisms and to understand their mechanisms in axonal stress responses.

1.8 Mechanisms for restraint and activation of DLK signaling

Essential for the current model that DLK gates responses to axonal stress is that its mechanism is tightly tuned to axonal damage and restrained in healthy/undamaged neurons. One important mechanism of control is at the level of protein stability and turnover. Genetic perturbations in multiple components of ubiquitin ligase complexes and deubiquitinating enzymes result in elevated DLK levels and chronically activated DLK signaling (Baker et al. 2014; Brace et al. 2014; Collins et al. 2006; Nakata et al. 2005). Moreover, overexpression of DLK in neurons, and even ectopic expression of DLK in non-neuronal cell types, is sufficient to activate downstream signaling (Huntwork-Rodriguez et al. 2013; Collins et al. 2006; Fan et al. 1996). This is thought to be mediated by its capacity to dimerize via leucine zipper domains and phosphorylate itself (Nihalani, Merritt, and Holzman 2000). Once activated, downstream signaling via JNK stimulates DLK phosphorylation at additional sites and a decrease in DLK's turnover rate (Huntwork-Rodriguez et al. 2013). This feed-forward relationship may enable neurons to kick-start DLK signaling in response to a local damage event in axons. How does DLK become activated? A growing number of conditions, kinases, and some phosphatases have been implicated in its regulation (Börchers et al. 2017; Huang et al. 2017; Feoktistov and Herman 2016; Hao et al.

2016; Wong et al. 2015; C.-C. Wu et al. 2015; Baker et al. 2014; Huntwork-Rodriguez et al. 2013; Lizhen Chen et al. 2011; Daviau, Di Fruscio, and Blouin 2009; Shen and Ganetzky 2009; Robitaille et al. 2008; Fukuyama et al. 2000), and activated DLK is heavily phosphorylated across multiple sites (Hao et al. 2016; Huntwork-Rodriguez et al. 2013). However, the molecular mechanisms that link various stressors in axons (in Figure 1-1 and Figure 1-2) to DLK activation are still poorly understood. Recent work has indicated that Protein Kinase A (PKA) is an important mediator of DLK's activation following axonal injury (Hao et al. 2016), while Ste20 Kinases MAP4K4, MINK1, and TNIK promote DLK's activation in axons following trophic factor withdrawal (Larhammar, Huntwork-Rodriguez, Rudhard, et al. 2017). Whether these different stressors use overlapping or distinct mechanisms is not yet known. *C. elegans* DLK-1 contains a domain shared with MAP3K13/LZK that gates signaling activation in response to elevated calcium (Yan and Jin 2012). However, application of microtubule destabilizing agents to axons leads to the activation of DLK signaling independently of calcium (Valakh et al. 2015). Hence it is likely that multiple distinct mechanisms regulate DLK activation in neurons.

DLK's retrograde signaling functions require that DLK is physically present to become activated in axons. A conserved site for palmitoylation allows DLK to associate with vesicles that are transported in axons, and palmitoylation is essential for DLK's signaling ability (Holland et al. 2016). Since defects in axonal transport and the cytoskeleton lead to DLK activation, is DLK transport directly linked to its activation mechanism? It is intriguing that a major negative regulator of DLK, the PHR ubiquitin ligase, localizes to presynaptic terminals (C. Wu et al. 2005; Schaefer, Hadwiger, and Nonet 2000; Zhen et al. 2000), hence may promote the destruction of DLK at synapses (Figure 1-3). It is also intriguing that PHR regulates axonal degeneration via an additional target, the protective enzyme NMNAT2 (Babetto et al. 2013; Xiong et al. 2012) and (Figure 1-2).

PHR's regulation of DLK is best documented in the context of synapse development, where PHR's regulation of DLK becomes apparent with a timing that coincides with termination of axonal out-growth and the initiation of synaptogenesis (M. Borgen, Wang, and Grill 2017; Collins et al. 2006). Since axonal damage inherently disrupts synaptic connections in axons, whether PHR influences DLK's activation mechanisms following axonal damage remains an interesting future question.

1.9 Conclusion

We propose that a higher-order function for DLK signaling may be to promote a damage-response state in neurons that enables plasticity in neuronal circuits. In this state, the ultimate response may be strongly influenced by the circumstance of the damage. In some contexts, such as PNS injury, neurons may be supported for growth and inhibited for death. However, in other contexts, in order to incur the least damage or the best adaptation within a neuronal circuit, it may be more advantageous for the damaged neuron to degenerate and be removed. As an evolutionarily conserved sensor of axonal stress and injury, DLK's regulation and modes of action are tightly coordinated with the integrity of the axonal cytoskeleton and transport machinery. As a critical mediator of injury responses and neurodegeneration pathways, future work is needed to understand the cellular responses that DLK regulates and the mechanisms that control its activation in the nervous system.

1.10 Acknowledgments

The Collins lab is supported by a grant from the National Institute of Health, R01NS069844. We thank Aaron DiAntonio, Dion Dickman, Roman Giger, Ashley Kalinski, and Claire Le Pichon for helpful comments on the manuscript.

Table 1-1 Functions ascribed to DLK signaling in different paradigms and model systems

Function	Context
Axonal regeneration in PNS	DLK is required for axonal regeneration following laser axotomy in *C. elegans* GABA motoneurons (Hammarlund et al. 2009) and ALM and PLM touch neurons (Yan et al. 2009; Lizhen Chen et al. 2011), and in D. melanogaster larval motoneuron (Xiong et al. 2010a) and sensory neurons (Stone et al. 2014). Following sciatic nerve injury in mice, DLK is required in motoneurons for reinnervation of motoneuron endplates (Shin et al. 2012). DRG neurons deleted for DLK fail to undergo enhanced regeneration stimulated by a conditioning injury (Fernandes et al. 2014; Shin et al. 2012).
Axonal regeneration in CNS	DLK is required for PTEN−/− induced regeneration in the mouse optic nerve (Watkins et al. 2013).
Wallerian degeneration of injured axons	Modest defects in Wallerian degeneration have been observed for DLK mutants in D. melanogaster olfactory neurons (Miller et al. 2009), cultured embryonic DRGs (Yang et al. 2015; Miller et al. 2009), and in the mouse sciatic nerve (Miller et al. 2009). Combined knockout of DLK with other components of MAPK signaling leads to a strong inhibition of Wallerian degeneration of RGC axons in the optic nerve (Yang et al. 2015).
Chemotherapy-induced axonal degeneration	DLK-deficient mouse DRG axons are protected after vincristine exposure (Miller et al. 2009). Loss of DLK in taxol-treated Drosophila axons prevents degeneration (Bhattacharya et al. 2012).
Resistance to axonal degeneration	DLK activation following a conditioning lesion in larval PNS motoneurons protects axons from degeneration following subsequent injuries (Xiong and Collins 2012).
Neuronal remodeling in response to cytoskeletal stress	The growth of *C. elegans* in the presence of microtubule destabilizing agent colchicine causes changes in the levels of many touch receptor proteins via DLK-1 signaling (Bounoutas et al. 2011). Genetic perturbations in microtubules cause synaptic remodeling of C. elegans GABA dorsal D-Type (DD) neurons via DLK-1 signaling (Kurup et al. 2015). D. melanogaster mutations in alpha-spectrin and ankyrin, which should chronically impair cytoskeleton, cause retraction and loss of presynaptic boutons; genetic manipulations in upstream and downstream components of the DLK signaling pathway modify these phenotypes (Massaro, Pielage, and Davis 2009).

Neuronal Death	Mouse embryonic DRGs deleted for DLK fail to undergo cell death following trophic factor withdrawal (Larhammar, Huntwork-Rodriguez, Rudhard, et al. 2017; Hirai et al. 2006). Mouse retinal ganglion cells (RGCs) deleted for DLK fail to undergo cell death following optic nerve injury (Fernandes et al. 2014; Watkins et al. 2013; Welsbie et al. 2013) and in a cellular model of stress/glaucoma (Welsbie et al. 2013). DLK inhibition in adult mice is also protective against cell death in models of excitotoxicity (Pozniak et al. 2013), subarachnoid hemorrhage (Yin et al. 2017), and 6-OHDA-induced dopaminergic cell death (X. Chen et al. 2008).
Neural degeneration in disease models	In two different mouse models of Alzheimer's Disease (AD) and a mouse model of ALS, conditional deletion of DLK in the adult nervous system shows neuroprotective phenotypes (Le Pichon et al. 2017). These include reduced loss of axons and NMJ synapses and reduced inflammation in the spinal cord of $SOD1^{G93A}$ mice; reduced memory impairment and dendritic spine loss in PS2APP mice, and reduced neuron loss in TauP301L mice. Neither A-beta nor Tau pathology was affected by DLK knockout, suggesting a downstream role for DLK in promoting degeneration (Le Pichon et al. 2017). In D. melanogaster, heterozygous mutations in DLK/Wnd rescue premature lethality in a TDP-43 overexpression model of ALS, however homozygous mutations enhance lethality in this model (Zhan, Xie, and Tibbetts 2015).
Synaptic decline	DLK activation in both *C. elegans* and D. melanogaster leads to defects in the structure of presynaptic terminals (Collins et al. 2006; Nakata et al. 2005). Electrophysiology recordings at D. melanogaster NMJ synapses indicate that DLK signaling activation in motoneurons induces both presynaptic reductions in synaptic vesicle release and post-synaptic responses to neurotransmitter (J. Li et al. 2017; Goel and Dickman 2018).
Developmental axonal outgrowth and neuronal migration	DLK-deficient mice show defects in neocortical radial migration and reduced axon tracts in the anterior commissure, internal capsule, and corpus callosum (Hirai et al. 2006). Dissociated cortical neurons knocked down for DLK have reduced axonal growth (Eto et al. 2010). Double mutants of DLK with JNK1 have severe defects in axon formation (Hirai et al. 2011).
Neuroinflammation	Inhibition of DLK leads to reduced microglial responses in a mouse model of neuropathic pain (Wlaschin et al. 2018) and in a mouse model of ALS (Le Pichon et al. 2017).

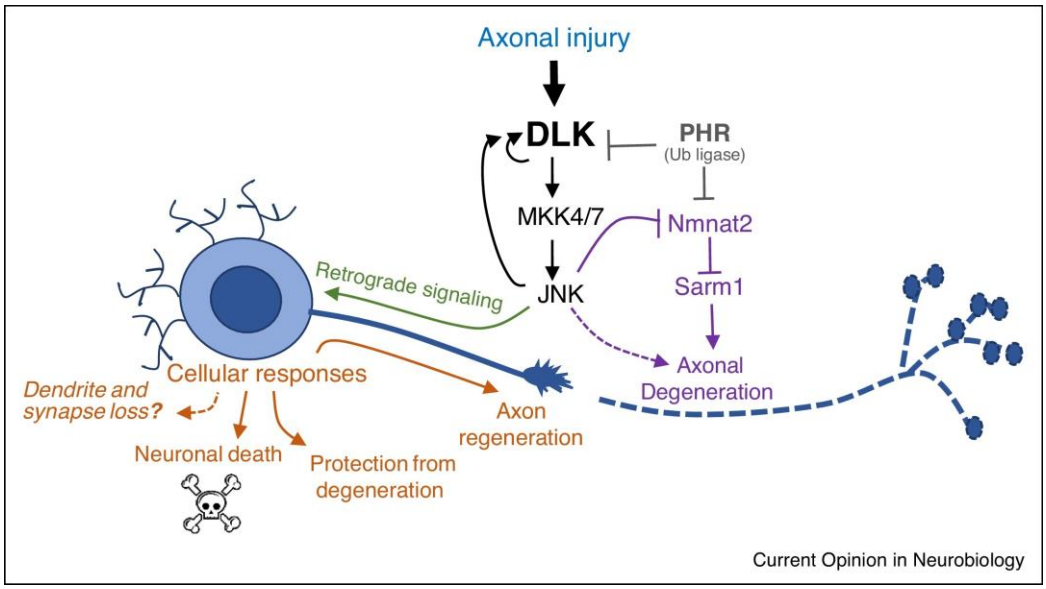

Figure 1-1 ***DLK regulates multiple responses to axonal damage.*** *DLK signaling becomes activated following axonal injury and regulates multiple cellular responses (in orange): neuronal death (Watkins et al. 2013; Welsbie et al. 2013), axonal regeneration (Shin et al. 2012; Xiong et al. 2010; Hammarlund et al. 2009; Yan et al. 2009) and/or protection from degeneration (Xiong and Collins 2012), depending upon the context (Table 1-1). Whether DLK promotes loss of dendrites and synaptic inputs is hypothesized based on discussed data (Le Pichon et al. 2017; Wang et al. 2013; Navarro et al. 2007; Purves 1975) but remains to be determined. The distal part of the axon, which becomes removed from the cell body undergoes Wallerian degeneration. This is also influenced by DLK signaling (Yang et al. 2013; Xiong and Collins 2012; Miller et al. 2009). In addition, DLK and downstream signaling components crosstalk with other factors that influence axonal degeneration, the NMNAT enzyme and Sarm1 NADylase (Walker et al. 2017; Yang et al. 2015; Babetto et al. 2013; Xiong et al. 2012).*

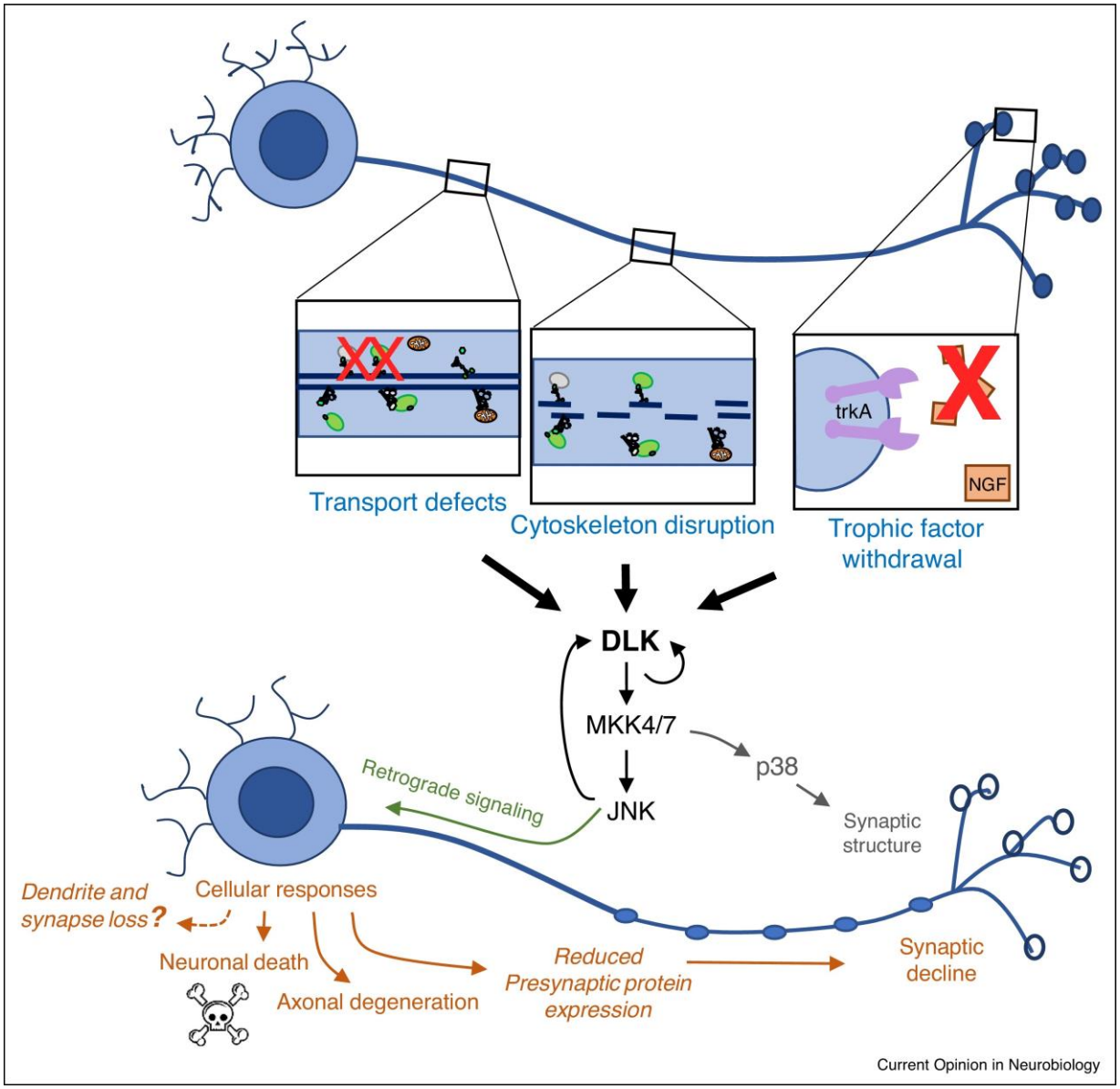

Figure 1-2 ***Examples of axonal stress that lead to activation of DLK.*** *Defects in axonal transport (Li et al. 2017), disruption of cytoskeleton within axons (Valakh et al. 2015; Valakh et al. 2013; Massaro et al. 2009), and inhibition of trophic factor signaling (Larhammar et al. 2017; Huntwork-Rodriguez et al. 2013; Ghosh et al. 2011) all result in the activation of DLK signaling. Downstream responses (in orange) include reduced expression levels of presynaptic proteins (Li et al. 2017) and yet unknown signals that impair postsynaptic receptor function and synaptic homeostasis mechanisms (Goel and Dickman 2018). Over time these responses are expected to promote synaptic decline and loss.*

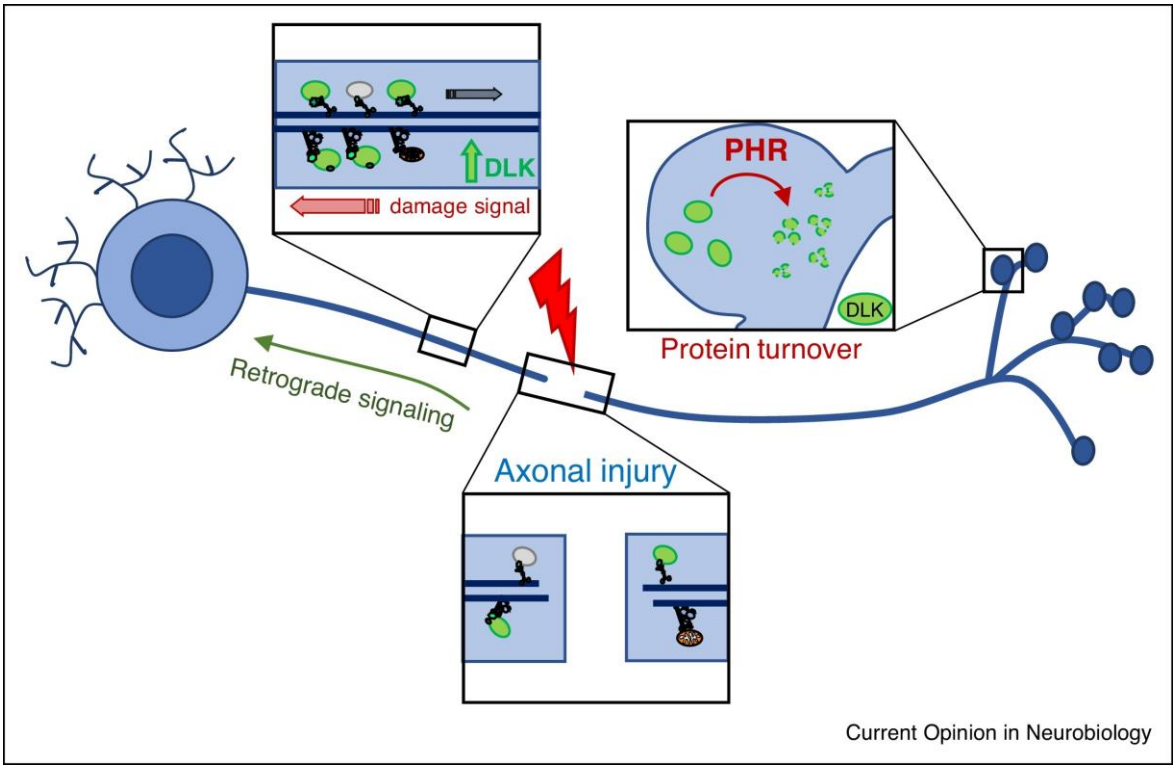

Figure 1-3 ***Regulation of DLK.*** *DLK associates with vesicles that are transported in axons (indicated in green) (Larhammar et al. 2017; Xiong et al. 2010). DLK protein is regulated by ubiquitin ligases, including the highly conserved synaptic protein PHR (Pam/Highwire/Rpm-1), which regulates DLK during synaptic development (Collins et al. 2006; Nakata et al. 2005).*

Chapter 2 Profiling Molecular Responses to DLK Activation in Injured Motoneurons

MAP Kinase signaling downstream of DLK mediates dichotomous context-dependent outcomes, ranging from cell death and synapse loss to initiation of axonal regeneration and degeneration. To identify molecular pathways regulated by DLK, we used RiboTag technology to profile the DLK-dependent translatome of injured motoneurons (MNs) following peripheral nerve injury (PNI). Contrary to expectations, we found that regenerative associative genes (RAGS) are robustly activated in MNs in the absence of DLK. Consistent with this observation, we found that DLK is not essential for MNs to initiate axonal regeneration and reconnect lost neuromuscular junction (NMJ) terminals. Out of 2085 differentially expressed genes 3 days post PNI we found that only 310 of these genes are DLK-dependent. Gene set enrichment analysis (GSEA) of the DLK-dependent genes identified secreted proteins and components of the immune system as major functional categories. Our data frame a model that DLK signaling in injured neurons governs the release of extracellular signals to other cells, including the immune system, to organize responses to axonal damage.

2.1 Introduction

Responses to DLK activation can be considered as both beneficial and deleterious. Beneficial responses include reformation of lost synaptic connections in the peripheral nervous system, while neuronal death in models for glaucoma, optic nerve injury, and ALS may be considered deleterious. (Watkins et al. 2013; Huntwork-Rodriguez et al. 2013; Welsbie et al. 2013, 2017; Le Pichon et al. 2017). DLK can also have a role in the cytoskeletal

organization (Kurup et al. 2015; C.-H. Chen et al. 2014; Valakh et al. 2013; Bounoutas et al. 2011; Massaro, Pielage, and Davis 2009), mitochondrial transport (Han, Baig, and Hammarlund 2016), and synaptic protein regulation (J. Li et al. 2017; Goel and Dickman 2018; Collins et al. 2006; Nakata et al. 2005). Despite these important and dichotomous functions ascribed to DLK, we still have very little understanding of the molecular mechanism(s) by which DLK achieves these functions. The overarching goal of this project has been to identify the cellular pathways that are regulated by DLK.

While the early stages of my thesis work initiated approaches to this goal in flies, I was drawn to use mice for several reasons. One is that the paradigm of peripheral nerve injury is well studied in mice (Magill et al. 2007). Many previous studies have described how DRG and motoneurons (MNs) respond to peripheral nerve damage and this form of damage has been demonstrated to activate DLK (Antoni Valero-Cabré et al. 2004; Magill et al. 2007; Itoh et al. 2009; Shin et al. 2012, 2019). Hence peripheral nerve injury (PNI) enables us to study the functional consequences of endogenous DLK activation. By contrast, in flies, many conditions lead to activation of DLK's homolog Wallenda, (for instance mutations in a ubiquitin ligase or kinesin motor), but these are all in the context of another mutation. Activation of DLK by PNI enables us to study what DLK does in an otherwise healthy and wild-type nervous system. A second reason to study DLK in the context of PNI in mice is that functional regeneration of lost NMJ synapses is well documented in mice (Antoni Valero-Cabré et al. 2004; Magill et al. 2007). Based on previous studies (Shin et al. 2012; Hammarlund et al. 2009; Yan et al. 2009) we expected that this would require DLK. In contrast, injured MNs in Drosophila larvae fail to re-establish functional NMJ synapses (Lucas Junginger and Laura Smithson, unpublished communication).

Finally, the mouse tissues are much larger than flies making biochemical approaches more feasible.

To profile molecular responses to DLK activation in motoneurons (MNs) we used the RiboTag method (Lesiak, Brodsky, and Neumaier 2015), which enables the Cre-dependent introduction of HA tag into Ribosomal Protein 22 (Rpl22). This protein gets recruited to ribosomes and transcripts from specific cell types are isolated (Figure 2-1A). We chose The RiboTag method for the following reasons. One challenge is that while we know DLK activates cell-autonomous responses in damaged neurons, most of the cells in nervous system tissue are not activated for DLK. Hence important cell-autonomous responses may be buried in the noise of whole tissue sequencing data. In addition, methods to isolate individual cells (eg, by FACS sorting) are expected to induce axonal damage, so may indirectly activate DLK signaling. These considerations made the RiboTag approach attractive.

This cell-type-specific approach of the RiboTag enabled us to identify genes regulated by DLK cell-autonomously in injured MNs. Previous functional studies of DLK led us to expect that DLK would regulate numerous cell-autonomous processes in neurons, including synaptic proteins (J. Li et al. 2017; Goel and Dickman 2018; Collins et al. 2006; Nakata et al. 2005), mitochondria, and metabolism (Han, Baig, and Hammarlund 2016; Byrne et al. 2016) and cytoskeletal proteins (C.-H. Chen et al. 2014). It was therefore somewhat surprising that the major functional classes of DLK-regulated genes include secreted proteins, cytokines, and immune-related genes. These findings turned our attention from the cell-intrinsic roles of DLK in neurons to its potential extrinsic and non-autonomous functions, which may be achieved through signals released to other cells.

2.2 Material and Methods

2.2.1 Animals:

All procedures involving mice were performed in accordance with guidelines developed by the National Institutes of Health and were approved by the Institutional Animal Care and Use Committee (IACUC) at the University of Michigan. Adult (12 – 15-Week-old) males and females on a C57BL/6 background were used in this study.

To render conditional KO of DLK and RiboTag in motor neurons, Rpl22HA/HA and DLK fx/fx were crossed with ChAT-Cre mice to generate Rpl22HA/HA; DLK fx/fx; ChATCre/+ (RiboHO; DLKfloxed; ChATCre) and Rpl22HA/HA; DLK +/+; ChATCre/+ (RiboHO; DLKWT; ChATCre) were used as controls. To test DLK reduction we used DLK fx/fx; UBC-CreER/+ and DLK fx/fx; +/+ mice with tamoxifen treatment.

2.2.2 Surgical Procedures:

2-3% Isoflurane mixed with Oxygen was used to anesthetize the mice, Carprofen was administered subcutaneously as analgesic 15 minutes before performing the surgery and then once a day for 48 hours post-surgery. At the level of mid-thigh, a 1 cm incision was made through the skin, and muscle and sciatic nerve were exposed. Using fine forceps (#11399-80, Fine Science Tools), the sciatic nerve was crushed. Sutures were used to close the muscles and to close the skin, and clips (Roboz, RS-9258) were used. Naive mice received no injury.

2.2.3 Tamoxifen treatment

To knock down DLK in adult mice post developmentally, 3-month-old Dlk fx/fx; UBC-CreER and Dlk fx/fx; +/+, received tamoxifen by oral gavage for 5 days and then a waiting period

of 10 days, after which they are tested for DLK protein levels. 20 mg/ml of tamoxifen was made in corn oil as our stock. Our working dose was 0.025 mg/g body weight.

2.2.4 Tissue preparation:

Phosphate buffer saline (PBS) was used to perfuse mice transcardially. To isolate the entire spinal cord, the hydraulic extrusion method from (Kennedy et al., 2013) was used. The lumbar spinal cord was then divided from the midline to uninjured (contralateral) and injured (ipsilateral) sides and flash-frozen in liquid nitrogen. Samples were similarly collected from naïve mice. For degeneration and reinnervation analysis, TA, EDL, gastrocnemius (GP), and Soleus (Sol) were collected. Muscles were fixed for 20 minutes at room temperature using 4% paraformaldehyde (PFA), while spinal cords and nerves were fixed with 4% PFA overnight. Samples were washed 3 times with 1X Phosphate buffer Saline (PBS) after fixation and transferred to 30% sucrose and kept at 4 ˚C. After sucrose saturation was done, samples were embedded in O.C.T. Compound (Fisher, 4585). For histochemical purposes spinal cords were sectioned 20 μm, longitudinally using a cryostat (Leica 3050S). Muscle sections were 60 μm thick and sciatic nerves were 15 μm thick.

2.2.5 Immunohistochemistry:

Samples were washed with 1X PBS to remove the OCT for 5 min, a ring was drawn around them using the ImmEdge hydrophobic pen (Vector Biosciences). Samples were permeabilized for 30 minutes using 0.1% Triton X-100 and then blocked for 30 minutes to 1 hour at room temperature in 1X PBS containing 0.1% Triton-X, 10% donkey serum (Jackson ImmunoResearch), and M.O.M blocking reagent (Vector Laboratories). Slides were then incubated with primary antibodies dissolved in 1X PBS containing 0.1% Triton-X, and 5% donkey

serum/goat serum. For Choline Acetyltransferase (ChAT) staining, Antigen retrieval is required before permeabilization. To do so, samples were treated with 10 mM Sodium Citrate pH:6 at 95 ˚C for 3 min and then washed once with 1X PBS. Primary antibodies used: goat anti-ChAT (Sigma, 1:100), Rabbit anti- HA (Cell Signaling, 1:100), Mouse anti- NeuN (Sigma, 1:500), Rabbit anti-CJun Serine 73 phosphorylated (Cell signaling, 1:100), Rabbit anti-SCG10 (Novus Biologicals, 1:100), mouse anti-beta-Tubulin III (Sigma, 1:200). Secondary antibodies used were as follows: 543 Donkey anti Rabbit, 488 Donkey anti-Mouse, 647 Donkey anti-goat (all from Jackson Laboratories) along with conjugated α-Bungarotoxin CF®543A (Biotium, 1:75).

2.2.6 Protein isolation and western blotting

We copurified proteins while we isolated our RNAs using RNeasy Plus Micro Kit (Qiagen). At the stage that RNA is binding to the cup, the flowthrough is used as a protein containing supernatant. We precipitated the proteins on ice for 30 min using ice-cold acetone. Centrifugation for 10 min at max speed led to the formation of the protein pellets which were washed again with 100% ice-cold ethanol and post centrifugation were resuspended in water. For denaturation, 2X SDS sample buffer was added to each sample, and samples were boiled at 100°C for 10 min.

SDS-PAGE Electrophoresis was done with 12-14% resolving SDS gels and ran proteins got transferred to polyvinylidene fluoride (PVDF) membranes. Our blocking solution contained Tris buffer Saline (TBS) with a pH of 7.4 with 0.1% Tween-20 and 4% skim milk. After blocking the membrane for 1 hour at room temperature, Rabbit anti- DLK primary antibody was added (Sigma, 1:1000) to 3% bovine serum albumin (BSA) and membranes were incubated in this solution overnight at 4°C. Membranes were washed 3 times the next day Rabbit anti-HRP (horseradish peroxidase) secondary antibody was again dissolved in 3% BSA and samples were

incubated for an hour. For visualization, a chemiluminescent substrate was used. ImageJ was used for quantification purposes and the integrated density of the signal was calculated for the DLK bands and the Actin bands as loading controls. DLK protein expression is shown as DLK/actin integrated density of the band in different genotypes.

2.2.7 Immunoprecipitation and RNA isolation

To homogenize and for immunoprecipitation (IP) of the HA-tagged ribosomes, we used (Sanz et al., 2009) protocol with some modifications. In short, IP buffer containing 50 mM Tris, pH 7.4, 100 mM KCl, 12 mM MgCl2, 1% Nonidet P-40 [NP-40] supplemented with 200 U/mL Promega RNasin, 1 mg/mL heparin, 100μg/mL cycloheximide, and protease inhibitor mixture [Sigma-Aldrich] were made fresh. Tissues were placed in a glass Dounce and homogenized with the pestle that fits tightly with the Dounce. After the homogenization is done, samples were toppled for 20-30 minutes at 4 ˚C, then were centrifuged at 10,000 Xg at 4 ˚C for 10 minutes. Normally at each step, we collected 50 μl of supernatants for future processing or analysis of input RNA. The supernatants at this step were then precleared at 4 ˚C for an hour with Protein G magnetic beads (New England Biolabs). Samples at this step need to be under constant rotation. After separating supernatants from the magnetic beads using a magnetic rack (company), samples were incubated for 4 hours with HA antibody (Biolegend, MMS-101P). The concentration of HA antibody was 1:150. At this step, samples are toppled at 4 ˚C. After the 4-hour incubation is done, Protein G magnetic beads are applied along with an overnight incubation under rotation at 4°C.

The next day, supernatants were separated from the magnetic beads. The immunoprecipitated ribosomes are now associated with magnetic beads. The beads were washed in a high salt buffer containing 50 mM Tris, pH 7.4, 300 mM KCl, 12 mM MgCl2, 1% NP-40 supplemented with 100 μg/mL cycloheximide 3 times. At the end of the third wash lysis buffer is

added to the beads and vortex for 30 seconds, then back on magnetic racks and the drawn supernatants are used for RNA isolation using RNeasy Plus Micro Kit (Qiagen) per manufacturer instructions.

2.2.8 RNAScope In situ hybridization

Fixed frozen samples were used for the *in situ* and to probe for multiple targets, RNAscope® Multiplex Fluorescent v2 Assay was used. The experiment was done based on the manufacturer's manual for fixed frozen tissue. Briefly, samples were washed with 1X Phosphate Buffer Saline (PBS) to remove OCT for 5 minutes. Samples were then baked in a 60˚C oven for 45 minutes. Samples were then post-fixed with 4% Paraformaldehyde (PFA) in 1X PBS for 60 minutes at room temperature. After this, samples are dehydrated with 50%, 70%, and 100% ethanol each dehydration step is for 5 minutes, at the end of the slides are removed from 100% ethanol and immersed again in fresh 100% ethanol for another 5 minutes. In the end, slides are left to dry for 5 minutes. To block endogenous peroxidase enzyme activity, hydrogen peroxide is then applied to the tissues for 10 minutes. Samples are then washed with deionized water (dH2O) for 10-15 seconds and then samples are put in the antigen retrieval solution that is in the steamer at 95 ˚C for 5 minutes.

Samples are then dried again in a 60 ˚C oven for 45 minutes. ACD oven needs to be turned on 30 minutes before use to make sure the 40 ˚C and humidity are acquired. After the samples were dry a hydrophobic ring was drawn around each tissue using an ImmEdge pen (Vector Laboratories, H-4000). Protease II is applied to each tissue and samples are left in the ACD oven for 40 minutes at 40 ˚C. Protease III is a broad-spectrum protease that is intended to permeabilize the samples adequately to allow the probes to reach the target mRNA.

The probe mix that we plan to use is the combined 50X of C1 probes with 1X of C2 and 1X of C3 probes. Slides are washed with dH2O and then the probe mix is applied, and samples are left at 40 ˚C for 2 hours. Samples are then washed with 1X Wash buffer for 2 minutes, twice. We stop at this step and store our slides in a jar containing 200 ml of 5X Saline Sodium Citrate (SSC) buffer (from 20X SSC buffer, 51205, AccuGENE^{TM}, Lonza). On the second day, samples are washed again with a 1X wash buffer twice each for 2 minutes. Amplification steps are then performed using A1, A2, and A3 solutions for 30, 30, and 15 minutes respectively at 40 ˚C. For the developing step, C1 is applied for 15 minutes at 40 ˚C. The TSA secondaries (NEL741001KT, NEL745001KT, NEL744001KT; Akoya Biosciences) are used at a concentration that works best for each probe and incubated for 30 minutes at 40 ˚C. Samples are washed at the end of each step twice with 1X wash buffer for 2 minutes. HRP block solution is then added, and samples are incubated for 15 minutes at 40 ˚C. Samples are then washed the same way and C2, and C3 developing solution and TSAs are added the same as C1 step. When the last wash was done, samples were mounted with DAPI Fluoromount-G (SouthernBiotech, 0100-20) and imaged in 3-5 days.

2.2.9 RT-qPCR

RNA concentration was measured using nanodrop and sending the samples (2 µl) to the core to be read by 2100 Bioanalyzer Instrument (Agilent Genomics). The remainder of the sample was used for cDNA preparation. We used Superscript III First-Strand Synthesis SuperMix (Invitrogen). RT-qPCR was performed using necessary primer sets, FastStart Universal SYBR Green Master Mix (Roche), and a 7900HT Fast Real-Time PCR System (Applied Biosystems). For each sample, we had 3 technical replicates and 2-3 biological replicates. We averaged the resulting CT of our 3 technical replicates per sample (biological replicate). Data is eventually

normalized to a loading control like actin, the result was log2 transformed and then relative expression was graphed compared to input for each gene.

The concentration of isolated RNA was determined by running samples on a 2100 Bioanalyzer Instrument (Agilent Genomics). cDNA was then synthesized with the remainder of the RNA sample (~12 μl) using Superscript III First-Strand Synthesis SuperMix (Invitrogen). Subsequent RT-qPCR was performed using a 7900HT Fast Real-Time PCR System (Applied Biosystems) with the appropriate primer set (Table S1) and FastStart Universal SYBR Green Master Mix (Roche). All samples were run in triplicate and the resulting CTs were averaged. Data were normalized to loading control (B2M, Figure 3 and Actin, 6 and 7), while normalization to a loading control was not performed in Figure 2. Following normalization, data were log2 transformed and then relative expression was calculated for each gene set examined.

2.2.10 RNA seq library preparation and analysis:

RNA sequencing was performed on 3 animals per condition, 3 days post SNC. Isolated RNAs after the IP (RNA integrity value (RIN) > 7.5) were sent to the University of Michigan Sequencing Core for library prep using "SMART-Seq v4 Ultra Low Input RNA Kit for Sequencing". The core used the covaris shearing and ThruPlex library prep of the cDNAs, along with PolyA selection. Paired end 50 bp sequencing was performed on a HiSeq4000 platform. Fastq files were received from the core. We quality-checked the files using FastQC (Andrews and Others 2010) and performed adapter trimming using Illumina Thruseq adaptors and BBDuk ("BBMap" n.d.). Trimmed reads were then mapped to the mouse genome (GRCm38.p6) using the STAR/2.5.2a aligner (Dobin et al. 2013). We performed post mapping quality control using QoRTs (Hartley and Mullikin 2015). One of the *Dlk* KO naive samples was behaving a little differently from other samples and showed bias towards its 3' end. We decided to remove this sample for our

downstream analysis and only used 2 *Dlk* KO naive samples. DESeq2 package was used in R for differential expression analysis (Love, Anders, and Huber 2014). Multiple differential expression analysis was performed using either control naive or control uninjured as the reference point. Heatmaps were generated using the ggplot2 package (Wickham 2011). Volcano plots were generated using the EnhancedVolcano package (Blighe, Rana, and Lewis 2019). For gene set enrichment analysis and pathway analysis, we used the DAVID platform ("DAVID Functional Annotation Bioinformatics Microarray Analysis" n.d.) and the GeneSCF in bash script (Subhash and Kanduri 2016). For DAVID we used all the genes that were identified in our sequencing as a background input. To plot the gene sets a combination of ggplot2 (Wickham 2011) and GoPlot (Walter, Sánchez-Cabo, and Ricote 2015) packages were used. The codes can be found in the appendix B.

2.2.11 Quantification of Immunohistochemical and In situ Hybridization analysis:

Regeneration analysis: To recognize the site of injury we used a few criteria. First, at the time of performing the injury, we used charcoal to mark the site of the injury. Second, after the fixation and sucrose saturation, we shorten the size of the proximal site to be able to find the injury site easier after sectioning. Third, after staining, and for analysis, we made bins of 50 μm width and measured the intensity along our nerves. The highest mean intensity for SCG10 was chosen as the area we begin our regeneration analysis (site of injury). Distance from the crush site until the point where SCG10 intensity dropped to 50%, is used as a regeneration index (Shin et al. 2012). For ChAT analysis, we use the site of injury based on SCG10 levels and calculate the length until the last ChAT positive axon tip is seen.

Reinnervation analysis: For innervation analysis, we looked at days 21 and 50 post SNC. We made a scoring system for reinnervation, 0 = not innervated at all or completely denervated

(this is chosen by looking at the amount of Tuj1 in the Bungarotoxin positive post synaptic pretzels, in this case, there is no nerve to be seen). 1 = Nerve has reached the BTX positive structure but hasn't entered. 2 = less than 50% of the BTX structure is filled with the Tuj1 positive axons. 3 = more than 50% of the BTX structure is filled with the Tuj1 positive axons. 4 = The nerve is filling up the BTX structure but there are still loose axons that are not fit in the structure. 5 = Fully Innervated.

P-cJun quantification: DAPI was used to circle around nuclei of motor neurons in the L3-L6 level at the injured (IL) and uninjured (CL) side of the spinal cord. Mean pixel intensity for p-cjun was measured at Day1 post SNC. At day 3 post SNC, the number of p-cJun positive nuclei in the injured side of the spinal cord was counted for both control and *Dlk* KO. This number was divided by the total number of MNs (marked by ChAT) to measure the percentage.

2.3 Results

2.3.1 Establishing the RiboTag assay to profile DLK-regulated responses in injured MNs from the mouse spinal cord

Validating *Dlk* KO in motor neurons

RiboTag technology makes use of tagging exon 4 of a ribosomal protein (Rpl22) to HA using Cre-recombinase expression (Figure 2-1A). To express HA-tagged Rpl22 in motor neurons in the spinal cord, we used Choline acetyltransferase (ChAT) to drive the expression of Cre recombinase. Using this method, HA-tagged Rpl22 will be expressed in somatic motor neurons and a group of lateral autonomic motor neurons, and some neurons around the central canal (Figure 2-1A). To address the question of what is downstream of DLK, we used a conditional *Dlk* KO line (Miller et al. 2009) in which exon 9-11 (Kinase domain) of DLK is floxed and wherever Cre is expressed can lead to excision of this segment (Figure 2-1A).

Before performing the actual RiboTag experiment, we first wanted to confirm that the *Dlk* KO mice are healthy and that DLK transcript and protein are indeed knocked out in MNs in these mice. Measurements of weight over developmental time showed that Dlk-fx/fx; ChAT-Cre (Dlk KO) mice are slightly reduced in weight starting at postnatal day 15 (P15) (Figure 2-2A and B). However, these animals still grow normally to viable adults and appear similarly healthy and as alert as the WT mice. Consistent with a prior study (Ghosh et al. 2011; Itoh et al. 2011), we noticed that *Dlk* KO animals have a larger number MNs (Figure 2-2C and D). Since previous studies have demonstrated a requirement for DLK in the death of embryonic DRG neurons following NGF withdrawal (Ghosh et al. 2011; Huntwork-Rodriguez et al. 2013; Larhammar, Huntwork-Rodriguez, Jiang, et al. 2017), we hypothesize that the extra MNs failed to undergo developmental neuronal death. To check for protein levels of DLK, we performed western blot on the lumbar segment of the spinal cord but given that DLK is expressed in all cell types, it was difficult to see a reduced expression of it in MNs. However, we were able to confirm that the Dlk-fx/fx mice enable DLK knockout with a ubiquitous UBC-CreER driver (Figure 2-3A-B). Since constitutive *Dlk* KO mice die within a month of birth (Itoh et al. 2011; Ghosh et al. 2011), the tamoxifen-inducible method is needed to delete DLK post-developmentally in adult mice. The successful depletion of DLK protein from both the lumbar spinal cord and sciatic nerves (Figure 2-3A-B) confirms our ability to delete DLK.

We then wanted to confirm that DLK signaling is indeed robustly activated in MNs following sciatic nerve crush. Previous studies have described DLK-dependent induction of phosphorylated cJun (p-cJun) in injured DRG neurons and retinal ganglion cell neurons following sciatic nerve and optic nerve crush, respectively (Herdegen et al. 1998; Kenney and Kocsis 1998; T. a. Watkins et al. 2013). We, therefore, examined the entire population of MNs in lumbar

segments L3 to L6 for p-Jun staining 1 and 3 days following unilateral sciatic nerve crush (Figure 2-1A and C). At one day post injury, there is no detectable p-cJun staining (above background) in the uninjured spinal cord and there is a 3-fold increase in p-cJun intensity in the ipsilateral side (axotomized MNs) but not the contralateral side of the spinal cord in wild type animals (Figure 2-1B). There is no induction of p-cjun at day 1 in the *Dlk* KO animals and all the nuclei quantified had similar p-cjun levels to the contralateral uninjured side. At day 3 post SNC, p-cJun is dramatically induced in many 44% MNs in the ipsilateral side of the spinal cord. In contrast, the p-cJun induction was strongly diminished in DLK KO mice with only 14% of MNs in the ipsilateral side of the spinal cord 3 days post SNC (Figure 2-4A and C). These data confirm that DLK signaling, assessed by p-cJun induction, is indeed activated in MNs following sciatic nerve crush.

Validating the specificity of RiboTag affinity isolation of mRNAs from MNs

We then confirmed the ability and specificity of the RiboTag purification method to enrich for MN transcripts. Quantitative RT-PCR with immunoprecipitated (IP) samples compared to total spinal cord extract showed enrichment of motor neuron marker *Chat* and *Dlk* (neuronal transcript) in the RiboTag IP, while other markers such as Calbindin (a marker for interneurons) and CNpase (a marker for oligodendrocyte) were heavily depleted in the IP samples (Figure 2-5A). The reduction of *Dlk* transcript levels in *Dlk* Fx/fx; ChATCre+/- samples serves as an independent confirmation of Dlk KO in MNs (Figure 2-5B).

2.3.2 RiboTag profiling of injured MNs at Day 3 post SNC

RNAs were isolated from control and KO animals 3 days post SNC (Figure 2-1B). To make sure the transcripts in the uninjured side of the spinal cord are not affected by the injury on the

ipsilateral side, we also collected RNAs from intact (naive) control and *Dlk* KO animals (Figure 2-1B).

Reads were mapped to the genome using STAR, and the Deseq2 package was used for differential expression analysis. We then performed analysis using QoRTs to perform QC analysis (Figure2-6A and B). This showed that all of our samples are of good quality and are behaving normally. Since the QoRTs analysis normally gives tables containing read counts ready to be used with the Deseq2 package, we used these read count tables for our differential expression analysis.

Principal Component Analysis (PCA) (Figure 2-7A) established the grouping of conditions and revealed the strongest differences between injured samples (isolated from the SC hemisegements ipsilateral (IL) to the injury) and uninjured samples. Samples isolated from the contralateral (CL) side should not contain injured MNs, hence it was reassuring to see that these samples closely grouped with samples from naive animals. We also noticed significant differences between *Dlk* KO samples from WT samples, both amongst uninjured samples and injured samples. However, the differences were greater between *Dlk* KO and WT injured samples (Figure 2-7).

Consistent with the PCA analysis, an initial heatmap of the top 60 most variable genes (Figure 2-7B) with hierarchical clustering, showed strong clustering of the samples from uninjured (Naïve and CL) both WT and *Dlk* KO mice, in addition to clustering of the injured samples (Figure 2-7B). Since the differences between naïve and uninjured samples were minor, we decided to use uninjured control (CL) samples from control (WT) animals as our baseline for future analysis. A volcano plot of the 2085 genes that are differentially expressed post injury (p adjusted value < 0.05) in WT animals confirms that the injury induces a large increase in expression of many genes, consistent with an induction of large-scale transcriptional responses to axonal injury (Figure 2-7C).

Prior studies of responses to PNI in DRG neurons have noted a large induction of Regeneration Associated Genes (RAGs), several of which have been shown to be required for regenerative axonal growth (Martin et al. 2019; Shin et al. 2019; Guan et al. 2016). Many of the known RAGs in DRGs are also strongly induced in MNs (Figure 2-8) Intriguingly, many known RAGs that have been functionally associated with axonal regeneration are still strongly induced in *Dlk* KO MNs. These include Atf3, Serpinb1a, etc., and cytokines such as Ccl2 and Ccl7. Out of the 30 most strongly changing genes following injury, we noted DLK-dependence for only a small subset (Figure 2-8A). It is striking that this subset contains several secreted peptides: Npy (neuropeptide Y), Gal (Galanin), and Fgf (Figure 2-8A).

Out of the 2085 genes that are differentially expressed in MNs post injury, only 310 of these genes are partially or completely dependent on DLK (Log2 fold change of 1.5 and adjusted p-value of less than 0.05) (Figure 2-8B). To better see the genes and differences between each condition we plotted multiple volcano plots for each type of comparison (Figure 2-9). It is observed that *Dlk* KO injured, and control injured have multiple enriched and depleted genes (Figure 2-7C). While some of these genes are different at the baseline level (Figure 2-9B), most are affected by axotomy in a DLK-dependent manner (Figure 2-9A). There are only a couple of genes that are transcriptionally affected in the uninjured side of the spinal cord compared to the intact animals (Figure 2-9C and D).

2.3.3 DLK is not essential for axonal regeneration in MNs

Given that most of the RAGs are still upregulated in *Dlk* KO animals, we wondered whether DLK is required for regeneration in our mouse model of SNC. We looked at regeneration at different time points post SNC (Day 1, 3, 21, and 50). One day after SNC, there is no difference in the amount of regeneration between WT and *Dlk* KO conditions (Figure 2-10A and B). At day

3 post SNC, there is a considerable amount of regeneration occurring in both motor (labeled by SCG10 and ChAT) and sensory (just SCG10 and no ChAT) axons. The new growth in *Dlk* KO injured axons is reduced while the sensory neurons in this background are capable of growing as long as wild-type axons (Figure 2-10C and D). This result shows a role for DLK in initiating a quick growth, but it doesn't address the question of whether it is required for functional regeneration. To address this, we looked at Day 21, where most axons should have fully come back to the muscles, and Day 50 where functional regeneration must be complete. Not to our surprise, we observed that both WT and *Dlk* KO muscles are fully innervated at these time points (Figure 2-10E and F).

2.3.4 DLK regulates RiboTag associated with mRNAs encoding multiple secreted proteins

To better understand what is being regulated by DLK signaling pathway, we performed Gene set enrichment analysis on our DLK-dependent DEGs, using a combination of the DAVID platform and GeneSCF package. Figure 2-8C showed multiple GO terms enriched that are associated with neuropeptides, and immune and inflammatory responses. Most of the cellular component terms were also related to the membrane and extracellular matrix (Figure 2-8C). Looking at the genes in each of these sets can help us frame some new ideas. In the immune terms, we saw members of the complement cascade C1q and MASP1 being upregulated post injury in a DLK-dependent manner. In the neuropeptides signaling/activity term, we have *Gal*, *Npy*, *Ngf*, *CRH*, *Adcyap1*, and other genes. The expression of these genes in the *Dlk* KO animals has reduced by 6, 10.5, 10, 2, and 5-fold respectively. We have also noticed that certain cytokines such as Cxcl13 that are not normally expressed in neurons show a 160-fold enrichment in the control 3 days post axotomy and only 13-fold increase in the axotomized motor neurons from the *Dlk* KO animals. Prior functional studies of DLK and its homologs in flies, *C.elegans*, and mammalian

neurons led us to expect we would find cytoskeletal, mitochondrial, and synaptic proteins regulated by DLK (J. Li et al. 2017; Goel and Dickman 2018; Han, Baig, and Hammarlund 2016; Byrne et al. 2016; C.-H. Chen et al. 2014; Collins et al. 2006; Nakata et al. 2005). However, these functions were not strongly represented in the RiboTag dataset of transcripts regulated by DLK in injured MNs. The strong enrichment of extracellular and secreted proteins suggests that DLK signaling has the capacity to organize responses made by other cells to respond to nerve damage.

2.3.5 The regulation of Galanin expression by DLK

To validate that the RiboTag approach indeed revealed DLK-dependent genes in MNs, we performed *in situ* hybridization for one of the strongly regulated secreted proteins, Galanin (Gal). In the uninjured condition, the level of *Gal* RNA is low throughout the spinal cord ventral horn In WT animals 3 days post injury, *Gal* is strongly induced in a subset of the injured MNs, identified by ATF3 expression (Figure 2-11A and B). Interestingly, the expression level of Gal shows a broad range amongst individual MNs, suggesting potential cell-type-specific variability. In contrast, *Dlk* KO animals do not show any elevation in their *Gal* expression (Figure 2-11A and B). We conclude that Gal expression is indeed strongly induced by DLK in injured neurons and that the RiboTag approach is successful at identifying DLK-regulated genes in MNs.

2.4 Discussion:

2.4.1 Axonal regeneration is not the primary function of DLK in mouse MNs

The axonal damage activated kinase DLK is best studied for its role in axonal regeneration. Its homolog DLK-1 was originally discovered in *C. elegans* screens for its essential role in enabling damaged axons to regenerate. It was therefore initially surprising that RAGs are still robustly induced in *Dlk* KO motoneurons. A previous study suggested that motoneuron

regeneration is impaired focused on 14 days post-injury (Shin et al. 2012). We note that while *Dlk* KO MNs are delayed in regeneration, full recovery of NMJ endplates and motility was observed 28 days post injury. While *Dlk*'s homolog Dlk-1 is essential for regeneration in *C. elegans* (Hammarlund et al. 2009), our observation in mammalian motoneurons is compatible with recent studies in zebrafish, which noted robust axonal regeneration in *Dlk* mutants. The zebrafish study noted a redundant requirement for the related kinase LZK for axonal regeneration, together with a role for both kinases in restraining the plasticity of spared branches (Adula et al. 2021). We conclude that axonal regeneration is not an essential function of DLK in the mammalian nervous system. In our RNA sequencing, we indeed found a set of genes that were strongly DLK dependent.

2.4.2 DLK regulates the expression of secreted and immune proteins from injured MNs

While most RAGs are DLK-independent in MNs, our data identified a unique subset of injury-induced genes that require DLK. Intriguingly, this gene set includes several neuropeptides: ADCYAP1 which encodes for Pituitary adenylate cyclase activating polypeptide (PACAP), Galanin (Gal), Neuropeptide Y (NPY). All of these neuropeptides are strongly induced in injured MNs and are strongly gated by DLK. We confirmed DLK regulation of Gal expression using RNAscope. Interestingly, *Gal* KO animals have a 35% reduction in the rate of peripheral nerve regeneration following SNC and a 40% reduction in neuritogenesis from cultured adult DRG neurons (Holmes et al. 2000), which can be rescued by the addition of galanin peptide (Mahoney et al. 2003). Besides its role in regeneration, Gal has been shown to alleviate limbic seizures (McCown 2009). It has been shown to play a role in pain processing (Wiesenfeld-Hallin, Bartfai, and Hökfelt 1992) and is responsible for a change in the gene expression in macrophages such as

anti-inflammatory cytokines in type1 macrophages (Koller et al. 2019). All of these roles for Gal make it an interesting signaling molecule that can regulate the responses from other cell types.

The DLK-dependent gene set also includes multiple immune response genes. One pathway that is strikingly represented is the complement pathway, a critical arm of innate immunity. The RiboTag data suggests that DLK triggers the induction of expression of all 3 subunits of C1q. In addition, DLK triggers the expression of Mannan-binding lectin serine protease 1, MASP-1, a parallel upstream activator of complement. Therefore, both the classical and lectin pathway arms of complement activation may be boosted by DLK signaling.

The finding that secreted and immune molecules are amongst the most strongly DLK-dependent transcripts has modified our original view of DLK's functions in injured neurons. Thus far most prior studies have focused on cell-intrinsic changes regulated by DLK. These include changes in the organization of the cytoskeleton (C.-H. Chen et al. 2014), changes in mitochondria transport and dynamics (Han, Baig, and Hammarlund 2016), and changes in the levels of synaptic proteins (J. Li et al. 2017; Goel and Dickman 2018; Collins et al. 2006; Nakata et al. 2005). We were originally surprised to find that these pathways are not strongly represented in injured MNs. It remains possible that they are redundantly regulated by the sister kinase LZK. Alternatively (or in addition) these processes may be less prominent in the post-developmental context of our experiment in adult mice.

Regardless of the reason for the lack of emphasis on intracellular pathways, the identification of secreted proteins regulated by DLK stimulates new thinking about the roles and contributions made by other cell types to respond to nerve injury. In this case, DLK may influence responses to nerve injury through non-cell-autonomous mechanisms, by triggering or gating responses made by other cells to the injury. It is indeed well established that many cell types

participate in the responses to peripheral nerve injury. These include local responses from Schwann cells and macrophages at the site and distal to the site of injury and microglial and astrocyte responses at the spinal cord level. Post injury, Schwann cells go through reprogramming to turn into repair Schwann cells for debris/myelin clearance, macrophages invade the distal site of injury and provide the factors required for the change in the Schwann cell phenotype (Martini et al. 2008; Jessen and Mirsky 2019). Far from the site of injury, in the lumbar spinal cord, microglia and astrocytes become activated surrounding the cell bodies of the axotomized neurons (Qian et al. 2018; Aldskogius 2011). Since DLK is known to regulate retrograde responses to the cell body, chapter 3 takes a deeper investigation into the inflammatory responses made by cells that surround the injured MNs in the spinal cord.

2.4.3 Revisiting the dichotomy of DLK-regulated responses

The consideration of contributions by the non-injured cells brings a reconsideration of potential mechanisms that underlie the dichotomy of DLK's known functions. The nature and state of other cells may contribute to the ultimate outcome. For example, triggering innate immunity or neuropeptide signaling may yield very different consequences depending upon whether the neuron is in the CNS or PNS, and the identity and state of its neighboring cells, as well as the partner cells in its circuit(s).

In addition, the finding that DLK regulates neuropeptides suggests a new potential mechanism for its dichotomous roles. It is noteworthy that neuropeptides including Galanin, and Neuropeptide Y are known for neuroprotective roles in models of ischemia, neurodegenerative diseases, as well as nerve injuries (I. Kim et al. 2021; Borbély, Scheich, and Helyes 2013; Somogyvári-Vigh and Reglodi 2004). We speculate that neuropeptide induction enables the engagement of pro-survival pathways to counteract cell death pathways, which previous studies

suggest are also induced by DLK. It is interesting to contrast the response of retinal ganglion cells to nerve injury, which die in a DLK-dependent manner, to injured MNs, which do not necessarily die, however, do undergo death in injuries that prohibit repair (Y. Liu and Wang 2020; Hoang et al. 2003; A. Valero-Cabré and Navarro 2001; Ma et al. 2001). We propose that neuropeptide expression enables a counteracting mechanism to cell death. As a stress response, DLK may trigger dueling pathways, enabling time and context to determine which outcome wins.

The possibility that DLK regulates neuropeptides and pro-survival pathways also offer a new view into recent considerations of DLK as a therapeutic target to delay neuronal loss in neurodegenerative diseases. Its role in neural death in models of trophic factor withdrawal and loss of MNs in a mouse model of ALS made DLK an attractive candidate target. Unfortunately, phase 1 clinical trials of DLK inhibitors in humans led to deleterious side effects and early cessation of the study (Katz et al. 2022). Our deeper view of the pathways regulated by DLK may shed light on new ways to target deleterious arms of DLK signaling while preserving or re-supplying protective arms.

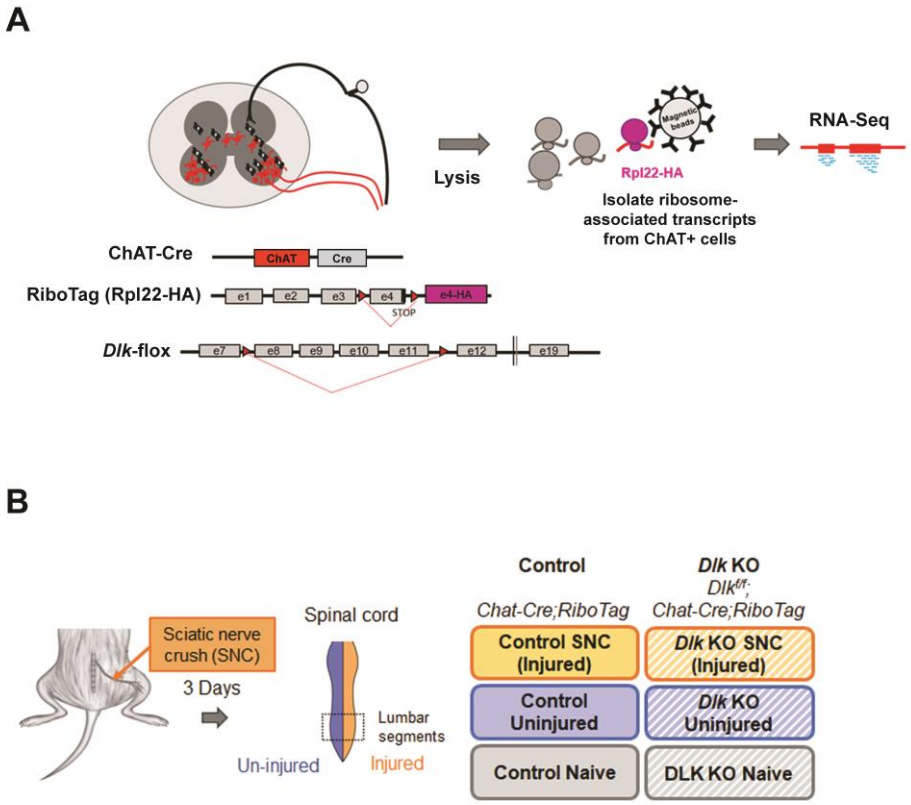

Figure 2-1 ***Schematic of RiboTag approach and experimental conditions.*** *A) Schematic of our RiboTag approach and Dlk KO in motoneurons. Use of ChAT-Cre recombinase limits the tagging of Rpl22 and excision of e8-11 of Dlk to cholinergic neurons. After the lysis and HA precipitations, transcripts associated with the MN ribosomes are isolated and sequenced. B) 3 days post unilateral sciatic nerve crush, we divided the lumbar L3-L6 injured and uninjured side of the spinal cord from both control and Dlk KO animals. We also collected lumbar spinal cords (L3-L6) from naive animals in both genotypes.*

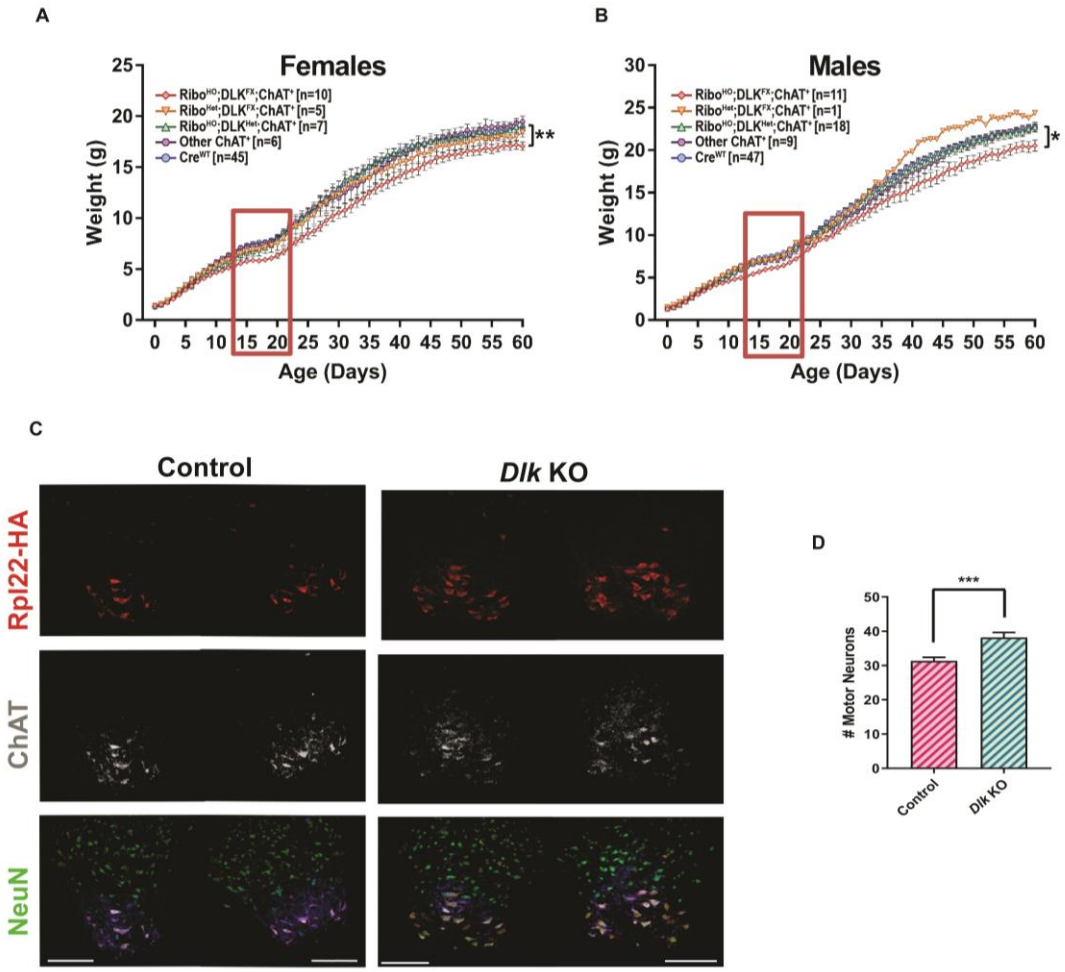

Figure 2-2 ***Dlk KO animals have excess motor neurons but are otherwise healthy.*** *A-B) Growth curves of females and males in different genotypes. Only Dlk KO (DLKFX; Chat+) animals show reduced weight which starts at P15. These mice are otherwise alert. C) Immunohistochemistry of transverse 20 µm section of the lumbar spinal cord with Choline acetyltransferase (ChAT) to mark motor neurons, NeuN (Marker for all neurons), and HA (to show the specificity of our ChAT-Cre in ventral motor neurons (MNs). D) quantification of C, there are more motor neurons per 10^6 um2 in Dlk KO animals.*

*For the Growth curves, an area under the curve was used and one Way ANOVA with Tukey test was performed. For D) a two-sided student t-test was performed. P-Values for * < 0.05, ** < 0.005, *** < 0.001. Scale bar is 200 µm.*

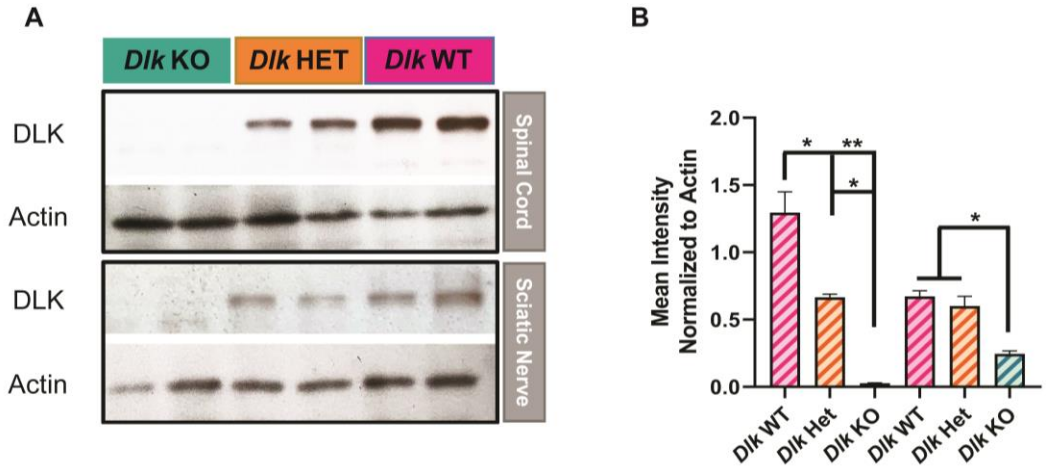

Figure 2-3 ***Validation of DLK Knockout.*** *A) Western blot of spinal cord and sciatic nerves from animals carrying either Dlk +/+ (WT), Dlk Fx/+ (HET), Dlk Fx/Fx (KO) using a UBC-CreER and tamoxifen gavage in adult to induce the excision of exon 8-11 in the Dlk gene. Actin is used as a loading control. DLK protein level is extremely down in the KO but not WT conditions. (B) Quantification of integrated density in A using ImageJ (Fiji), every lane is normalized to the loading control (actin). One way ANOVA with Tukey test is performed for spinal cords and sciatic nerves separately. P-Values for * < 0.05, ** < 0.005.*

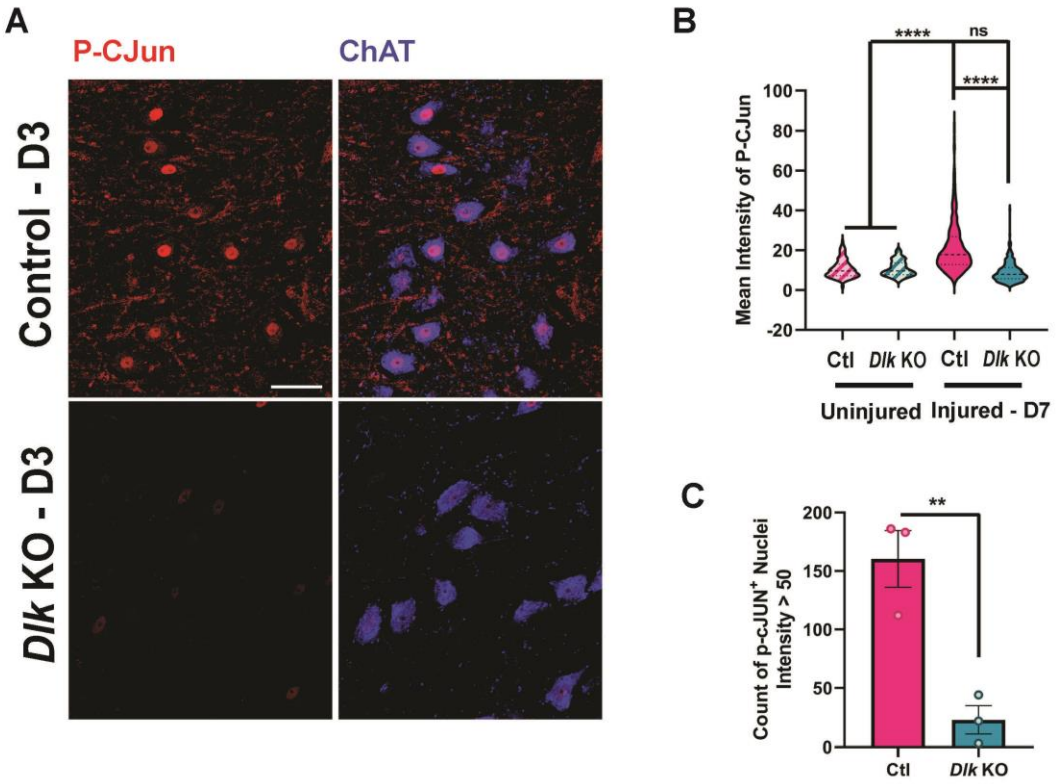

Figure 2-4 ***Phosphorylation of c-jun is diminished in Dlk KO.*** *A) Immunohistochemistry of ChAT (for MNs) and p-cJun (marker of DLK signaling activation) 3 days post SNC. Control neurons are highly elevated for their p-cjun expression while the Dlk KO counterparts are not. B) Quantification of mean intensity of p-cjun one day after SNC. There is a 2-fold increase in the mean intensity of p-cjun in control compared to the uninjured. Dlk KO takes away this induction. C) Quantification from A, number of p-cjun positive cells with high intensity is dramatically reduced in Dlk KO animals, 3 days post SNC. For (B) One way ANOVA with Tukey test was performed. P-value for **** < 0.0001. For C, unpaired two-tailed t-test is performed. P-value for ** is 0.0069.*

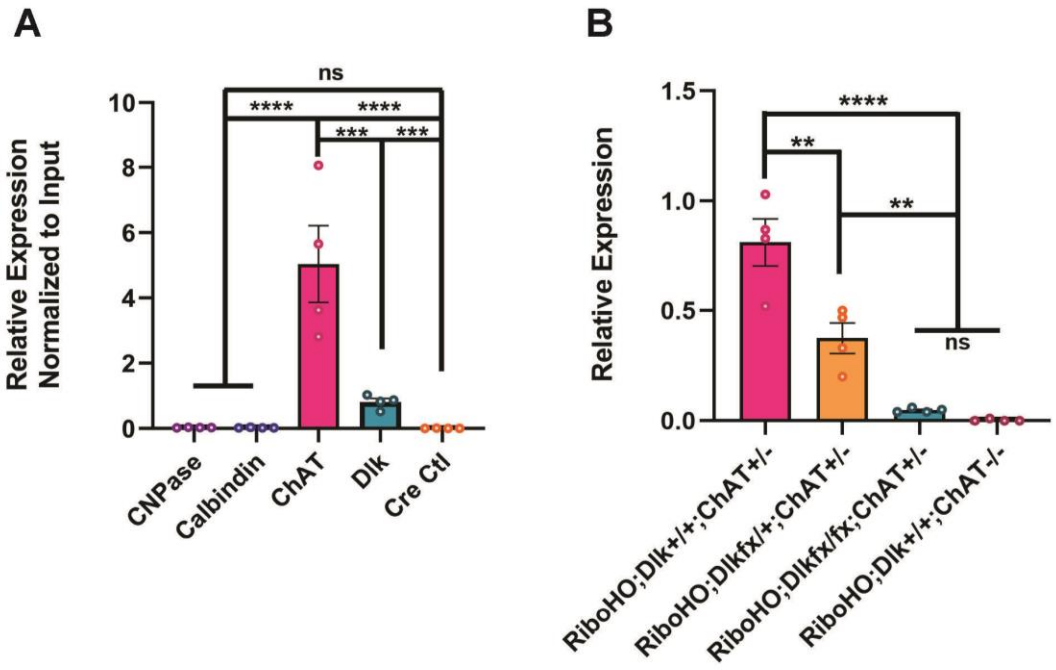

Figure 2-5 ***RiboTag purification enriches transcripts from MNs.*** *(A) Relative expression of different transcripts normalized to our input RNA. RiboTag enriches for MN transcripts ChAT and neuronal transcript Dlk, it does not enrich transcripts from other cell types such as CNPase (Oligodendrocytes) and Calbindin (Interneurons).(B) Relative expression of Dlk transcript in Dlk WT (Dlk+/+), Het (Dlkfx/+), and KO (Dlkfx/fx) along with Cre negative control shows reduction of the transcripts in both Het and Dlk KO. One way ANOVA with the Tukey test was performed. P-value for ** < 0.005, *** < 0.0005, **** < 0.0001.*

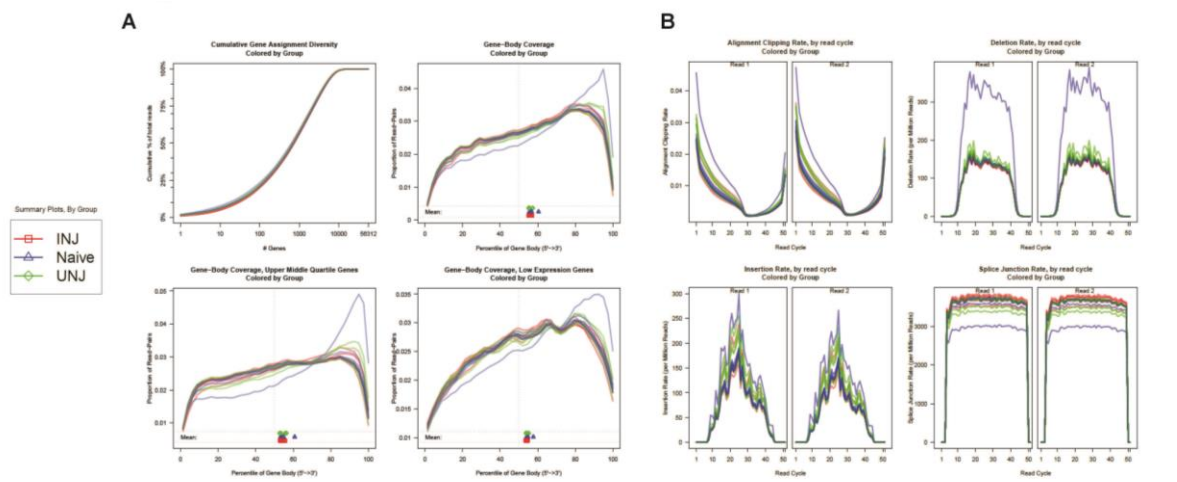

Figure 2-6 ***QoRTs analysis for quality control after reads are mapped to the genome.*** *(A) and (B) plots show that everything follows the regular pattern it should; however, there is one sample from the naive (see material and methods) that is behaving differently. In our gene body coverage plots, everything looks normal as we performed PolyA selection for our mRNA there is a bias towards 3' end, however the one sample mentioned is still acting different from the other samples which may mean, having degraded RNA to begin with.*

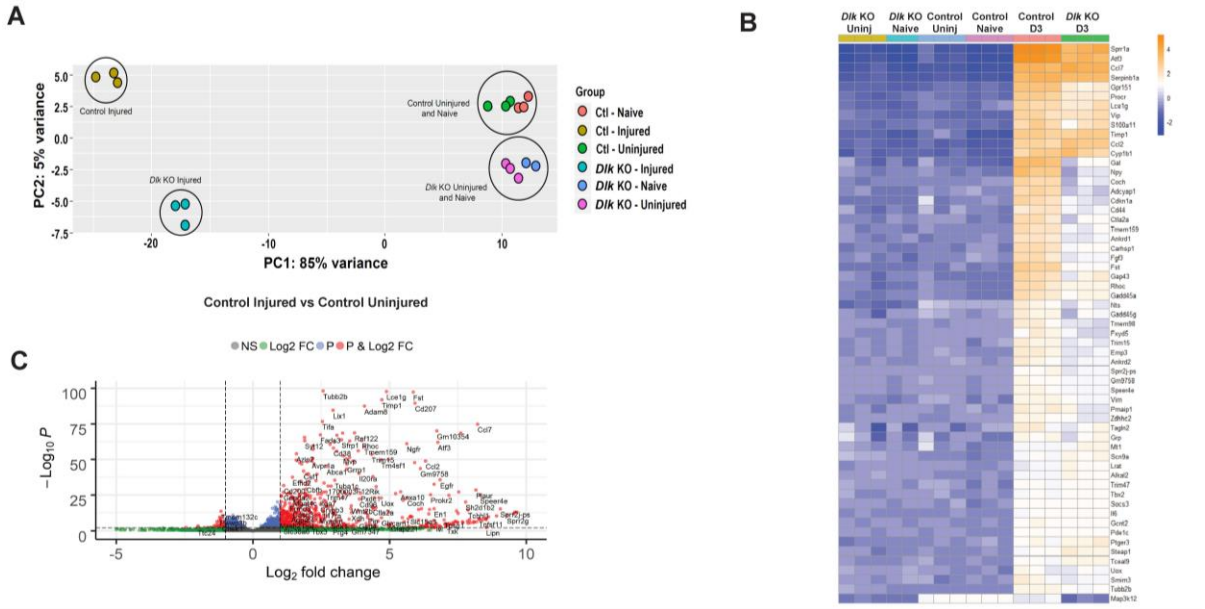

Figure 2-7 ***Analysis of transcripts affected by injury and DLK activation.*** *(A) Principal Component Analysis (PCA) plot shows grouping among replicates of each condition and the most variability is seen between injured and uninjured and then control injured and Dlk KO injured. (B) Volcano plot showing that injury causes changes in 2085 genes, mostly upregulated (Log2 Fold change of 1 and P-adjusted value of <0.05). (C) Heatmap of first 60 genes that are most variable among conditions shows upregulation of many regenerative associative genes (RAGs) in both control and the Dlk KO. Many neuropeptides are heavily diminished in the Dlk KO.*

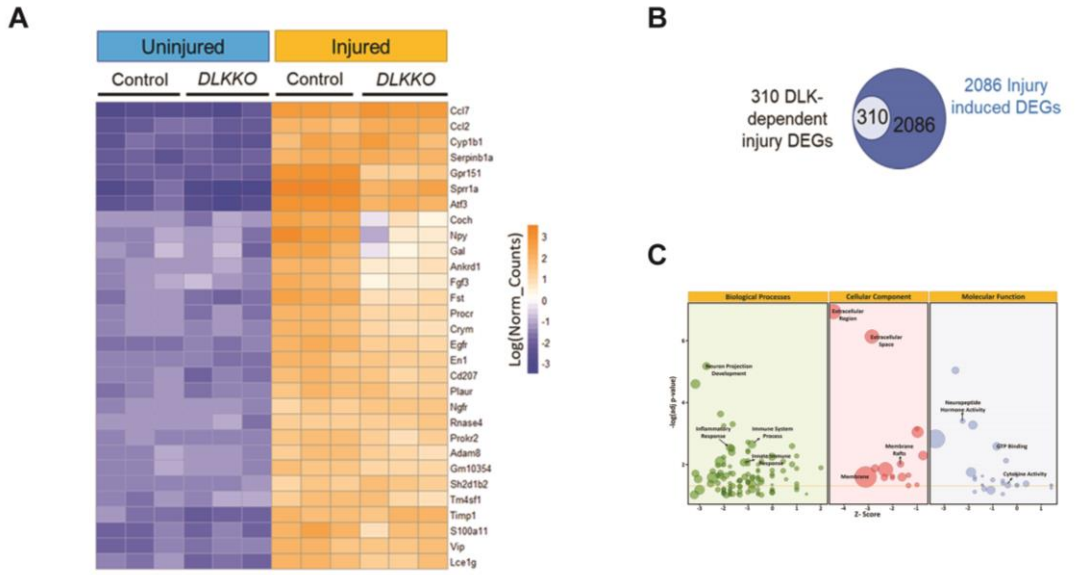

Figure 2-8 ***Comparison between Control and Dlk KO 3 Days post SNC.*** *(A) Heatmap of the first 30 most variable genes post SNC is shown. Most of the RAGs are still upregulated in the Dlk KO although upregulation of some is diminished strongly like Coch, Npy and Gal. (B) Venn Diagram of differentially expressed genes (DEGs). From 2086 DEGs, a distinct subset (310) of the SNC-induced DEGs showed strong dependence on DLK (based on 1.5-fold change, adjusted p-value of less than 0.05). (C) Bubble plot of GO analysis in 3 categories of Biological Processes (BP), Cellular Component (CC) and Molecular Function (MF). Z-score is just a value to suggest whether the genes in each significant Go Terms are likely to deplete (negative value) or increase (positive value). It is defined by a simple calculation of the number of upregulated genes in each Go term is subtracted by the downregulated genes and divided by square root of counts of genes in that Go term. (For more info check Goplot documentation).*

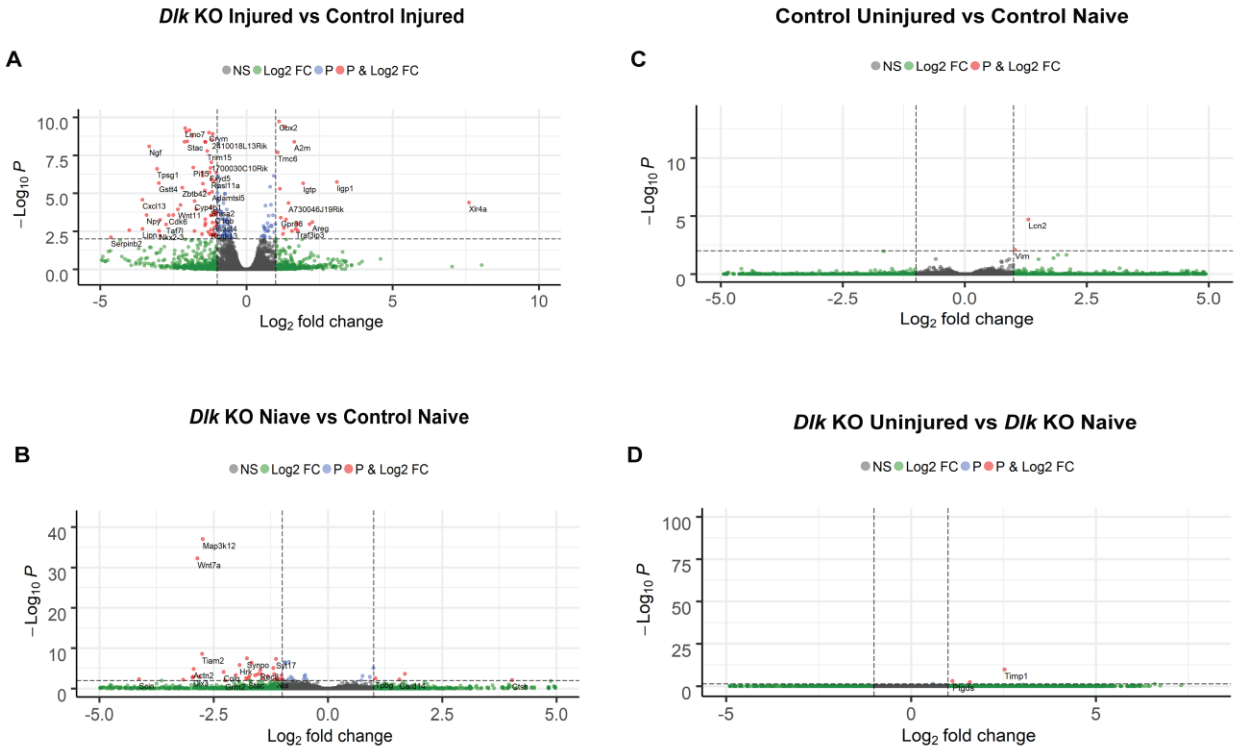

Figure 2-9 ***Multiple Volcano plots to visualize the differences between multiple conditions.*** *(A) Volcano plot comparing differentially expressed genes between control and Dlk KO injured shows that from 310 DEGs, most are attenuated or not upregulated in the KO conditions, and these are mostly neuropeptides, immune genes and cytokines. (B) There are not many genes that are different at baseline level between control and Dlk KO condition. (C-D) In both control and Dlk KO conditions, there are few genes that are affected in the uninjured side of the spinal cord compared to intact naive mice.*

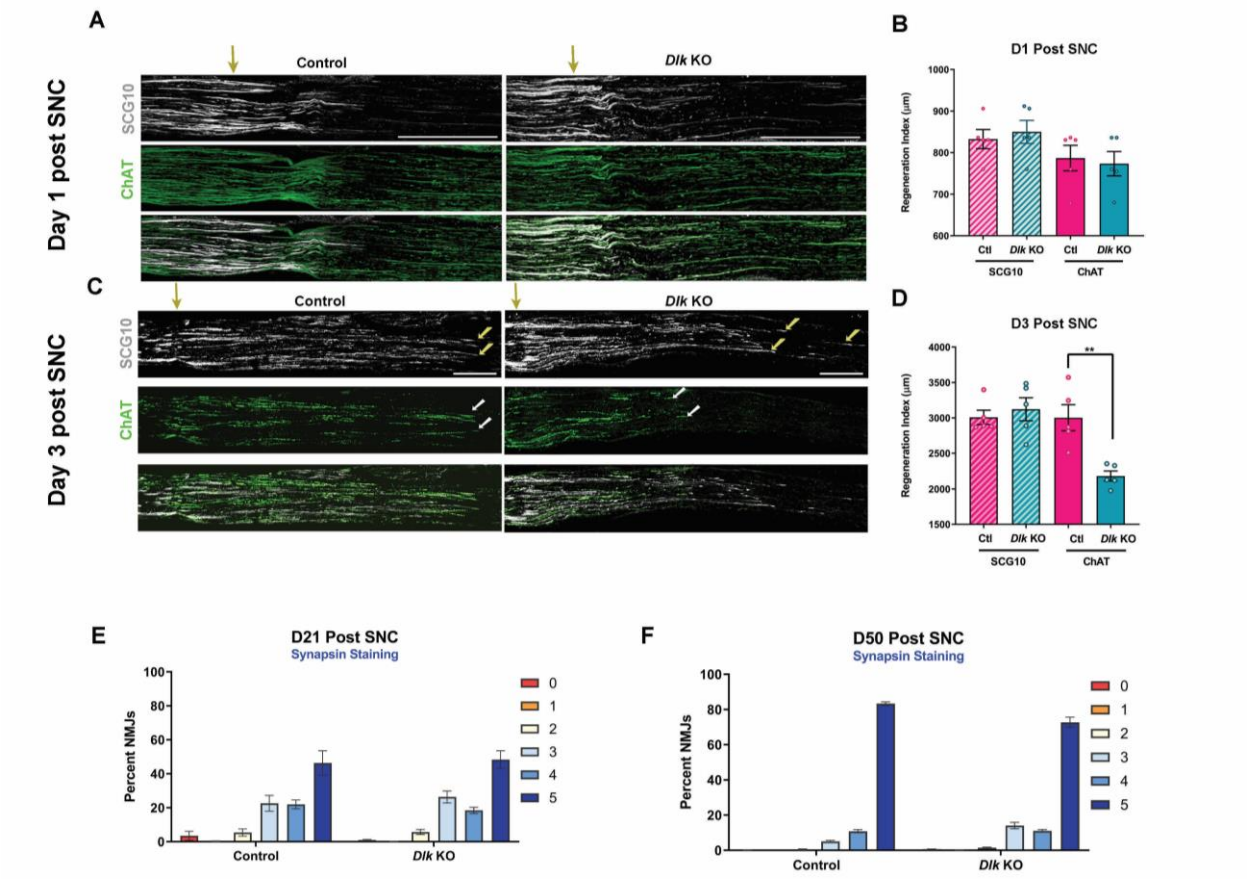

Figure 2-10 ***Functional regeneration still occurs in Dlk KO animals despite initial delay.*** *(A) and (C) Immunostaining of Sciatic nerves (15 µm section thickness) for SCG10 (new axonal growth), ChAT (motor axons) at day 1 (A) and day 3 (C) post SNC. On day 1, no difference is detected between control and Dlk KO regeneration levels but on day 3, regeneration is clearly delayed in Dlk KO animals. (B) and (D) Quantification of regeneration at day 1 and 3 post SNC. 50 µm bins were placed from the site of injury and mean intensity of SCG10 was calculated when the intensity drops to half that's the length, we consider for the regeneration index. For ChAT, we calculate the length from the site of injury until the last ChAT+ tip of axons. (E) and (F) Quantification of percent NMJs that are fully (5) innervated (5) or not innervated (0) at all at day 21 (E) and 50 (F) post SNC. As seen in the figure, Dlk KO animals, although delayed, can fully regenerate their NMJs after SNC. One Way ANOVA is performed and P-value for ** < 0.005.*

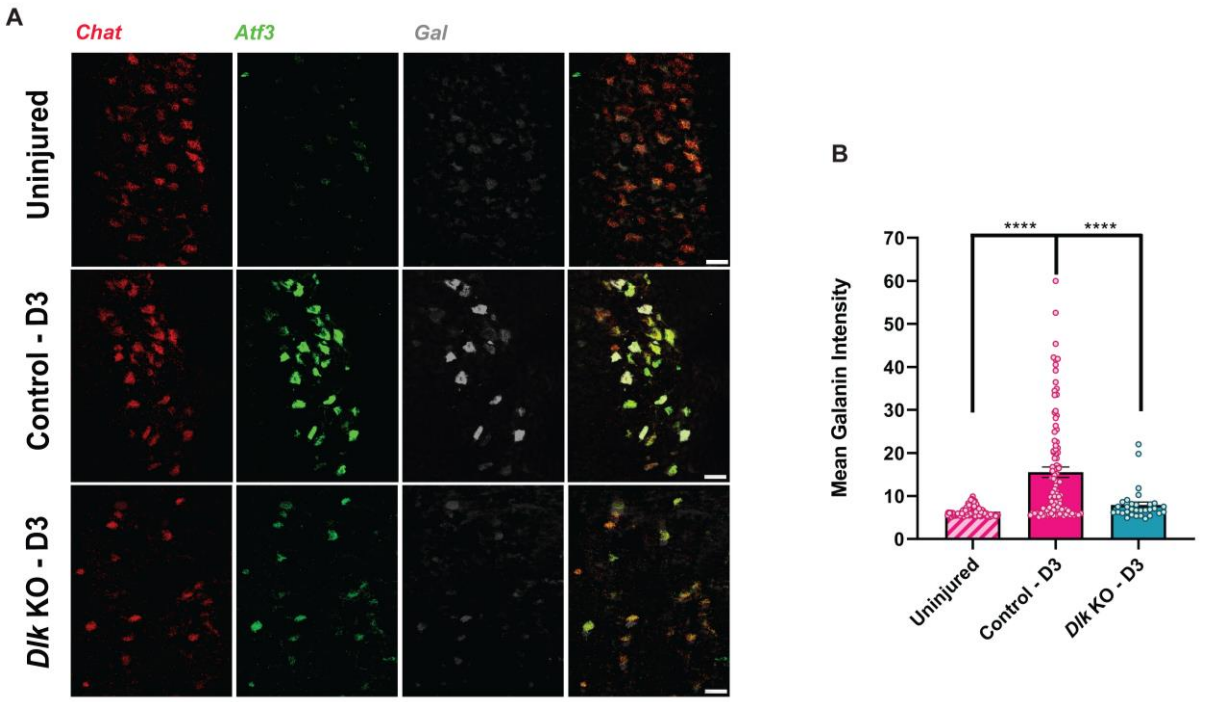

Figure 2-11 ***Galanin (Gal) expression is regulated by DLK.*** *(A) In situ Hybridization at ventral horn of the spinal cord, 3 days post sciatic nerve crush (SNC). Chat is used to mark MNs, Atf3 probes are used to mark injured neurons. Gal expression is heavily upregulated in axotomized neurons marked by Atf3 in control but not Dlk KO MNs. Scale bar is 50 μm. (B) Quantification from (A) mean intensity of Galanin expression in each Atf3+/Chat+ cell for the injured (IL) side of the spinal cord and Chat+ for the uninjured (CL) side is measured. One Way ANOVA is performed with the Tukey test, and P-value for **** < 0.0001.*

Chapter 3 DLK Signaling Triggers Complement Directed Loss of Upstream Synapses from Axotomized Motoneurons

The loss of synaptic inputs from axotomized motoneurons (MNs) following peripheral nerve injury (PNI) is associated with an inflammatory response by spinal cord microglia. However, the functional contributions of microglia to this form of synapse loss have been questioned, since its mechanism is poorly understood. Here we identify the neuronal kinase DLK/MAP3K12 as an orchestrator of both inflammation and synapse loss from axotomized MNs. Using conditional *Dlk* knockout mice we found that DLK is required within axotomized MNs for the loss of multiple presynaptic markers for different synapse types and for the induction of phagocytic microglia surrounding MN cell bodies, indicating a non-cell-autonomous role for DLK in the spinal cord following PNI. Depletion of microglia via the Csf1r inhibitor PLX5622 in conjunction with *Dlk* KO led to complete inhibition of synaptic loss. Using RiboTag profiling to identify DLK-gated genes in axotomized MNs identified the classical and lectin pathways of complement as downstream targets of DLK in MNs. RiboTag profiling to identify DLK-regulated genes in axotomized MNs led to the identification of C1q and MASP1, upstream regulators of complement, as candidate effectors of DLK. We found that DLK triggers C1q expression first from the axotomized MN, and then later in surrounding microglia which become enriched in CDd68-positive structures that colocalize with presynaptic bassoon. C3 KO mice phenocopy *Dlk* KO mice. This microglial response and synapse loss are blocked in C3 knockout mice. Together the observations suggest that DLK activation in injured MNs directs the activation of complement and

which then directs synaptic clearance by microglia. This work implicates the DLK kinase as a new neuronal regulator of complement, inflammation, and synapse loss.

3.1 Introduction:

Synapse loss in both development and disease has been associated with the induction of complement, a major arm of innate immunity (Gomez-Arboledas, Acharya, and Tenner 2021; Druart and Le Magueresse 2019; Presumey, Bialas, and Carroll 2017; Stephan, Barres, and Stevens 2012). Opsonized complement has been observed to accumulate near the locations of synapses which are then cleared by microglial phagocytosis (Stevens et al. 2007; Werneburg et al. 2020). While the complement system has become a target of great interest for managing neuroinflammation and synapse loss in the diseased brain (Schartz and Tenner 2020; Carpanini, Torvell, and Morgan 2019), the upstream triggers that lead to the induction of complement to delineate specific synapses for clearance are not well understood. During developmental pruning, complement becomes induced within an aseptic environment not exposed to damage or pathogens. It is hypothesized that neuron-intrinsic signals render synapses to be vulnerable to complement, however, the nature of the signals and the mechanisms that generate them are still poorly understood.

This study brings attention to the neuronal dileucine zipper kinase DLK (MAP3K12) as an upstream regulator of complement-mediated synapse loss. DLK is best known for its roles in responses to axonal damage, including the ability of neurons to regenerate or die (Asghari Adib, Smithson, and Collins 2018; Welsbie et al. 2017; Le Pichon et al. 2017; Watkins et al. 2013; Huntwork-Rodriguez et al. 2013; Welsbie et al. 2013). Here we studied DLK's role in the loss of synapses from the cell body of axotomized motoneurons following PNI. This form of synapse loss involves aseptic inflammation in the spinal cord distant from the injury site in the periphery and

was originally coined as ‘synaptic stripping’, based on the observation that microglia interdigitate their processes between the cell bodies and presynaptic boutons, suggesting an active role in ‘lifting’ or removing synapses from the axotomized MN (Alvarez et al. 2020). However, whether microglia play an active role in axotomy-driven synapse loss has been strongly questioned (Alvarez et al. 2020; Kettenmann, Kirchhoff, and Verkhratsky 2013), since previous manipulations aimed at reducing the population of microglia in the spinal cord have not yielded strong impairments to the global loss of presynaptic markers from injured MNs (Rotterman et al. 2019; Svensson and Aldskogius 1993; Kalla et al. 2001). It has alternatively been proposed that synaptic loss is initiated within neurons, however, the mechanisms that initiate and execute the loss are not known.

We considered the neuronal kinase DLK to be an attractive candidate regulator of synapse loss from axotomized MNs. DLK is transported in axons, becomes activated by PNI, and signals retrogradely to mediate transcriptional responses in the cell body (Shin et al. 2019, 2012; Itoh et al. 2009). DLK has also been shown to influence inflammation following PNI and in an ALS model (Wlaschin et al. 2018; Le Pichon et al. 2017). Using mice conditionally deleted for DLK in MNs, we found that DLK concomitantly orchestrates microglial inflammation and synapse loss from axotomized MNs in the lumbar spinal cord following sciatic nerve crush. Our studies of this mechanism indicate that DLK signaling within injured MNs triggers the activation of complement, which directs the clearance of many presynaptic structures by phagocytosis. These findings shed new light on the mechanisms of synapse loss from axotomized neurons and implicate DLK signaling as a new regulator of complement activation from damaged neurons. DLK is known to become activated in various paradigms of neuronal stress and injury (Asghari Adib, Smithson, and Collins 2018; Welsbie et al. 2017; Le Pichon et al. 2017; Watkins et al. 2013; Huntwork-Rodriguez

et al. 2013; Welsbie et al. 2013). Therefore, this work brings a new view of DLK as an attractive candidate regulator of complement activation and synapse loss in multiple scenarios of injury and disease.

3.2 Materials and Methods

3.2.1 Animals

All procedures involving mice were performed in accordance with guidelines developed by the National Institutes of Health and were approved by the Institutional Animal Care and Use Committee (IACUC) at the University of Michigan. Adult (12 – 15-Week-old) males and females on a C57BL/6 background were used in this study.

DLK fx/fx (Miller et al. 2009)

B6N.129-Rpl122tm1.1Psam/J (JAX stock # 011029)

ChAT-IRES-Cre: B6;129S6-ChATtm(Cre)/Lowl/J (JAX stock #006410)

Rosa-tdTomato line (JAX stock # 007914 (Ai14))

Tmem119-2A-EGFP reporter mouse line (JAX stock # 031823)

B6.129S4-C3tm1Crr/J (JAX stock #029661)

For histological analysis regarding conditional KO of DLK, RiboTag and DLK fx/fx conditional mice were crossed with ChAT-Cre mice to generate Rpl22HA/HA; DLK fx/fx; ChATCre/+ (RiboHO; DLKfloxed; ChATCre) experimental mice. Additionally, C57BL/6J mice and Rpl22HA/HA; DLKfx/fx; ChAT+/+ (RiboHO; DLKfloxed;ChATWT) were used as control. For RNA-seq analysis Rpl22HA/HA; DLK +/+; ChATCre/+ (RiboHO; DLKWT; ChATCre) were used as controls.

For stripping studies and to be able to mark the perimeter of the motor neurons, Rosa-Tdtomato/Rosa; DLK fx/fx; ChATCre/+ (Rosa-tdtomatoHO; DLKFloxed; ChATCre) were used

as DLK conditional knockout along with Rosa-Tdtomato/Rosa; DLK +/+; ChATCre/+ (Rosa-tdtomatoHO; DLKWT; ChATCre) as the controls.

For the PLX experiment, Tmem119EGFP/EGFP; DLKFX/FX; ChATCre/+ (Tmem119HO; DLKFloxed; ChATCre) were used as conditional DLK KO and Tmem119EGFP was used as an endogenous microglia reporter, Tmem119EGFP/EGFP (TmemHO) was used as a control in these experiments.

For genotyping the following primers were used:

ChAT-Cre: Forward - wildtype 5' GCA AAG AGA CCT CAT CTG TGG A 3' and Forward - Mutant 5' CAA AAG CGC TCT GAA GTT CCT 3' and reverse primer 5' CAG GGT TAG TAG GGG CTG AC 3'

UBC-CreER: Forward primer 5' GTG AAA CAG CAT TGC TGT CAC TT 3' and reverse primer 5' GCG GTC TGG CAG TAA AAA CTA TC 3' along with the internal control forward primer 5' CTA GGC CAC AGA ATT GAA AGA TCT 3' and reverse primer 5' GTA GGT GGA AAT TCT AGC ATC ATC C 3'

RiboTag-HA: Forward primer 5' GGG AGG CTT GCT GGA TAT G 3' and reverse primer 5' TTT CCA GAC ACA GGC TAA GTA CAC 3'

TdTomato Reporter: Forward primer 5' CTC TGC TGC CTC CTG GCT TCT 3' and reverse - wildtype 5' CGA GGC GGA TCA CAA GCA ATA 3' and reverse - mutant 5' TCA ATG GGC GGG GGT CGT T 3'

Dlk KO: Forward primer 5' GGA AAG GTG TGG CCC TGG CTG GCT TGG AAG 3' and reverse primer 5' CAG GTG CAG CAA GAT CTG TCG GAA TGA TGG 3'

Tmem-EGFP: Forward - wildtype 5' GTC AGG AGG AGG CCC AGG AA 3', Forward - Mutant 5' CTG CTG CCC GAC AAC CAC TA 3' and reverse primer 5' GTT TCC TGG GGT GCA CCA GA 3'

3.2.2 Surgical Procedures:

2-3% Isoflurane mixed with Oxygen was used to anesthetize the mice, Carprofen was administered subcutaneously as analgesic 15 minutes before performing the surgery and then once a day for 48 hours post-surgery. At the level of mid-thigh, a one-centimeter incision was made through the skin, and muscle and sciatic nerve were exposed. Using fine forceps (#11399-80, Fine Science Tools), the sciatic nerve was crushed. Sutures were used to close the muscles and to close the skin, clips were used. In cases of Sciatic nerve transection, instead of a crush, 3-5 mm of the sciatic nerve was cut using fine scissors.

3.2.3 Tissue dissection and post processing:

Phosphate buffer Saline was used to perfuse mice transcardially. To isolate the entire spinal cord, the hydraulic extrusion method from (Kennedy et al., 2013) was used and then the lumbar segment of the spinal cord was pinned in a sylgard dish to help keep the spinal cord straight. Sciatic nerves were collected from both injured (IL) and uninjured (CL) sides and were pinned to a sylgard dish to keep straight. Spinal cords and nerves were fixed with 4% PFA overnight. Samples were washed 3 times with 1X Phosphate buffer Saline (PBS) after fixation and transferred to 30% sucrose and kept at 4 ˚C. After sucrose saturation was done, samples were embedded in O.C.T. Compound (Cat# 4585, Fisher). For histochemical purposes spinal cords were sectioned 20 μm, longitudinally using a cryostat (Leica 3050).

3.2.4 Immunohistochemistry:

Given that multiple antibodies were used in our experiments, we had multiple conditions for permeabilization and blocking. Please refer to the table for the conditions related to each antibody. In general, samples were washed with 1X PBS to remove the OCT, a ring was drawn around them using the ImmEdge hydrophobic pen (Vector Biosciences). Samples were permeabilized for 30 minutes using 0.1% Triton X-100 and then blocked for 30 minutes to 1 hour at room temperature in 1X PBS containing 0.1% Triton X-100 (PBS-T), 10% donkey serum (Jackson ImmunoResearch), only in case of goat antibodies we used donkey serum, otherwise, regular goat serum was used, and M.O.M blocking reagent (Vector Laboratories). Slides were then incubated with primary antibodies dissolved in 1X PBS containing 0.1% Triton X-100, and 5% donkey serum/goat serum. For Choline Acetyltransferase (ChAT) staining, antigen retrieval is required before permeabilization. To do so, samples were treated with 10 mM Sodium Citrate pH:6 at 95 ˚C for 3 min and then washed once with 1X PBS. For primary antibodies, 5% donkey/goat serum is used in 0.1-0.3% Triton X-100 and is left overnight. The next day, samples are washed 3X with PBS-T, and then secondary antibodies are added to 0.1-0.3% Triton X-100 with 5% donkey/goat serums. This solution is then added to the samples and the incubation time is 1 hour. After the incubation time is over, samples are washed 2X with PBS-T and once with 1X PBS. Samples were mounted using anti-fade Fluoromount-G with DAPI and imaged using a Leica Scanning Microscope (SP5).

3.2.5 RNAScope In situ Hybridization:

Fixed frozen samples were used for the *in situ* and to probe for multiple targets, RNAscope® Multiplex Fluorescent v2 Assay was used. The experiment was done based on the manufacturer's manual for fixed frozen tissue. Briefly, samples were washed with 1X Phosphate

Buffer Saline (PBS) to remove OCT for 5 minutes. Samples were then baked in a 60˚C oven for 45 minutes. Samples were then post-fixed with 4% Paraformaldehyde (PFA) in 1X PBS for 60 minutes at room temperature. After this, samples are dehydrated with 50%, 70%, and 100% ethanol each dehydration step is for 5 minutes, and at the end of the slides are removed from 100% ethanol and immersed again in fresh 100% ethanol for another 5 minutes. In the end, slides are left to dry for 5 minutes. To block endogenous peroxidase enzyme activity, hydrogen peroxide is then applied to the tissues for 10 minutes. Samples are then washed with deionized water (dH2O) for 10-15 seconds and then samples are put in the antigen retrieval solution that is in the steamer at 95˚C for 5 minutes.

Samples are then dried again in a 60 ˚C oven for 45 minutes. ACD oven needs to be turned on 30 minutes before use to make sure the 40 ˚C and humidity are acquired. After the samples were dry a hydrophobic ring was drawn around each tissue using an ImmEdge pen. Protease II is applied to each tissue and samples are left in the ACD oven for 40 minutes at 40 ˚C. Protease III is a broad-spectrum protease that is intended to permeabilize the samples adequately to allow the probes to reach the target mRNA.

The probe mix that we plan to use is the combined 50X of C1 probes with 1X of C2 and 1X of C3 probes. Slides are washed with dH2O and then the probe mix is applied, and samples are left at 40 ˚C for 2 hours. Samples are then washed with 1X Wash buffer for 2 minutes, twice. We stop at this step and store our slides in a jar containing 200 ml of 5X Saline Sodium Citrate (SSC) buffer (from 20X SSC buffer, Cat# 51205, AccuGENE^{TM}, Lonza). On the second day, samples are washed again with 1X wash buffer twice each for 2 minutes. Amplification steps are then performed using A1, A2, and A3 solutions for 30, 30, and 15 minutes respectively at 40 ˚C. For the developing step, C1 is applied for 15 minutes at 40 ˚C. The TSA secondaries (Cat#

NEL741001KT, NEL745001KT, NEL744001KT; Akoya Biosciences) are used at a concentration that works best for each probe and incubated for 30 minutes at 40 ˚C. Samples are washed at the end of each step twice with 1X wash buffer for 2 minutes. HRP block solution is then added, and samples are incubated for 15 minutes at 40 ˚C. Samples are then washed the same way and C2, and C3 developing solution and TSAs are added the same as C1 step. When the last wash was done, samples were mounted with DAPI Fluoromount-G (Cat# 0100-20, SouthernBiotech) and imaged in 3-5 days.

3.2.6 PLX Treatment:

Csf1r inhibitor, PLX5622 (from Plexxikon, chow was produced by Research Diets Incorporated) with the dosage of 1200 ppm (1200 mg of active form of PLX per kg of the diet), was administered orally by chow starting 2 weeks prior to the experiment and continued until the mice are sacrificed. Control mice were kept on regular diet. Sciatic nerve crush was performed after the 2 week diet, and animals were kept on either PLX or regular food and spinal cords were collected at the end time point.

3.2.7 Quantification of Immunohistochemistry and In situ Hybridization

Synaptic quantification:

For all the quantifications, we are using Volocity software. We also were blinded to the genotypes in all quantifications.

Synaptophysin: To quantify global marker Synaptophysin, we used Tdtomato and a freehand tool to trace the perimeter of MNs. Injured neurons in the ipsilateral side of the spinal cord were labeled with ATF3. Sum pixel intensity for each MN was then divided by its surface area and reported as the mean intensity of synaptophysin. Each number was then normalized to

the mean intensity of synaptophysin in the uninjured (CL) area and was reported as mean intensity (IL/CL). For the injured side 100-150 neurons were counted per animal and for the uninjured 50-80 neurons were used for analysis. The mean intensity was measured by calculating the average of all neurons' mean pixel intensity in the injured or uninjured side of the spinal cord.

Bassoon: Given that bassoon was coating the perimeter of the motor neuron cell body, we quantified it differently from synaptophysin. We initially traced the MN using the freehand tool in the velocity software and then used the dilate option to dilate 20 μm around the cell body. The Sum intensity in this donut was then divided by the area to give us the mean synaptic density for Bassoon.

VGluT1 and VAChT: These synapses have individual puncta/boutons around the motor neuron cell body and on primary dendrites. We traced the perimeter of the cells, using tdTomato and the freehand tool and quantified the perimeter of each cell. We used the find object option in velocity to find and count each VGluT1 and VAChT boutons. The total count was then normalized to the perimeter to address differences in the size of MNs and was presented as VGluT1/VAChT synapses per 100 μm.

Microglial and CD68 quantification:

We used velocity software and by defining the size/ standard deviation (SD) threshold in the find object option, we selected each microglia.

To measure microglia density, the mean area that was each microglia was measured and divided by the total area that was covered to select the microglia. The number was then presented as Microglia density per 200 μm^2 by multiplying it by 200. With the same selection, we could also measure the mean Iba pixel intensity in each microglia. To measure the amount of CD68 in each selected microglia, we measured the sum of the mean pixel intensity of CD68 in each microglia.

For CD68 counts, we simply used the same method of using the size/ standard deviation (SD) threshold in the found object option to select CD68 puncta and measure the counts divided by the area that was covered. The counts were then reported as counts per 200 μm^2.

C1q *In situ* hybridization and immunostaining quantification:

In situ hybridization: With RNAscope *In situ* hybridization, we decided to count the number of injured neurons (using ATF3) that contain any C1q puncta. This number was then divided by the total number of MNs counted and presented as the percent injured MNs with C1q expression.

Immunostaining: For Day 3 post SNC, C1q quantification was performed by tracing around each motor neuron and finding the Mean C1q pixel intensity in the area selected around each MNs. For each animal, the mean intensity C1q pixel intensity was calculated in the uninjured (CL) part of the spinal cord and individual numbers were normalized to this mean and presented as Mean intensity Injured (IL)/Uninjured (CL).

Quantification of Tmem119+ microglia post PLX treatment and injury:

Microglia were counted manually while blind and normalized to the sum surface area and presented as percent microglia per 500 μm^2.

3.3 Results:

3.3.1 Neuronal DLK is required for axotomy-induced synapse loss

To ask whether DLK is required cell-autonomously in motoneurons (MNs) for axotomy triggered synapse loss, we used previously characterized Dlk fx/fx conditional Dlk KO mice (Miller et al. 2009), together with ChAT-Cre and Ai14 Rosa-tdtomato reporter. These mice developed normally and did not exhibit overt phenotypes (Supplemental Figure 1A-B). We assessed the presence of multiple synaptic markers on the cell body of MNs by confocal

microscopy, using TdTomato and NeuN to delineate the cell body surface. We imaged injured MNs and their uninjured counterparts from equivalent locations in the ipsilateral (IL, injured) and contralateral (CL, uninjured) sides of the same tissue sections following unilateral sciatic nerve crush (SNC). Activating Transcription Factor 3 (ATF3), which becomes induced specifically in axotomized MNs (Tsujino et al. 2000), confirmed the identification of injured MNs.

In control (WT) animals, within 7 Days post SNC, the cell body surface and surrounding area of axotomized MNs showed a dramatic loss in synaptophysin. This abundant and ubiquitous presynaptic protein is expected to mark most synapses, and the loss of intensity for synaptophysin staining in the region of axotomized MNs has been described in previous studies (Oliveira et al. 2004; Berg et al. 2012; Campos, Barbosa-Silva, and Ribeiro-Resende 2021). This loss in synaptophysin was significantly reduced in *Dlk* KO animals (Figure 3-1A-C). Since *Dlk* is deleted specifically in cholinergic neurons (including MNs), while synaptophysin should mark inputs from all cell types, the loss of synaptophysin represents a non-cell-autonomous effect of *Dlk* loss in MNs, affecting the presence of presynaptic inputs.

We then examined the presence of presynaptic cytomatrix protein, Bassoon, surrounding injured and uninjured MNs. Bassoon coats the surface of uninjured MNs with a uniform density. 7 days post SNC, WT MNs show a reduction in bassoon density on the cell body surface (Figure3-1 D-E), in addition to a non-uniform clumping distribution (discussed later in Figure 3-6). Compared to WT, we observed a higher density of Bassoon surrounding both injured and uninjured MNs in *Dlk* KO mice. Strikingly, we observed no significant difference in Bassoon density or distribution between injured and uninjured *Dlk* KO MNs (Figure 3-1D).

We also examined the distribution of specific synapses. VGluT1 (Vesicular Glutamate Transporter 1) is localized specifically at afferent synapses made by muscle spindle Ia axons

(Burke, Walmsley, and Hodgson 1979; Brown and Fyffe 1981). WT MNs showed a 20% reduction in VGluT1 synapse density 7 days post SNC. In contrast, *Dlk* KO MNs showed no significant reduction. (Figure 3-1F-G). The cholinergic C-bouton inputs from V0c interneurons, visualized by staining for VAChT (Vesicular Acetylcholine Transporter) undergo a 28% reduction in number/density and 1.5-fold increase in size on the cell bodies of injured WT MNs (Figure 3-1H-J). In contrast, *Dlk* KO MNs showed significant changes in density or size following axotomy. Collectively, these observations suggest that DLK function is required in injured MNs to induce the remodeling and loss of multiple synaptic inputs.

3.3.2 Neuronal DLK is required for microglial response around axotomized MNs

Previous studies of synaptic 'stripping' from axotomized MNs have hypothesized and debated the role of microglia in synaptic loss (Spejo and Oliveira 2015; Alvarez et al. 2020). We, therefore, asked whether the microglial response was altered around *Dlk* KO MNs. We probed the ipsilateral (IL) and contralateral (CL) ventral horn which contains injured and uninjured MNs for the microglia and macrophage markers ionized calcium binding adapter molecule 1 (Iba1) and lysosomal marker CD68, which is upregulated phagocytic microglia (Perego, Fumagalli, and De Simoni 2011; Chistiakov et al. 2017; Janda, Boi, and Carta 2018) In WT animals, SNC induces a large increase in microglial density in the IL region of the injured MNs (Figure 3-2A-B and D). The increase in density still occurs in *Dlk* KO animals, however, is more variable and less pronounced (Figure 3-2A-B). More strikingly, the number of microglia that show close associations with the injured MNs is reduced for *Dlk* KO MNs (Figure 3-2F-G). In addition, microglia surrounding injured MNs in WT animals show a strong increase in the lysosomal marker CD68 as well as Iba1 intensity (Figure 3-2C and E), compared to uninjured MNs. The increased Iba1 and CD68 intensities surrounding injured MNs are strongly dampened in *Dlk* KO mice. We

interpret that specific microglial responses to axotomized MNs require cellular events regulated by DLK function in MNs.

3.3.3 Addressing the role of microglia in synaptic loss

To further address the role of microglia in axotomy triggered synapse loss, we use the Csf1r inhibitor PLX5622 to deplete microglia before the SNC injury. Adult (3-month-old) Tmem119-EGFP transgenic mice were fed PLX chow for 7 days prior to SNC. This treatment led to a 20-fold reduction in the density of Tmem119-EGFP positive cells in the IL ventral horn (containing injured MNs) and a 6-fold reduction in the CL ventral horn (containing uninjured MNs). In both WT and *Dlk* KO genotypes, a small increase in Tmem119-GFP cells was still detected in the IL region of axotomized MNs (Figure 3-3A-B).

MNs in PLX-treated animals showed high variability in synaptophysin density, independent of sex and regardless of the injury. For unknown reasons, MNs in 3 of the PLX-treated animals showed significant synaptophysin loss, while 3 showed no synaptophysin loss independent of sex (Figure 3-3E-G). In contrast, synaptophysin intensity was equivalent around both injured and uninjured MNs in *Dlk* KO animals treated with PLX (Figure 3-3C-D). While *Dlk* KO MNs raised on normal chow still show some degree of synaptophysin loss (Figure 1A), the combination of *Dlk* KO with PLX depletion of microglial leads to complete inhibition of synaptophysin loss (Figure 3-3D). At face value, these data imply that DLK signaling in MNs works in concert with the recruited microglia to promote synapse loss.

3.3.4 DLK function in injured motor neurons triggers the induction of complement

Since the microglial response to injured MNs is strongly regulated by DLK, we focused our attention on immune system genes gated by DLK in injured MNs. While known neuronally expressed cytokines CCL2, CCL7, and Csf1 (previously proposed to be regulated by DLK in injured DRGs (Hu et al. 2019; Wlaschin et al. 2018) are not strongly DLK-dependent in injured MNs (Figure 3-4A), we noticed that all 3 subunits of C1q are induced in injured MNs in a DLK-dependent manner. In addition, Mannan-binding lectin serine protease 1 (MASP1), an alternative activator of complement in the C1q-independent lectin pathway, is also strongly induced by DLK in injured MNs (Figure 3-4B). These data led us to hypothesize that DLK signaling in injured MNs induces the activation of complement.

Complement components are normally highly expressed in glial cells, while neuronal sources of complement are not well known. So, we first examined the expression pattern of C1q in the spinal cord by *in situ* hybridization, using RNAScope probes to *C1qb*. At day 3 post SNC, *C1q* expression is predominant in microglia, particularly in microglia surrounding the injured MNs (Figure 3-4C-D). The enriched *C1q* expression in microglia (identified by Iba1 staining) surrounding injured MNs (marked by *Atf3* expression), was strongly reduced in microglia surrounding *Dlk* KO MNs (Figure 3-4D-E).

The RiboTag data predicted the expression of *C1q* in MNs. From the strong expression of *C1q* in associated microglia, we could not confirm *C1q* expression in MNs at Day 3. However, at 24 hours post-SNC (Day 1), we observed a strong and specific C1q expression in injured MNs, identified by the expression of *Atf3* (Figure 3-4F-G). This early (and likely transient) expression of *C1q* in axotomized MNs is diminished in *Dlk* KO animals, consistent with the RiboTag RNA-seq data.

We then examined C1q protein by antibody staining (Figure 3-4G-I). Like naïve animals, C1q staining is only sparsely detected in contralateral uninjured MNs, however, a dense net-shaped pattern of C1q is present in the vicinity of WT injured MNs at Day 3 post SNC. C1q staining is particularly intense in the area immediately surrounding injured MNs in WT animals. This MN-associated C1q was greatly reduced in *Dlk* KO tissues (Figure 3-4G-I). C1q was still present in *Dlk* KO tissues, however, showed an altered localization, predominantly close to nuclei of non-neuronal cells (arrows in Figure 3-4I). From these data, we infer that DLK signaling in injured MNs triggers cellular events that lead to the accumulation of C1q.

3.3.5 Microglia eat presynaptic components from axotomized MNs

Complement is previously known for its role in directing the phagocytosis of synaptic components by microglia. However, in contrast to developmental pruning, prior studies of synaptic stripping from axotomized MNs have not detected evidence for microglia 'eating' synaptic components and have instead proposed alternative relationships of microglia with injured MNs (Alvarez et al. 2020; Kettenmann, Kirchhoff, and Verkhratsky 2013; Perry and O'Connor 2010). In our studies of synaptic components, we noticed that Bassoon showed an altered localization in a clump-like pattern around the cell body of WT axotomized MNs. Co-staining with Iba1 revealed that the clumps of Bassoon were localized inside microglia associated with injured MNs (Figure 3-5A). Microglia-internalized clumps of Bassoon were detected surrounding the cell body of MNs and close to dendrite/processes in WT animals. Interestingly, a small frequency of internalized Bassoon were detected near uninjured MNs, and they were greatly increased surrounding axotomized WT neurons at day 7 post SNC (Figure 3-5B). Coincident with the reduction in CD68 surrounding axotomized *Dlk* KO MNs (Figure 2), the microglia-internalized clumps of Bassoon

were strikingly absent in *Dlk* KO animals (Figure 3-5B). Together these observations suggest that cellular components of the presynaptic inputs onto axotomized MNs are phagocytosed by microglia, and this process is triggered by events in MNs regulated by DLK.

Complement is a logical mediator of microglial phagocytosis. In *C3* KO animals we observed a similar phenotype to *Dlk* KO (Figure 3-5B). The absence of bassoon clumps in the *C3* KO is not due to reduced levels of activated microglia or reduction of CD68 (data not shown). From the combined observations, we conclude that DLK functions within axotomized MNs to trigger the activation of the complement cascade and C3-dependent clearance of synaptic inputs (Figure 3-5C).

Table 3-1 List of primary antibodies used in this study

Antibody	Source	Cat#	Species	Concentration	Specific Condition
ATF3	Novus Biologicals, LLC	NBP1-85816	Rabbit	1:500	None
Bassoon	Abcam+	ab82958	Mouse (IgG2a)	1:500	0.1% Triton X-100
C1q	Abcam	ab182451	Rabbit	1:1000	None
CD68	Bio-Rad	MCA1957	Rat	1:1000	
ChAT	Millipore	AB144P	Goat	1:100	Antigen Retrieval
HA	Cell Signaling	3724	Rabbit	1:100	
Homer1	Synaptic Systems	160 006	Chicken	1:500	
Iba1	Wako	019-19741	Rabbit	1:500	Acetone (Best condition)
MMP9	Sigma	M9570-100UG	Goat	1:100	None

NeuN	Sigma	MAB377	Mouse IgG1	1:500	0.1% Triton X-100
p-c-Jun	Cell Signaling	3270S	Rabbit	1:100	
PSD95	Cell Signaling	2507	Rabbit	1:50	0.1% Triton X-100
Synaptophysin1	Synaptic Systems	101 004	Guinea pig	1:500	
SynCAM1	Medical and Biological Laboratories	CM004-3	Chicken	1:500	
SCG10	Novus Biologicals, LLC	NBP1-4946	Rabbit	1:100	
VAChT	Synaptic Systems	139 105	Guinea pig	1:500	Great in all conditions
VGluT1	Sigma	AB5905	Guinea pig	1:5000	

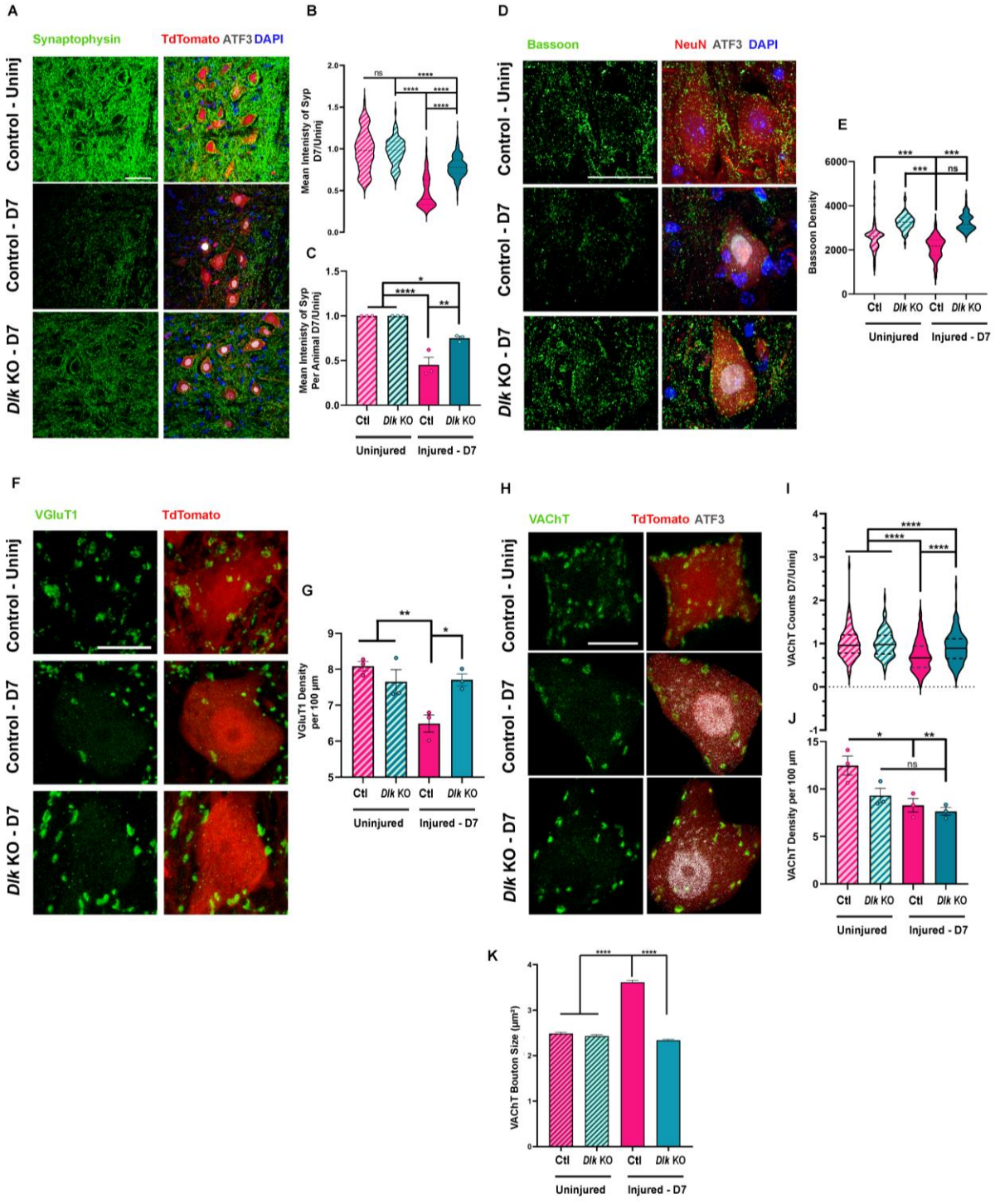
A
Synaptophysin
TdTomato ATF3 DAPI
Control - Uninj
Control - D7
Dlk KO - D7
B
Mean Intensity of Syp D7/Uninj
ns
****
****
****
****
C
Mean Intensity of Syp Per Animal D7/Uninj
*
****
**
Ctl
Dlk KO
Ctl
Dlk KO
Uninjured
Injured - D7
D
Bassoon
NeuN ATF3 DAPI
Control - Uninj
Control - D7
Dlk KO - D7
E
Bassoon Density
***
***
***
ns
Ctl
Dlk KO
Ctl
Dlk KO
Uninjured
Injured - D7
F
VGluT1
TdTomato
Control - Uninj
Control - D7
Dlk KO - D7
G
VGluT1 Density per 100 µm
**
*
Ctl
Dlk KO
Ctl
Dlk KO
Uninjured
Injured - D7
H
VAChT
TdTomato ATF3
Control - Uninj
Control - D7
Dlk KO - D7
I
VAChT Counts D7/Uninj
****
****
****
J
VAChT Density per 100 µm
*
**
ns
Ctl
Dlk KO
Ctl
Dlk KO
Uninjured
Injured - D7
K
VAChT Bouton Size (µm²)
****
****
Ctl
Dlk KO
Ctl
Dlk KO
Uninjured
Injured - D7

Figure 3-1 ***Neuronal DLK is required for axotomy-induced synapse loss*** *A) Synaptophysin (green) surrounding motoneurons (MNs) labeled by RosaTdtomato in ChAT-Cre; Ai14 mice, which are either wild type (+/+) or floxed (fl/fl) for Dlk. MNs in the L3-L6 lumbar segments of the ventral spinal cord that experienced axotomy from sciatic nerve crush (SNC), 7 days post-SNC, are identified by their expression of ATF3 (gray) in the Injured side (ipsilateral - IL) in lumbar segments L3-L6. These are compared to the uninjured contralateral (CL) found in the same tissue section (longitudinal sections). Scale bar is 50 μm.*

*(B) and (C) Quantification of synaptophysin intensity (shown in A) surrounding MN cell body surface. The intensity of synaptophysin surrounding each MN was measured using TdTomato to select the quantified pixel area. The mean synaptophysin intensity measured for each MN (sum green pixel intensity/area μm2 of Tdtomato) was normalized to the mean for MNs measured in the uninjured (CL) region of the same section. (B) shows measurements pooled for all MNs from 4-5 sections (n=110-150 for axotomized and n=80-100 for uninjured neurons) pooled from n=3 mice per genotype. (C) plots the mean intensity of all injured neurons in each animal (n=3). A One-Way ANOVA with Tukey test for multiple comparison was performed. * is P-Value < 0.05, ** is P-Value < 0.005 and **** is P-Value < 0.0001.*

(D) The presynaptic active zone component Bassoon (green), surrounding MNs, labeled by NeuN, in the L3-L6 lumbar segments of the ventral spinal cord 7 days post SNC. Injured MNs in the injured (IL) side of spinal cord sections are identified based on ATF3 staining (grey), Scale bar is 50 μm.

*(E) Quantification of Bassoon Density. The total intensity of Bassoon was measured as sum intensity of bassoon puncta in a 20μm distance from the surface of the neurons, divided by the area μm2. One-way ANOVA with Tukey test for multiple comparisons was performed. *** is P-Value < 0.001.*

(F) Immunohistochemistry of ventral spinal cord 7 days post SNC for presynaptic afferent onto motor neurons using VGluT1 (green). Tdtomato is used to visualize the perimeter of the motor neuron cell body. Scale bar is 20 μm.

*(G) Quantification of F. Average number of VGluT1 boutons was measured per animal and presented as a number of VGluT1 synapses per 100 μm. A One-Way ANOVA with Tukey test for multiple comparison was performed. * is P-Value < 0.05.*

(H) Immunohistochemistry of ventral spinal cord 7 days post SNC for a component of C-Boutons, VAChT (green), ATF3 (grey) and Tdtomato (red). Scale bar is 20 μm.

(I) Counts of VAChT per MN divided by average counts of VAChT in the uninjured (CL) side.

*(J) Average number of VAChT boutons was measured per animal and presented as a number of VAChT synapses per 100 μm. For both I and J, A One-Way ANOVA with Tukey test for multiple comparison was performed. * is P-Value < 0.05 and **** is P-Value < 0.0001.*

*(H) Size of each bouton that was selected in our protocol was analyzed as the selected area (μm2). **** is P-Value < 0.0001. IL (Ipsilateral), CL (Contralateral)*

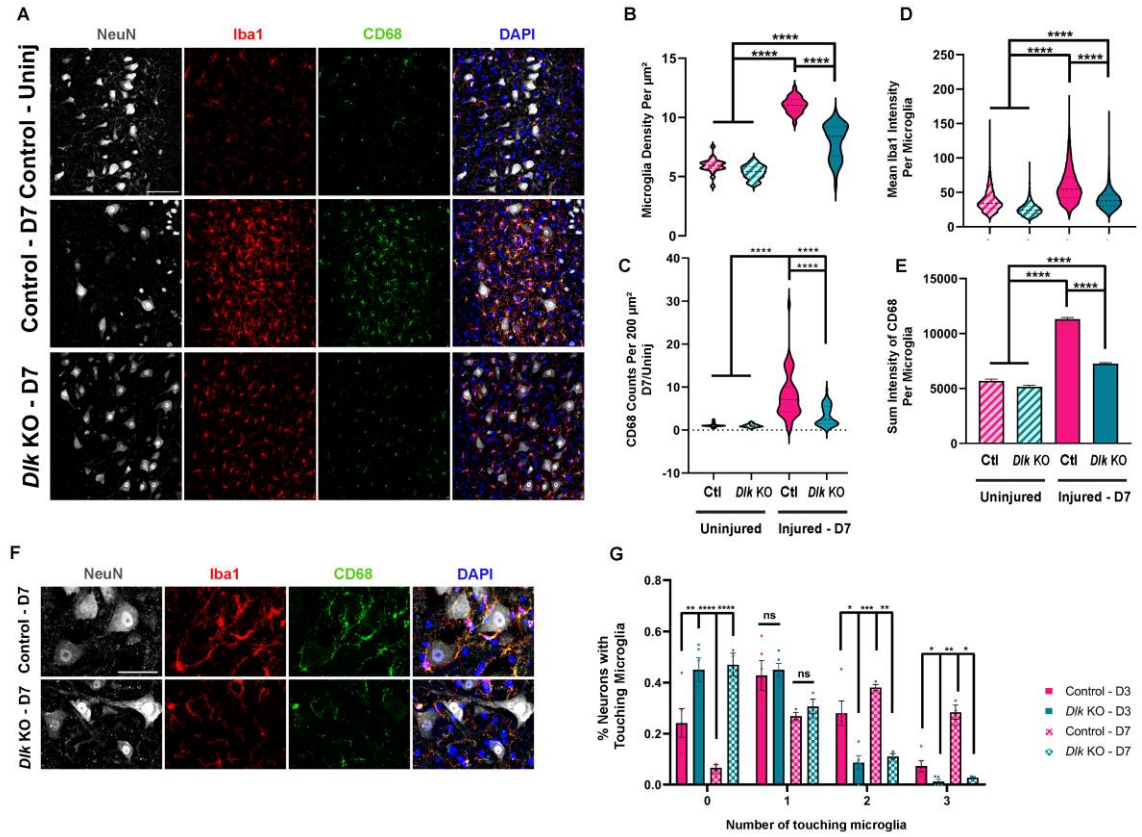

Figure 3-2 ***Neuronal DLK is required for microglial response around axotomized MNs****. A) Iba1 (Red) and CD68 (green) showing microglia and their lysosome respectively. The increase in both microglial density and their phagocytic capacity 7 days post SNC around axotomized neurons (Labeled by NeuN in gray) is attenuated in Dlk KO animals. Scale bar is 200 µm. (B)And (D) are quantification of data in A. Microglial density was calculated as the sum of Iba1 positive areas specifically selected by using Iba1 using our measurement protocol in each region of interest divided by the region of interest area (B). Mean Iba1 intensity in each microglia selected by our measurement protocol that would pick each microglia based on Iba1 threshold and standard deviation and measure the sum intensity of Iba1 in each of these microglia (see material and methods) (D).*

(C) CD68 puncta was counted in both injured and uninjured sides of the spinal cords and was graphed based on counts of CD68 puncta per 200 µm2. CD68 counts are heavily elevated 7 days post injury but the enhancement is diminished in Dlk KO animals.

*(E) Quantification of microglia phagocytic capacity. Sum intensity of CD68 positive puncta was measured in each microglia. CD68 intensity is heavily elevated in microglia 7 days post injury in the WT but not KO. For (B-E) A One-Way ANOVA with Tukey test for multiple comparison was performed. **** is P-Value < 0.0001.*

(F) In a close-up view of (A), it is apparent that microglia are not associating with the cell body of the axotomized MNs in the KO. Scale bar 50µm.

*(G) quantification of the number of microglia touching the cell body of the axotomized neurons at D3 and D7 post SNC. The number of associated microglia increases from D3 to D7 in injured WT animals but not KO. There is in general more microglia associated with the MN cell body at both D3 and D7 in the WT cases. A One-Way ANOVA with Tukey test for multiple comparison was performed at each time point. * is P-Value < 0.05, ** is P-Value < 0.005, *** is P-Value < 0.005 and **** is P-Value < 0.0001.*

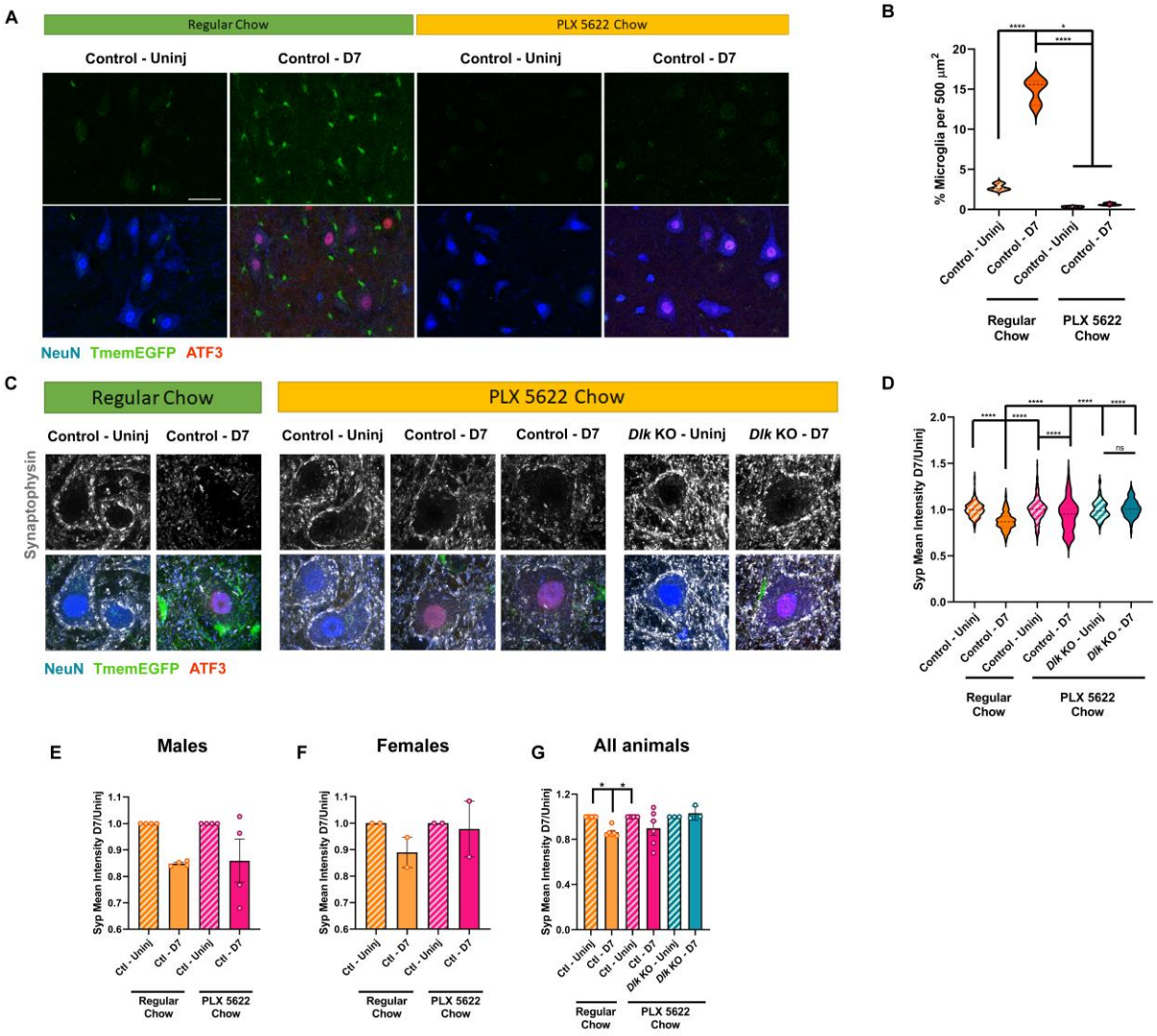

Figure 3-3 ***Addressing the role of microglia in synaptic loss.*** *(A) PLX5622 a Csf1r inhibitor was used to deplete microglia. Tmem119EGFP reporter mice were used to endogenously tag microglia. Animals were fed on PLX5622 7 days prior and then up to the time spinal cords are collected (here Day7 post SNC). Microglial activation post injury is depleted after feeding on PLX5622. (B) Quantification of microglia depletion post PLX5622 feeding. Percent microglia per 500 µm2 was measured by counting the number of microglia and dividing it by the sum of the injured or uninjured area. Scale bar is 50µm.*

(C) Immunostaining of spinal cords 7 days post SNC on regular or PLX5622 chow. Synaptophysin (gray) loss is reduced by PLX feeding in control, but it is completely rescued in Dlk KO animals fed on PLX. TmemEGFP; Dlk +/+, TmemEGFP; Dlk fx/fx; ChATCre are used for DLK WT and KO respectively. ATF3 (red) is used to mark the injured neurons and NeuN (Blue) to label MNs. (D) Quantification of synaptophysin intensity (shown in C) surrounding MN cell body surface. The intensity of synaptophysin surrounding each MN was measured using TdTomato to select the quantified pixel area. The mean synaptophysin intensity measured for each MN (sum green pixel intensity/area µm2 of Tdtomato) was normalized to the mean for MNs measured in the uninjured (CL) region of the same section. measurements pooled for all MNs from 3 sections (n=100-200 for both axotomized and uninjured neurons) and pooled from n=6 mice per control and n=3 for KO genotypes.

(E-G) Individual animals are represented for PLX treatment. The difference in the result of PLX-treated controls is sex-independent.

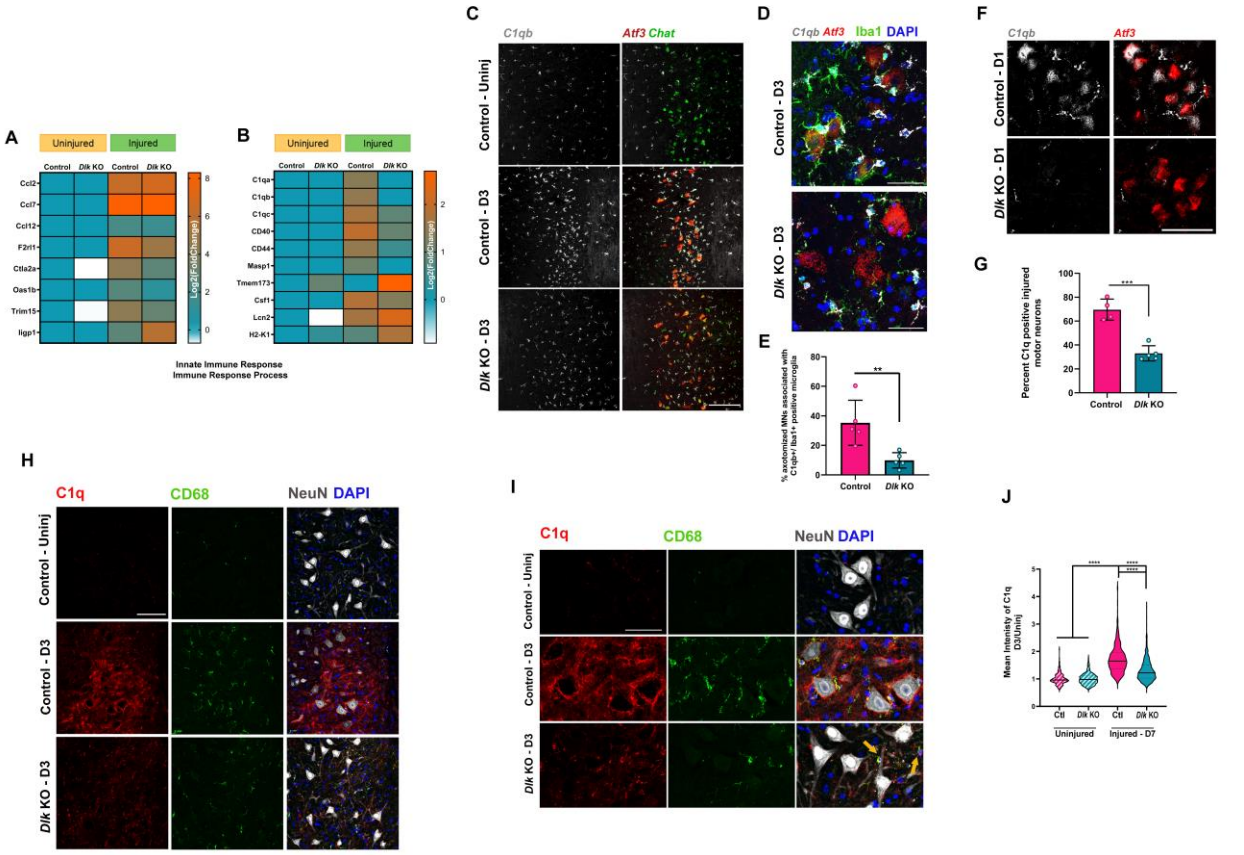

Figure 3-4 ***DLK function in injured motor neurons triggers the induction of complement*** *(A) and (B) Heatmaps of genes associated with GO terms (innate immune response and immune response process). Notice the cytokines such as CCL2 and 7 are not regulated by DLK but members of complement cascade such as C1q a,b and C and Masp1 are gated by DLK.*

(C) In situ Hybridization of C1qb (gray), Chat (Green) and Atf3 (red). Microglia are heavily expressing C1qb 3 days post SNC and microglial expression of C1qb is reduced in Dlk KO animals. Scale bar is 200µm.

(D) Close up look at In situ Hybridization of C1qb (gray), and Atf3 (red) immunostained for Iba1 (green) and DAPI. C1qb positive microglia surround axotomized MNs in WT and not KO animals. (E) Quantification in D, showing the reduction in the number of Iba1+/C1q+ microglia associated with Dlk KO axotomized MN.

(F) In situ Hybridization of C1qb (gray), and Atf3 (red), 1 day post SNC, shows MN expression of C1qb in WT and not KO animals.

(G) Quantification of E, percent C1qb positive axotomized MNs is calculated by counting the number of neurons that have C1qb puncta in them and dividing them by the total number of MNs.

(H) Immunostaining of C1q, 3 days post SNC. Control axotomized MNs are heavily coated by C1q positive puncta while this localization is changed and is more punctuated in the KO.

*(I) Zoom in view of (G), punctuated C1q staining in Dlk KO is mostly in non-neuronal cells (yellow arrows) (J) Quantification of intensity of C1q around axotomized MNs. NeuN is used to circle around MNs and sum intensity of C1q is divided by the area selected to give us mean intensity of C1q. This intensity is then divided by the average intensity of C1q around MNs in the uninjured part of the spinal cord. A One-Way ANOVA with Tukey test for multiple comparison was performed at each time point. **** is P-Value < 0.0001.*

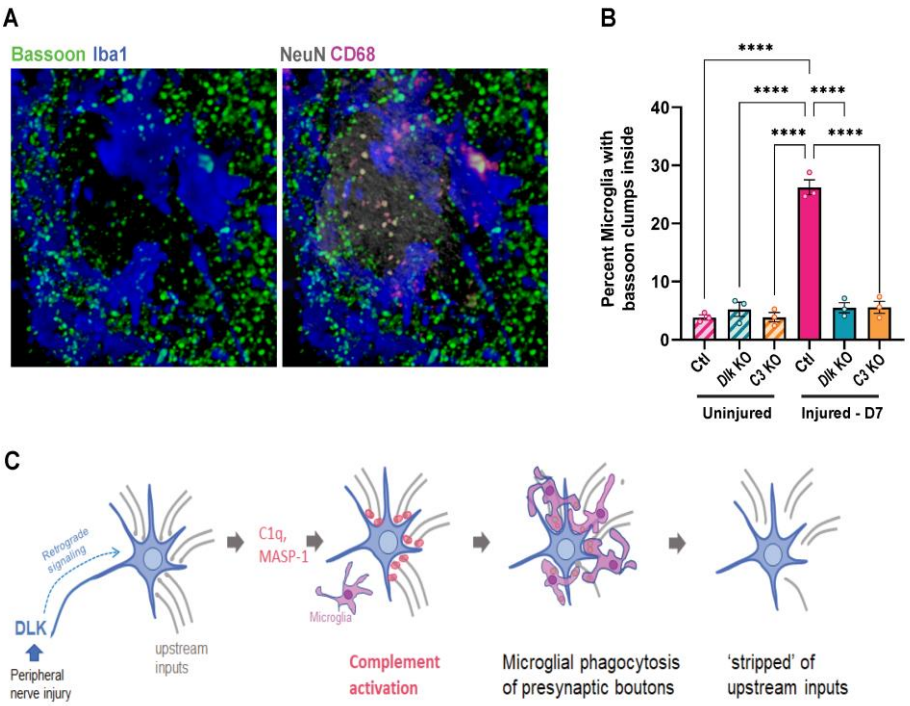

Figure 3-5 ***Microglia eat presynaptic components from axotomized MNs*** *(A) 3D rendering of a control neuron (Grey-NeuN) 7 days post SNC surrounded by multiple Microglia (Blue-Iba1). There are many Bassoon puncta (green) around the cell body and in the space around the neuron. Microglial engulfment of bassoon is seen by colocalization of green with lysosomal marker CD68 (magenta). (B) Quantification of percent microglia with bassoon clumps inside showed high frequency of engulfment post injury in the control but not Dlk or C3 KO.*

(C) Our Current model depicts that DLK activation post injury changes the expression of complement associated genes, leading to the activation of the cascade, recruitment of microglia and loss of upstream inputs on axotomized MNs.

Chapter 4 Comparison of our MN Specific RNA-Sequencing to Other Existing Datasets

Signaling downstream of the dileucine zipper kinase DLK is required for multiple responses to axonal injury. Previously published studies have profiled DLK regulated molecular responses in several different paradigms. These include injured DRG sensory neurons, induced cortical neurons (iNeurons in culture), and, in unpublished work that I was involved in, ectopically induced DLK signaling in *Drosophila* motoneurons (MNs). My thesis work focused on the identification of DLK-regulated responses in injured motoneurons (MNs) following sciatic nerve injury. My findings in mouse MNs brought attention to new DLK targets that were not previously acknowledged in the other studies. Moreover, the finding that DLK regulates the expression of complement inspired experiments that delineated a new role for DLK in triggering complement activation, inflammation, and synapse loss in the spinal cord following PNI. These findings established new questions which I sought to address with previously published datasets. In this chapter, I have asked whether DLK regulates common target genes and or common pathways in other published datasets. My analysis suggests DLK regulates a similar set of genes which include secreted peptides, and innate immunity genes across diverse models of DLK activation.

4.1 Introduction

In our study, we have shown that DLK is required for synaptic stripping and inflammation post peripheral nerve injury (PNI). As mentioned in earlier chapters, understanding how DLK can have its dichotomous responses after the activation can lead to finding better therapeutics as DLK has been associated with pathology in multiple neurodegenerative diseases (Le Pichon et al. 2017; Zhan, Xie, and Tibbetts 2015). We showed that DLK is required for the production of C1q from

injured neurons along with secreted proteins and certain cytokines that are not produced in normal conditions. Given that many different paradigms can activate DLK, we wanted to know whether inflammatory response term, neuropeptide secretions, and other sets of genes that we identified as DLK-dependent in injured MNs are also targets of DLK in other cell types and activation paradigms. We also questioned whether certain targets are amongst DLK-regulated genes in different paradigms.

In this Chapter, I have compared my dataset of DLK-regulated ribosome-associated transcripts in MNs, identified by RiboTag profiling at 3 days post sciatic nerve crush (SNC) to several different existing datasets. (1) The first dataset profiles DLK-regulated genes following the shared injury paradigm of SNC (Shin et al. 2019). However, instead of MNs, the Shin et al study sequences bulk transcripts from dorsal root ganglions (DRGs), which contain the cell bodies of sensory neurons in addition to multiple glial and immune cells. (2) The second dataset profiles MNs through the same RiboTag technique (Shadrach et al. 2021), however, does not directly investigate DLK. Instead, the Shadrach et al study profiles MN-specific transcript changes in the $SOD1^{G93A}$ model of Amyotrophic lateral sclerosis (ALS). Previous studies suggest that DLK signaling becomes activated and contributes to degenerative loss of MNs in this mouse model (Le Pichon et al. 2017). Although this dataset is not assessing the loss of DLK, we can see which DLK-gated genes in our dataset are showing up at different time points in the ALS model. (3) We then investigated a dataset that DLK-dependent gene expression changes in a different neuron type: cortical neurons derived from human iPSC (Tian et al. 2019). In the Tian et al study, the cortical neurons were not exposed to a specific stressor, however knockout of DLK via CRISPRi led to enhanced survival of neurons in the culture conditions (Tian et al. 2019). (4) We compared our dataset with a DLK- dependent gene expression change after nerve growth factor (NGF) deprivation in cultured embryonic DRGs

in the presence or absence of GNE-3511, a selective DLK inhibitor (Larhammar, Huntwork-Rodriguez, Jiang, et al. 2017). (5) Finally, we investigated a dataset generated in invertebrate *Drosophila* MNs, in which the *Drosophila* homolog of DLK, Wallenda (Wnd) was ectopically expressed in larval MNs. MN-specific transcripts were then purified using a TRAP approach (Zhang et al. 2016). The TRAP approach bears an analogy to the RiboTag approach since ribosome-associated transcripts are purified by the co-purification with a tagged ribosomal subunit, which is expressed specifically in *Drosophila* MNs using the Gal4/UAS system (Brand and Perrimon 1993).

Our comparisons identified DLK-dependent genes that were unique to single paradigms. However, strikingly, we found that neuropeptides and members of complement cascade were shared amongst four datasets generated from mammalian neurons but not the NGF withdrawal paradigm. In addition, neuropeptides and neuropeptide signaling were highly significant pathways affected by Wnd in the fly model. These findings suggest an ancient relationship between DLK/Wnd signaling and neuropeptide biology.

4.2 Material and Methods

4.2.1 RNA-seq Comparison:

For comparing our RiboTag MN-specific dataset to other datasets, we used the dplyr package and inter and outerjoin functions to find shared genes post differential expression analysis in each paradigm. For the Drosophila melanogaster dataset, we used a similar pipeline as to the one used in chapter 2. We used “Drosophila_melanogaster.BDGP6.22.dna.toplevel. fa” and it's equivalent “gtf” file to make an indexed reference genome and use it for mapping our reads to the indexed fly genome using star/2.5.2a. All the codes can be found in Appendix.

4.3 Results

4.3.1 Comparison to injury induced DLK signaling in DRG neurons

In recent years there have been multiple studies that looked at the DLK signaling pathway and performed RNA-sequencing in multiple models of DLK activation (Hu et al. 2019; Shin et al. 2019; Larhammar, Huntwork-Rodriguez, Jiang, et al. 2017). The DiAntonio lab specifically looked at downstream targets of DLK activation post SNC at D1 and D3 (Shin et al. 2019). They used the same *Dlk*-fx/fx transgenic mouse (Miller et al. 2009) crossed to advilin-Cre to knock out *Dlk* only in dorsal root ganglions (DRGs) -sensory neurons- that also send peripheral branch of their axons to the sciatic nerve. The way DRG are dissected is not as clean. As DRGs are not as isolated as one would imagine and we get changes in other cells such as satellite glia, microglia, and infiltrating immune cells as well. Therefore, some of the DEGs seen in the sensory neuron data post injury may be the non-cell-autonomous effects of DLK in other cell types. Although it is worth mentioning that we may get some background as well because of our method of isolation with magnetic beads and how there is a certain amount of background binding we can get. Knowing these shortcomings, finding shared genes sets in two different cell types with two different methods of isolation is still informative and can help us find a unifying feature for DLK activation. We compared our day 3 DLK-dependent DEGs in MNs to the day 3 DLK-dependent DEGs in sensory neurons. There were shared genes in our dataset that required DLK for their expression changes post PNI. 552 genes were specifically changing only in the DRGs, and 235 genes were specifically DLK dependent in MNs (figure 4-1A). In the shared DEGs 3 days post SNC, we can see enriched GO terms such as immune and inflammatory responses showing DLK dependence. We can also see the same extracellular preferences for the cellular component terms in the DRG dataset (Figure 4-2A-B, blue circles for DRGs and red circles for MNs). This

comparison and the unique subset of DLK-dependent genes in motor versus sensory neurons can be found in the appendix 1.

Our gene set enrichment analysis of unique DEGs in sensory and motor neurons showed interesting trends. In the injured sensory neurons, we see a trend for genes associated with ion transport and signal transduction, and perception of pain. We also have terms such as phagocytosis, inflammatory and immune response with a unique set of genes, response to interferon beta, and defense response to the bacterium. This may emphasize the point mentioned above that if DLK is also required for the inflammatory response post injury through secreted signals then it will affect the infiltration of immune cells and glial cells around the DRG. So, the method of DRG dissection may not be able to exclude these cells, therefore, some of the DEGs in the DRG data set may be DEGs unique to these other cells that are infiltrating the WT injured DRGs but not the *Dlk* KO ones. The other sets associated with ion transport and certain synapses raise the hypothesis that DLK may affect synapses of DRGs in a different paradigm as motor neurons residing in the spinal cord. The unique DEGs in motor neurons are associated with terms such as regulation of ERK1/2 signaling, Kinase activity, regulation of Wnt Signaling, actin/cytoskeletal organization, and cytokine activity. This unique map in motor neurons shows more intracellular changes in kinases and a unique set of cytokines produced by motor neurons post injury. This comparison and the specific subset of genes in motor versus sensory neurons is useful because it highlights the idea that DLK activation in different cells may yield different results and one should take this into account while considering DLK inhibitors as therapeutic agents (See Appendix 1 for the graphs).

4.3.2 Comparison to MN specific translatom in SOD1^{G93A} at different time points

Recently it has been established that DLK inhibition can attenuate cell death in SOD1^{G93A} mouse models of ALS (Le Pichon et al. 2017). Therefore, we compared our dataset to a recently

published and well-characterized dataset from Pierchala's lab in 1-, 3-, and 4-month-old $SOD1^{G93A}$ mice (Shadrach et al. 2021). 1- month old ALS mice are pre-symptomatic, while 3-month-old are early symptomatic, and 4-month-old are symptomatic (Shadrach et al. 2021). In this study, RNA-sequencing was performed on transcripts that are collected from MNs in the lumbar spinal cord using the RiboTag approach, making their dataset an interesting and convenient dataset to compare to ours.

In this paper, MNs from the ALS mice at the three mentioned time points were compared to D7 post sciatic nerve crush (an injury model). Given that we were interested in looking at possible DLK-regulated genes in disease conditions, we compared our DLK-regulated DEGs to the DEGs from the ALS mice. As seen by Pierchala's lab and presented in their paper (Shadrach et al. 2021), at 1 and 3 months of age, there are not many shared DEGs between injury and DLK induced, and ALS induced genes with only two shared genes at 1 month of age and nine at 3 months of age. The nine genes in 3 months old ALS mice, however, are intriguing, 3 members of the complement cascade C1q a, b, and c are upregulated at this time point in the ALS model. Galanin is the neuropeptide that is also upregulated. All these genes showed DLK dependence for their elevation post injury in motor neurons (Table 4-1). It is worth exploring what the early induction of C1q in motor neurons is doing since it can act as a signal to start an inflammatory response. However, it may also play a neuroprotective role, by clearing the debris.

At 4 months of age, when animals have clear symptoms and inflammation in their spinal cord, there are 80 shared DEGs with the DLK-dependent DEGs 3 days post SNC. Of these shared DEGs, neuropeptides such as Npy, Gal, and Adcyap1 that were heavily DLK dependent for their upregulation in our model, were also upregulated in the ALS model. Our gene set enrichment analysis (GSEA) showed that 4 months old ALS mice share terms with DLK-dependent DEGs

including neuropeptide signaling, regulation of ERK1/2, and hormone activity. Also, most of the shared CC terms are associated with extracellular region/space (Figure 4-3 A-B and Figure 4-4A-B orange circles). As mentioned previously DLK activation leads to multifarious and dichotomous outcomes. Recent clinical trials have also shown that long-term inhibition of DLK is deleterious for the patients' improvement and survival (Katz et al. 2022). Given the result of our comparison, it is possible that part of DLK activation and its role in the induction of neuropeptides is neuroprotective. It is also possible to imagine that an initial inflammatory response might help clear the debris, but the long-term existence of inflammation and gliosis can lead to synapse and cell loss.

4.3.3 Comparison to transcripts from human iPSC derived cortical neurons with CRISPRi (interference) for MAP3K12 (DLK)

In Tian et al 2019 study, the authors found that knockdown of MAP3K12 (DLK) improves neuronal survival (Tian et al. 2019). In their study, they developed a CRISPRi system to knock down multiple genes in human iPSC-derived cortical neurons. Their CROP-seq results in cortical neuron knockdown for DLK, and revealed enrichment for ribosomal and anti-apoptotic genes, and pro-apoptotic genes. Moreover, genes associated with cytoskeletal organization were depleted. We compared our Day 3 DLK-gated genes to this dataset. One would assume that in these cortical neurons, DLK's role is mostly related to neuronal survival and its context of activation is different from our paradigm. It is, however, of essence to see whether there are shared genes in these very different paradigms and whether a unifying feature for DLK activation can emerge. What we observed after our comparison was that only 12 genes are shared in these datasets, and they also don't necessarily up/downregulate in the same direction (Table 4-2). One of the genes in this set is Galanin (*Gal*) and given that it was also present in sensory neurons and motor neurons, it may

be one of the neuroprotective genes affected by DLK. We also have neurotensin (*Nts*) affected by DLK which is reduced in both CRISPRi and axotomized MNs knocked out for DLK (Table 4-2). The neuromodulation of the dopaminergic system by neurotensin raises a possible mechanism by which DLK can contribute to the pathology seen in diseases that have dopaminergic dysregulation such as Parkinson's Disease (PD) (Warren et al. 2017; Borbély, Scheich, and Helyes 2013). Dusp1 which is known as Puckard in flies, a phosphatase that dephosphorylates MAP kinases such as JNK, and P38 (Owens and Keyse 2007; Keyse 1998), is also not upregulated after knocking out or knocking down DLK. The fly homolog of Dusp1, Puckered, is normally upregulated after activation of JNK, one of the downstream targets of DLK (Martín-Blanco et al. 1998).

4.3.4 Comparison to DLK-dependent DEGs in an NGF withdrawal paradigm

It is established that NGF deprivation leads to DLK activation and DLK is required for the subsequent cell death and axonal degeneration (Ghosh et al. 2011). To study the DLK-dependent gene expression changes after NGF withdrawal, Watkins' lab performed RNA-sequencing on cultured embryonic DRGs after NGF deprivation in the presence and absence of DLK inhibitor, GNE3511 (Larhammar, Huntwork-Rodriguez, Jiang, et al. 2017). They showed in their study that DLK regulated the PERK stress signaling pathway (Larhammar, Huntwork-Rodriguez, Jiang, et al. 2017). Surprisingly, like the iNeurons, there are only a handful of genes that are shared in our injury paradigms and this NGF deprivation model (Table 4-3). There are a couple of shared Transcription factors and G-protein coupled receptors. Stathmin 4 (*STMN4*) showed up in this comparison as well as the iNeuron analysis.

4.3.5 Studying activation of DLK (Wnd) in an invertebrate model (Drosophila melanogaster)

DLK is a conserved enzyme and is found in invertebrates such as C. *elegans* and D. *melanogaster* (known as Dlk-1 and Wnd respectively) and has been shown to be activated and required for regeneration in injury models (Klinedinst et al. 2013; Hammarlund et al. 2009). DLK/Wnd has also been reported to lead to synapse loss in a kinesin-3 mutant model in flies (J. Li et al. 2017). We wondered whether DLK/Wnd activation in flies can also affect similar gene sets with what we observed in mammalian injury models. To address this question, we collaborated with the lab of Dion Dickman at the University of Southern California. While we compared DLK-Dependent gene expression changes in mammalian MNs post injury, in the Dickman lab, they directly activated DLK without injury through overexpression of DLK/Wnd in motor neurons, using the Gal4/UAS system (*BG380*-Gal4 and UAS-*Wnd*). The Dickman lab generously shared their data with us. Our initial analysis with a PCA plot showed that one of the overexpression samples is slightly different from the other 2 but in general, samples were grouped together (Figure 4-5A). Heatmap of the 50 most variable genes with hierarchical clustering showed a similar trend as 2nd wnd overexpression sample (Wnd.2) was not grouped like the other 2 wnd overexpression samples because of a group of genes that are behaving differently (Figure 4-5 B). Our volcano plot shows many genes with their gene symbols that are downregulated after overexpression of DLK (Wnd) (Figure 4-5 C). We performed gene set enrichment analysis (GSEA) and plotted the 20 first significant terms in all three categories of Biological Processes (BP), Molecular Function (MF), and Cellular Components (CC). We observed more genes that are associated with synapse activity and synaptic vesicle/organization and postsynaptic membrane terms. In the *Drosophila* dataset with ectopic DLK activation. Importantly, despite the different modes of DLK activation, we notice that neuropeptide related terms are depleted in fly motoneurons after DLK activation, which is like all the other paradigms of DLK activation (Figure 4-2 and 3 A-B, light green circles). G-

protein coupled receptor activity and hormone activity terms were shared between our MN dataset and this model of activating DLK in fly MNs (Figure 4-2 and 3 A-B light green circles).

4.4 Discussion

In this chapter, we sought to address the question of whether DLK activation in multiple contexts can regulate the same gene sets/ pathways. Our analysis showed that the C1q member of the complement cascade is expressed by neurons in stressed conditions and this enrichment requires DLK in multiple paradigms. We also depicted that the secretion of peptides is DLK-dependent in multiple contexts. Our gene set enrichment analysis showed that neuropeptide hormone activity is one of the terms that is DLK dependent in injury induced DLK activation paradigms, ALS model and it is conserved in invertebrates as well (Figure 4-3 A and B). Immune and inflammatory responses affected by DLK are also shared in the different contexts of neuronal stress/ different neuron types (Figure 4-2 A and B).

An interesting difference between mice and fly models of DLK activation is that synaptic genes seem to be affected transcriptionally when DLK is activated. One explanation can be that the mechanism of synapse plasticity is not the same in flies and mice. Based on our findings in chapter 2, transcriptional changes of synaptic genes are less prominent in mice. However, it is still exciting to see that DLK can contribute to synaptic loss although not in the same manner in both vertebrates and invertebrates. It is also worth noting that this method of DLK activation by overexpression is different from our injury model and a better comparison can be achieved if our dataset is compared to profiling post injury in *Drosophila*.

One of the surprising observations from our comparison was the very limited number of genes that were shared between our dataset and the two cultured models (iNeuron and NGF deprivation). NGF withdrawal activates DLK which in turn activates PERK and ATF4 changing

the set of genes that are being regulated by DLK drastically (Larhammar, Huntwork-Rodriguez, Jiang, et al. 2017). *Atf4* is not one of the genes regulated by DLK in the SNC model of DLK activation in both motor and sensory neurons (our data from chapter 2 and (Shin et al. 2019)). With iNeuron dataset, we noticed that there are still terms such as activation of innate immune response and immune response process but the DLK-dependent genes in these terms were not the same as the ones found in the SNC models of DLK activation. The most significant terms for the iNeurons were related to the regulation of rRNA, ribosomal assembly, and translation initiation. In vitro studies in our work showed little similarities to DLK-dependent gene expression changes in vivo. It needs to be considered that non-cell-autonomous responses such as microglial or immune responses are not present in the invitro culture of the iNeurons and that can change how and what genes get regulated by DLK. In short, we think that the context of DLK activation and the developmental stages that the cells are in can affect the transcriptional changes observed post DLK activation. This study can benefit from the addition of other datasets such as injury-induced gene expression changes in a *cJun* KO because cJun is one of the downstream targets of DLK and is phosphorylated by MAPKs and relocate to the nucleus, making dimers with other transcription factors and changing the expression of many genes (Mason et al. 2021). Such comparison can help us establish the set of genes that are regulated by Jun activation in our paradigm and separate the regeneration related genes as this study shows Jun is required for regeneration (Mason et al. 2021). It can also add to our understanding of DLK activation and downstream targets if we compare our dataset to a central nervous injury model gene expression changes (Watkins et al. 2013). Finding out the differences in models that lead to axonal degeneration and cell death compared to PNI that does not lead to cell death can help decipher the dichotomy of DLK responses. There may be

different transcription factors (TFs) or various forms of dimerization between the TFs leading to unique differentially expressed genes.

.

Table 4-1 ***Shared DEGs between DLK dependent DEGs 3 days post injury and 3month old ALS DEGs.*** *Members of complement such as C1qa-c are upregulated in the 3-month-old SOD1^{G693A} model of ALS. Galanin, one of the neuropeptides that is heavily DLK dependent in our model, is also upregulated in the 3-month-old ALS model.*

Gene	Ensemble ID	Log2FC - ALS	Log2FC - *Dlk* KO	P.Value - ALS	P.Value - *Dlk* KO	FDR - ALS	FDR - *Dlk* KO
Gal	ENSMUSG00000024907	1.07414	-2.626041995	5.00E-05	4.71E-30	0.0167663	2.30E-26
C1qb	ENSMUSG00000036905	1.55098	-1.077105698	5.00E-05	1.57E-06	0.0167663	0.000252983
Rhoc	ENSMUSG00000002233	1.57578	-0.737177691	5.00E-05	4.86E-06	0.0167663	0.000668886
C1qc	ENSMUSG00000036896	1.6283	-0.79330937	5.00E-05	5.76E-05	0.0167663	0.005414073
C1qa	ENSMUSG00000036887	2.17412	-0.981904691	5.00E-05	2.46E-05	0.0167663	0.002652725
Sprr1a	ENSMUSG00000050359	4.42518	-1.349444069	5.00E-05	4.24E-17	0.0167663	3.46E-14
Atf3	ENSMUSG00000026628	5.56077	-1.130410104	5.00E-05	1.49E-16	0.0167663	1.12E-13

Table 4-2 ***Shared DEGs between DLK-dependent DEGs 3 days post injury and CRISPERi method of knocking down DLK in IPSC-derived cortical neurons.*** *DLK (MAP3K12) is downregulated in both conditions. Neuropeptides such as Gal and NTS need DLK for their upregulation. Proapoptotic gene HRK also needs DLK for its enrichment. A few of the shared genes are not affected in the same manner in this comparison and are highlighted in green. Genes that are de-enriched in the absence of DLK are highlighted in blue and yellow are enriched.*

Gene	Ensemble ID	Log2FC - *Dlk* i	Log2FC - *Dlk* KO	P.Value - *Dlk* i	P.Value - *Dlk* KO	FDR - *Dlk* i	FDR - *Dlk* KO
MAP3K12	ENSG00000139625	-1.424299012	-2.170110336	1.86E-24	2.46E-29	6.27E-20	9.62E-26
STMN4	ENSG00000015592	-0.557636692	-1.530190347	6.55E-24	4.36E-15	1.10E-19	2.75E-12
DOK5	ENSG00000101134	0.493825025	-0.540801824	9.73E-09	0.000109735	1.09E-05	0.009123377
HRK	ENSG00000135116	-0.696589226	-2.346171916	5.13E-08	2.02E-14	4.43E-05	1.20E-11
RPL35A	ENSG00000182899	0.098195174	-0.590734466	4.05E-05	0.000420453	0.011160245	0.026758355
PPP1R1C	ENSG00000150722	0.45354039	0.643095496	4.34E-05	0.000646705	0.011711384	0.036709464
GAL	ENSG00000069482	-0.950810796	-2.626041995	8.47E-05	4.71E-30	0.019685862	2.30E-26
PKIB	ENSG00000135549	0.262893027	-0.774260641	0.000146418	1.99E-05	0.028190889	0.002224331
NTS	ENSG00000133636	-0.696222971	-0.774493713	0.000195565	0.000197121	0.033448484	0.014317252
SCRT2	ENSG00000215397	0.308008099	-0.526997292	0.000683481	0.0001989	0.078597935	0.01439298
PALLD	ENSG00000129116	-0.435695537	-0.491919775	0.000763602	0.00031	0.084356705	0.020531437
DUSP1	ENSG00000120129	-0.357797176	-1.159534125	0.001014964	3.67E-17	0.102074849	3.26E-14

Table 4-3 ***Shared DEGs between DLK dependent DEGs 3 days post injury and DLK dependent DEGs in NGF withdrawal paradigm using embryonic DRGs.*** *Most shared genes in this paradigm are transcription or translation associated.*

Gene	ID	Log2FC - NGF	Log2FC - *Dlk* KO	P.Value - NGF	P.Value - *Dlk* KO	FDR - NGF	FDR - *Dlk* KO
Bend5	ENSMUSG00000028545	0.792093088	-0.966812475	4.22E-47	1.08E-07	2.71E-45	2.34E-05
Prokr2	ENSMUSG00000050558	2.627352703	-0.76807022	1.66E-25	4.04E-05	4.99E-24	0.003982762
Mob3b	ENSMUSG00000073910	0.744917622	1.559177769	1.08E-13	2.95E-05	1.63E-12	0.00304899
Cdh12	ENSMUSG00000040452	0.682632524	0.684792119	7.03E-12	0.000273972	8.97E-11	0.018458128
Atf3	ENSMUSG00000026628	-3.941269206	-1.130410104	0	1.49E-16	0	1.12E-13
Nfil3	ENSMUSG00000056749	-1.477196048	-0.617188425	7.93E-165	1.07E-05	3.20E-162	0.001320827
Plat	ENSMUSG00000031538	-1.079563509	-0.81355253	3.20E-107	0.000445991	6.53E-105	0.028155988
Dusp1	ENSMUSG00000024190	-1.351512601	-1.159534125	1.27E-106	3.67E-17	2.55E-104	3.26E-14
Flrt3	ENSMUSG00000051379	-1.599123183	-0.632965339	1.65E-98	0.000269606	3.03E-96	0.018226838
Stmn4	ENSMUSG00000022044	-0.765691371	-1.530190347	3.17E-95	4.36E-15	5.53E-93	2.75E-12
Btg2	ENSMUSG00000020423	-1.094868618	-1.08301023	4.56E-56	9.15E-07	3.72E-54	0.000154045
Bdkrb2	ENSMUSG00000021070	-0.859015343	-1.02793575	5.27E-45	0.00048203	3.15E-43	0.029430934
Heca	ENSMUSG00000039879	-0.806473872	-0.597363555	9.68E-44	0.000391302	5.55E-42	0.025315395
Rnf122	ENSMUSG00000039328	-1.067634147	-0.45671094	2.22E-42	0.000266002	1.21E-40	0.018045637
Pxdc1	ENSMUSG00000021411	-0.825503325	-2.563476377	2.92E-30	4.25E-17	1.11E-28	3.46E-14
Mgat4c	ENSMUSG00000019888	-1.030912812	-0.685568527	3.57E-22	3.59E-06	9.09E-21	0.000519942
Eif4ebp1	ENSMUSG00000031490	-0.628870926	-0.759469091	2.37E-21	0.000171218	5.75E-20	0.012719611
Rnf165	ENSMUSG00000025427	-0.798641338	-0.849304912	1.58E-18	7.04E-05	3.28E-17	0.006308964
Cebpd	ENSMUSG00000071637	-0.762730295	0.566940717	4.30E-14	0.000229545	6.70E-13	0.016132523
Rnd1	ENSMUSG00000054855	-1.236274282	-0.545867243	1.78E-10	1.33E-05	1.95E-09	0.001551451
Sulf1	ENSMUSG00000016918	-0.83857998	1.041809198	1.44E-07	0.000461062	1.13E-06	0.028688617
Ccl2	ENSMUSG00000035385	-0.890433846	0.483610213	1.98E-06	0.000169437	1.32E-05	0.012635315
Steap1	ENSMUSG00000015652	-0.803863713	0.907084816	7.24E-06	1.88E-06	4.40E-05	0.000287087
Steap4	ENSMUSG00000012428	-1.010520558	3.013698781	3.90E-05	1.54E-16	0.000208	1.12E-13
Kcnk13	ENSMUSG00000045404	-1.195919217	-1.203145641	4.48E-05	2.28E-05	0.000236	0.002504084
Ano4	ENSMUSG00000035189	-0.63285287	-0.736723991	6.69E-05	7.95E-06	0.000341	0.00102871

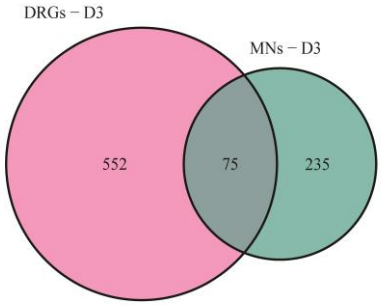

Figure 4-1 ***Venn Diagram of Shared DEGs between DRG and MNs 3 days post SNC.*** *75 genes are shared between the two.*

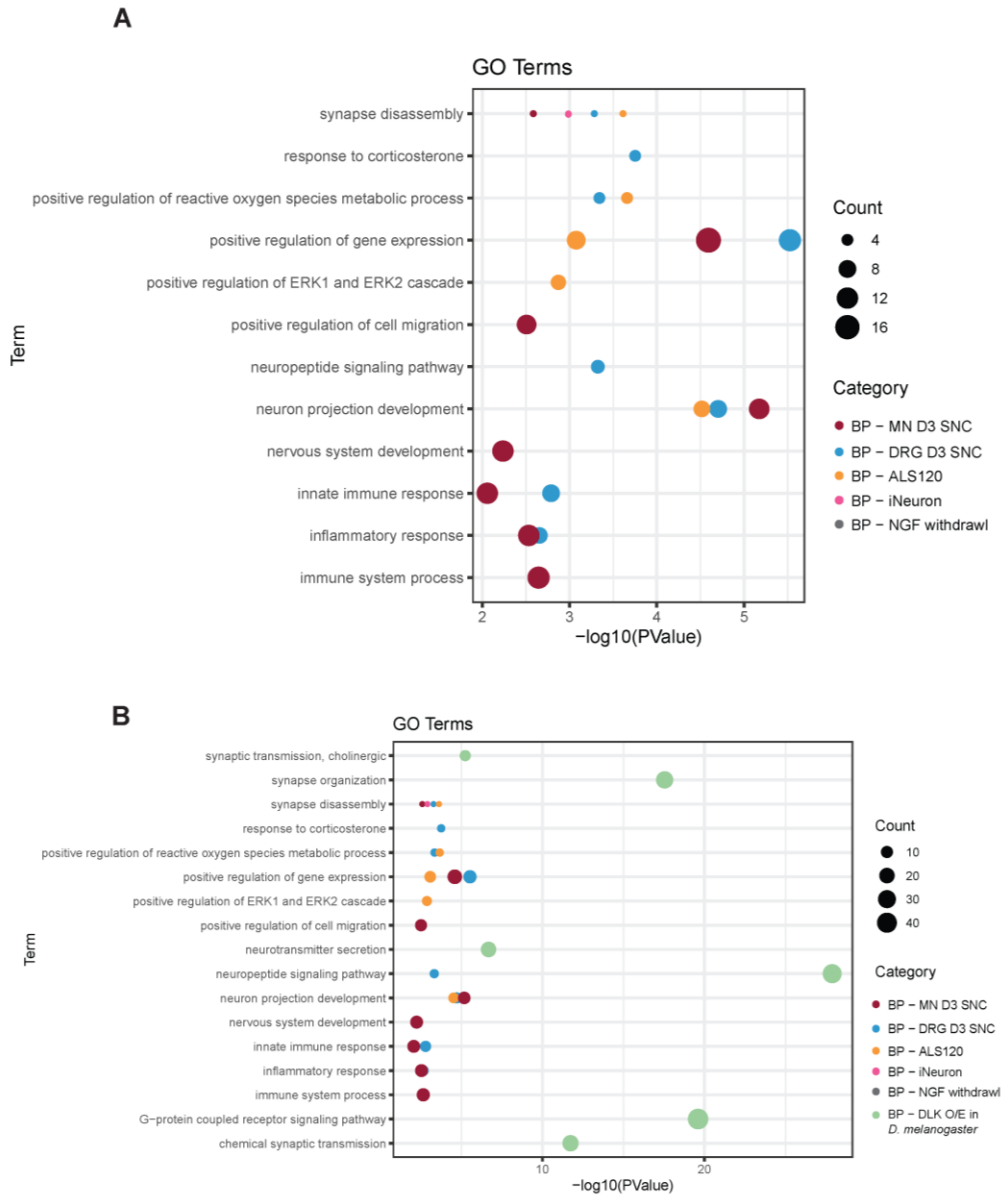

Figure 4-2 ***Biological Processes Terms****. (A) Bubble plot of biological processes terms that are shared among our comparisons in mammalian systems and different models of DLK activation. Inflammatory response and immune response terms are shared between the DRG and MNs post injury. Synapse disassembly term which contains the 3 members of complement is shared between DRG, MN, iNeuron and 4-month-old ALS. (B) Drosophila Melanogaster (DM) gene sets and terms are added to the comparison. Many of the Drosophila melanogaster DEGs fall into synaptic related categories and don't overlap with the other conditions.*

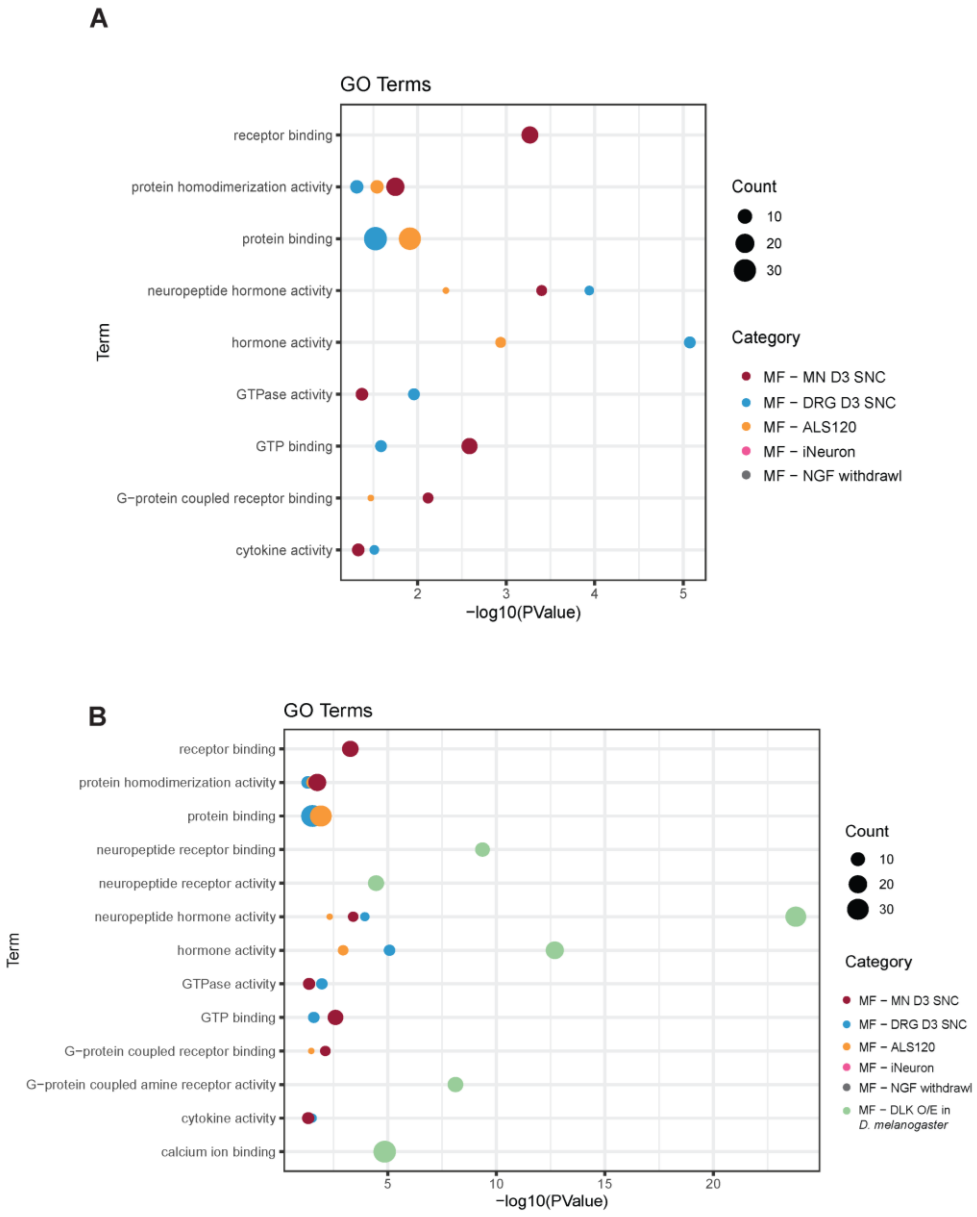

Figure 4-3 ***Molecular Function Terms****. (A) Bubble plot of Molecular Function terms that are shared among all the comparisons. In general, there are more shared terms between DRG and MN post injury, but Term "neuropeptide hormone activity" is shared with the ALS model as well. (B) In the invertebrate Drosophila Melanogaster model of DLK activation, we still have neuropeptide hormone activity as one of the significant terms. DLK regulation of neuropeptides seems to be conserved between invertebrate and vertebrate models.*

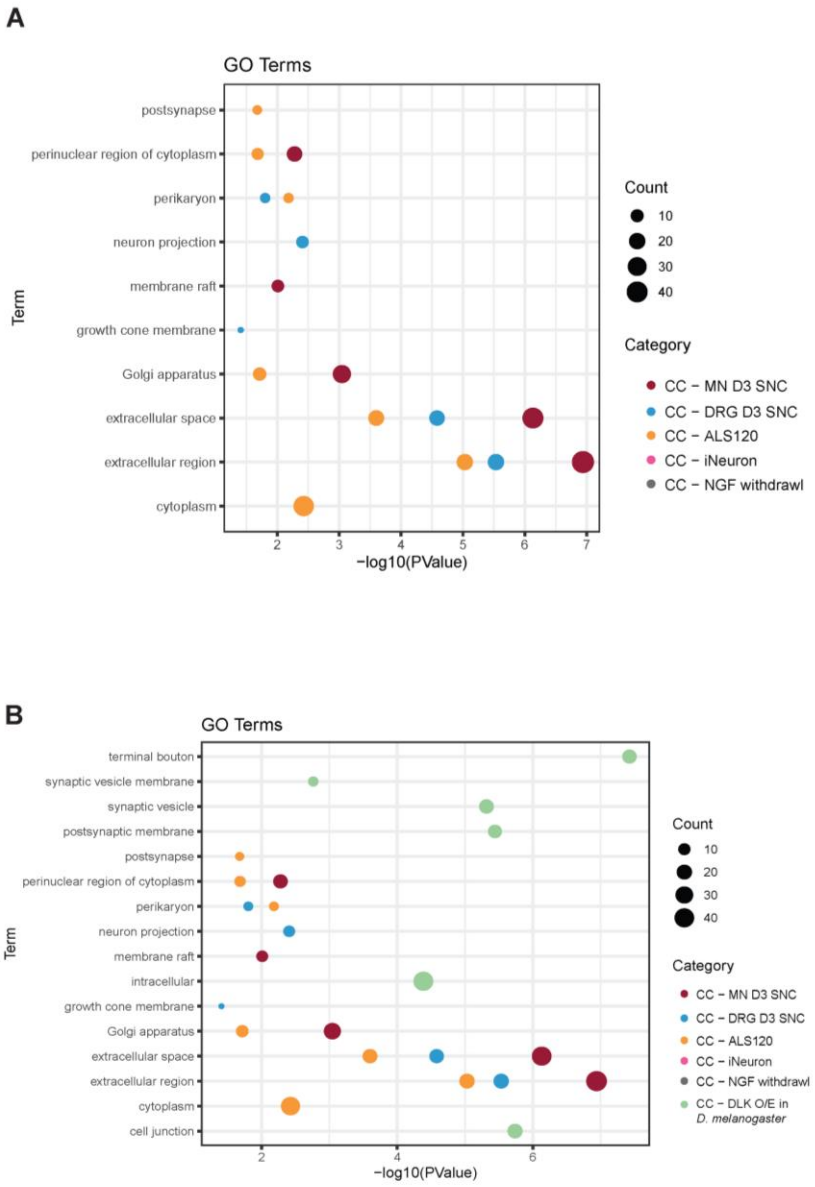

Figure 4-4 ***Cellular Component Terms****. (A) Bubble plot of Cellular component terms. The "Extracellular space/region" category is overrepresented in multiple paradigms emphasizing the role of DLK in the production of secreted molecules in multiple contexts of activation. (B) In the invertebrate Drosophila Melanogaster model of DLK activation, most genes are associated with intracellular space and synapse structure, showing that DLK method of synapse loss is most probably different in the invertebrates such as Drosophila.*

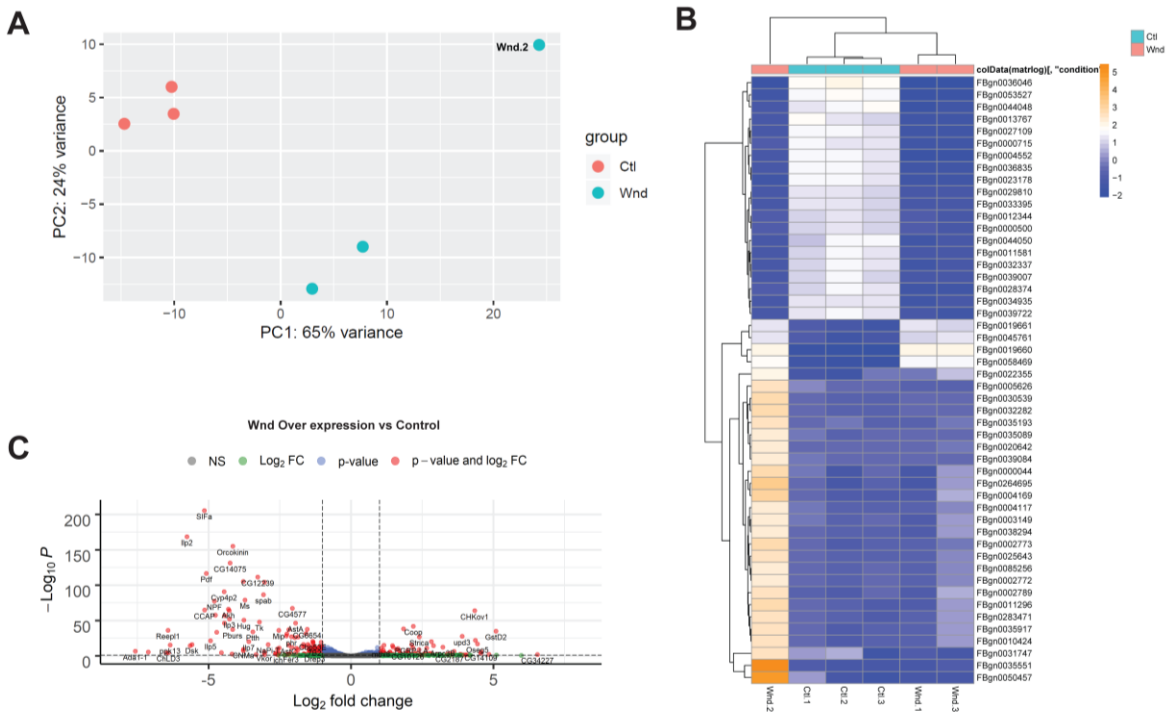

Figure 4-5 ***RNA-seq analysis of DLK/Wnd activation in Drosophila melanogaster Motoneurons.*** *(A) Principal Component Analysis shows clear grouping of the conditions although one of wnd overexpression samples (wnd.2) is slightly different from the other two. (B) Heatmap of most variable genes shows that many genes are downregulated when DLK/wnd is overexpressed. (C) Volcano plot of the comparison.*

Chapter 5 DLK Activation Causes Lethality and Degeneration in Adult *Drosophila*

The Dual Lucine Zipper Kinase DLK, known as Wallenda (Wnd) in *Drosophila*, controls a highly conserved signaling pathway that becomes activated in damaged axons and is required for multiple responses of neurons to axonal damage. We describe a new paradigm in the adult *Drosophila* nervous system to study degeneration and cell death. This new paradigm by taking advantage of the powerful genetic tools in *Drosophila* will enable future studies on the DLK-gated genes found in the RiboTag profiling data. We propose the use of the fly eye as a model to study the developmental role of DLK activation in neuronal death and degeneration. We also propose the use of induced Gal4 for assessing the lethality and degeneration caused by DLK/Wnd activation in flies. Our initial result showed that inhibition of the apoptotic or Sarm1 pathway cannot rescue the rough eye phenotype caused by DLK/Wnd overexpression, but it can rescue the premature lethality in the adult nervous system. Given our findings that DLK regulates non-cell-autonomous responses, we can study the contribution of immune-related genes and neuropeptides to degeneration and cell death gated by DLK.

5.1 Introduction

Wallenda (Wnd), DLK homolog in *Drosophila melanogaster* was initially discovered through a genetic screen to suppress lethality (Collins et al. 2006). Higher levels of DLK protein in this study caused synaptic overgrowth and lethality (Collins et al. 2006), suggesting a role for DLK/Wnd in neuronal degeneration and death. DLK-gated cell death has been shown in Retinal Ganglion Cells (RGCs) and fly and mouse models of neurodegenerative diseases (Le Pichon et al. 2017; Zhan, Xie, and Tibbetts 2015; Welsbie et al. 2013) where genetic manipulation or

pharmacological inhibition to reduce DLK levels, had neuroprotective effects (Le Pichon et al. 2017; Zhan, Xie, and Tibbetts 2015; Welsbie et al. 2013). In mouse DRGs after NGF deprivation, it has been shown that DLK induces the expression of pro-apoptotic Puma along with other caspases and contributes to axonal degeneration (Simon et al. 2016). The lethality and degeneration caused by DLK in the adult nervous system are not fully understood and it is hard to study DLK activation in adults because the global absence of DLK is developmentally lethal in flies. *Drosophila* provides a powerful model system for studying the mechanism(s) by which DLK/Wnd signaling promotes toxicity. To this end, we used two approaches:

1) We used the fly eye, a powerful model to study cellular mechanisms of degeneration (Bolus et al. 2020; Hirth 2010; Sang and Jackson 2005). It has suggested that overexpression of some of the disease transgenes such as TDP-43 and human polyQ protein and Ataxin 3 lead to degeneration of the eye (McGurk, Berson, and Bonini 2015). Moreover, a well characterized study on the photoreceptors has established that DLK overexpression in the R1-6 photoreceptor leads to degeneration while DLK activation in R7 and 8 photoreceptors have an axonal sprouting phenotype (Mecklenburg et al. 2018). Therefore, we used the fly eye model to perform a biased genetic screen and find targets of DLK that influence degeneration. Based on our previous knowledge of DLK targets and previously published dataset (Larhammar, Huntwork-Rodriguez, Jiang, et al. 2017), we picked RNAi lines to test. As expected, known downstream targets of DLK such as JNK and Fos are required for the degenerative effects of DLK in the eye as JNK and Fos knocked down rescued the rough eye phenotype. members of the integrated stress response (ISR) pathway which has been depicted to affect neuronal death via DLK in an NGF withdrawal paradigm of DLK activation (Larhammar, Huntwork-Rodriguez, Jiang, et al. 2017) showed little to no effect in rescuing the eye phenotype.

2) Neurons have limited capacity for repair in a mature state and neurodegenerative diseases are mostly late onset as well, emphasizing the importance of studying signaling pathways in adult, mature systems. To determine whether post-developmental activation of DLK in the adult nervous system is sufficient to cause toxicity, we used Geneswitch elavGal4 to specifically drive the expression of DLK in neurons of adult fly brains (Roman et al. 2001). With this approach, we found that acute induction of DLK in adult flies causes premature lethality. This lethality was rescued completely by overexpressing an apoptotic inhibitor- P35 and inhibiting a downstream target of Wnd activation- Jun N-terminal Kinase (JNK)- using JNK dominant negative. We also found that *Sarm* RNAi can partially rescue the lethality although based on the lengthened lifespan of the control *Sarm* RNAi flies on vector, we are not at this time confident that the partial rescue by *Sarm* RNAi is in the same pathway as DLK.

5.2 Material and methods

5.2.1 Drosophila stocks

The following strains were used in this study: *ELAV-GeneSwitch*-Gal4 (Osterwalder et al., 2001), UAS-fos^{DN} (Eresh et al., 1997), UAS-bsk^{DN} (Weber et al., 2000). Flies were raised at 25°C on standard Semidefined yeast-glucose media (Backhaus et al., 1984), *GMR*-Gal4, UAS-*Wnd E*, and UAS-*Wnd F*.

5.2.2 RU486 Administration

Standard Semi-defined yeast-glucose media (Backhaus, Sulkowski, and Schlote 1984) was microwaved to liquefy the medium, and after the food cooled down, RU486 (mifepristone, sigma, dissolved in 80% ethanol) was added to the food (from a 10 mM stock concentration to reach a

final concentration of 200 µM. Vehicle food contained an equivalent amount of ethanol (1.6%). *Geneswitch (GS)-elav* Gal4*;* UAS-*wnd* and *GS-elav* Gal4 *(Control)* flies and any other genetic necessary genotypes were raised in parallel at 25 ˚C on normal food before shifting to RU486 or vehicle containing food at 5-6 days post eclosion. Male and female (not virgins) flies were kept in separate vials, each vial containing 20-25 flies.

5.2.3 Survival Assay

After flies were shifted to food containing the drug or vehicle, live and dead flies were counted every day until no flies remained in each vial. Survival plots are defined as a fraction of animals that were alive each day.

5.2.4 Adult Fly Brain dissection and Immunohistochemistry

Male and female adult flies were anesthetized on a CO2 pad and then transferred to a plate filled with PBS, the head/cuticle is then ripped open to allow access to fixatives. These brains are not fully dissected. The partially dissected heads were then transferred to a 4-well plate filled with 4% Paraformaldehyde (PFA) (EMS, 15710) in 1% Phosphate Buffer Saline (PBS) and fixed for 45 min at room temperature. After the fixation, fly brains were washed 2-3 times with 1X PBS – Note to avoid adhesion of these brains to the pipet, use a glass pipet that is washed/coated with 1% BSA in 1X PBS. Fixed brains were then fully dissected in ice-cold 1X PBS. Dissected brains were then transferred to a blocking solution of 0.3% Triton, 1% BSA, and 5% Normal Goat Serum (NGS) in 1X PBS. The tissues were blocked for 1h at room temperature. Primary antibodies were added to the blocking medium and primary staining was performed for 4 days at 4 ˚C. Primary antibodies and the concentration used were as follows; Anti- Brp (DSHB, nc82, mouse IgG1)

1:100, Anti-Synapsin (DSHB, 3C11, mouse IgG2b) 1:30, anti- Fas II (DSHB, 1D4, mouse IgG1) 1:500. After the primary antibody staining, brains were washed with 0.3% Triton in 1X PBS. Secondary antibodies were all used at 1:500; Goat anti-mouse IgG1- 568, Goat anti-mouse IgG2b (488), and Goat anti-HRP- 647. Secondary staining was performed at 4 ˚C for at least 3 days, in cases of dim result, we lengthen the incubation time to 4-5 days. Vectashield antifade mounting media was used and brains were mounted as described in (Kelly, Elchert, and Kahl 2017).

5.2.5 Fly Brain Imaging and quantification

Confocal images were collected as described in (Xiong et al. 2010) 10X and 40X objectives were used to collect images of the brain or specifically the mushroom bodies. At least 5 brains of males and 5 brains of females were imaged per genotype and condition. We used a 2 μm step size for our Z stacking. We used Volocity software and the line drawing tools to measure the width of the alpha lobe. Each dot in the plot is a mean of 4 width measurements per brain (2 per lobe).

5.3 Results

5.3.1 Biased screen for targets of degeneration in the fly eye

We used the fly eye model to discover the potential pathways by which DLK promotes lethality, using the eye tissue screen. Based on previous RNA-seq data, from an NGF withdrawal paradigm in DRG cultures (Lewcock paper), we chose fly homologs of subsets of DLK-regulated genes and screened for targets that can suppress eye degeneration. This is a faster method to find targets and study them in our adult brain model. We looked at a series of RNAi lines (Table 5-1). We assayed genes in the following groups. JNK signaling, ISR pathway, transcription factors, and cell death pathway genes (Table 5-2).

To drive the expression of each RNAi or overexpression line in our DLK induced eyes, we used GMR-Gal4; UAS-*Wnd* (DLK) in the presence of either a UAS-specific RNAi/overexpression line or a UAS-Control RNAi/overexpression line. The result for each category we tested was as follows:

JNK Signaling

Known targets of MAPK signaling such as *Fos, Bsk* (*JNK*), *Jra* (*Jun*) RNAis, or dominant negatives suppressed the rough eye phenotype caused by overexpression of DLK (Figure 5-1). This is consistent with our expectation as all these genes are known downstream targets of the DLK - JNK pathway.

Integrated Stress Response (ISR) Pathway

The NGF withdrawal paradigm in cultured DRGs has proposed a role for DLK in activating ISR and contributing to cell death (Larhammar, Huntwork-Rodriguez, Jiang, et al. 2017). PERK, one of the known kinases in this pathway, and its downstream effector ATF4 get phosphorylated which causes a global halt on translation following the specific translations for genes with ATF4 activating sequence (Larhammar, Huntwork-Rodriguez, Jiang, et al. 2017). Flies have two of the kinases in ISR; GCN2 and PERK. We tested both *GCN2* (*dGCN2*) and *PERK (dPERK or PEK*) along with *Cryptocephal* (*Crc*), a member of the CREB/ATF pathway in flies with high similarity to ATF4 (Lee et al. 2015; Pomar et al. 2003; Olsen et al. 1998; Santoyo et al. 1997). When we tested two RNAi lines for both *GCN2* and *PERK*, we noticed that offspring with the right genotype carrying either *GCN2* or *PERK* RNAi and UAS-*wnd* failed to eclose. Those that did eclose show no suppression of the rough eye phenotype and the eye size was even smaller than *Wnd* overexpression alone (Figure 5-1). These observations suggest that the ISR pathway is either developmentally required or does not work downstream of DLK to cause neurodegeneration in the

eye. It is also possible that ISR is still downstream of DLK, but its activation is neuroprotective and removing it makes the phenotype worse. *ATF4* (*Crc*) knockdown showed no effect in suppressing the rough eye phenotype.

Transcription/ Translation Factors:

We tested a series of transcription/translation factors. *Vrille (Vri)*- homolog of NFIL3 is a transcription factor previously shown to be activated via Protein Kinase A (PKA) contributing to regeneration (MacGillavry et al. 2009). It has also been associated with ALS motor neuron loss (Tamai et al. 2014). *Thor*, homolog of EIF4EBP 1 and 2, a translation initiation factor shown to be affected by DLK activation in the NGF withdrawal paradigm (Larhammar, Huntwork-Rodriguez, Jiang, et al. 2017). *SoxN* and *Pointed* (*Pnt*)- a transcription factor and homolog of ETS-1 with with similarity to ELK, are two other genes affected by DLK activation in the (Larhammar, Huntwork-Rodriguez, Jiang, et al. 2017) dataset. *Rps6,* Ribosomal protein S6 (Rsp6) homolog of mammalian Rps6 which encodes a key component of the small (40S) ribosomal subunit was also among the candidates we tested. Reduction in the expression of none of these genes suppressed the rough eye phenotype caused by overexpression of DLK.

Cell Death Pathway

To assess whether caspase dependent apoptosis is involved in the neuronal loss, we made use of a baculovirus P35 pan-caspase inhibitor (LaCount et al. 2000; Hay, Wolff, and Rubin 1994) and saw no eye suppression. Inhibition of JNK mediated apoptosis can lead to activation of necrosis dependent cell death (M. Li et al. 2019) which can be the reason we didn't see a suppression using P-35 overexpression. A key driver of Wallerian degeneration – a programmed pathway of axonal destruction - is the TIR-domain protein Sarm1, which functions as a NADase enzyme, degrading the essential metabolite NAD+ (Essuman et al. 2017; Gerdts et al. 2015). Yang

et al. observed that genetic inhibition of MAPK signaling could blunt degeneration induced by ectopic activation of Sarm1 in DRG explants, and proposed a role for MAPK in promoting degeneration downstream of Sarm1 (Yang et al. 2015). In our eye screen, we observed a complete and partial rescue of the eye phenotype by two of the three *Sarm* RNAi lines, the other one has no positive effects on the rough eye and size and degeneration of the eye (Figure 5-1).

With our screen, we found out that the ISR pathway is developmentally required, and inhibition of caspase dependent cell death is not sufficient to rescue the eye phenotype.

5.3.2 Acute induction of DLK/Wnd in the adult brain leads to premature lethality.

To assess whether acute induction of DLK/Wnd is sufficient to cause degeneration and lethality in adult animals, *Geneswitch (GS)-elav* Gal4*;* UAS-*DLK/wnd,* and *GS-elav* Gal4 *(Control)* flies were shifted to food containing 200 µM RU486 or vehicle (80% ethanol), 5-6 days post eclosion. Both male and female flies with *Wnd* overexpression showed a 50% reduction in their life span compared to the controls (Figure 5-2A-B). Females with UAS-*DLK/Wnd* on vehicles showed a slightly reduced lifespan (Figure 5-2B).

5.3.3 Neuronal overexpression of DLK causes degeneration in the mushroom bodies lobes

We wanted to probe whether our findings from the eye screen are relevant for whole animal survival in a non-developmental paradigm in adult animals.

Initially, we asked whether overexpression of Wnd/DLK acutely in the brain leads to synapse and neuronal loss. Grace Zhai's lab has shown that TDP-43 R406W overexpression leads to the formation of holes in the brain due to excessive loss of neurons and synapses (Ali, Ruan, and Zhai 2012). These holes were visualized by staining for markers such as Bruchpilot- a presynaptic marker. We used Brp (data not shown) and synapsin as markers for the presynaptic

proteins and also FasII. Fas II staining identifies alpha and beta lobes of mushroom bodies so we could examine whether DLK expression leads to alterations in their stereotyped morphology. flies were raised in parallel at 25 ℃ on normal food before shifting to RU486 or vehicle containing food at 5-6 days post eclosion. Animals fed on RU486 start expressing the UAS-*DLK/Wnd* causing overexpression and activation of DLK signaling. We observed excessive loss of axonal tracts in the alpha and beta lobes of the mushroom bodies 12 days post induction of DLK/Wnd (Figure 5-3A-C and 5-4A). Using Brp and Synapsin staining, we did not observe any vacuolization in most of the brains analyzed (15-20). We did have one brain that showed holes in the synapsin staining and this brain has completely lost its mushroom body structure as well (Figure 5-4B). Most probably, the animals with excessive degeneration and vacuolization in their brain are dead before we can assess their brains.

5.3.4 Axonal disintegration and loss is starting as early as 4 days after acute induction of Wnd

As shown in Figure 5-3A and 5-4A-B, we observed severe axonal loss and degeneration 12 days post DLK/Wnd induction. We wanted to see how early this degeneration is starting, so we examined two earlier time points: day four and day eight. Interestingly, we noticed that axonal loss is starting as early as day four as mushroom body alpha lobes show less width. The alpha lobe still has its stereotypical morphology but is thinner than the control condition. This specific difference is seen in both sexes (Figure 5-5A-C). At day eight, although the width of the lobe is not significantly less than day four, morphological disintegration of the alpha and beta lobes is observed (Figure 5-6A); as there are round bulbous structures at the tip of both alpha and beta lobes as if the axons are retracting or degenerating at the tip (Figure 5-6A'-A'').

5.3.5 Premature lethality induced by Wnd overexpression is JNK dependent

Following up on the eye data, we looked at the possible role of JNK in lethality caused by induction of DLK/Wnd in adults, we used JNK dominant negative (JNK DN) transgene flies. This transgene has been shown to effectively stop the activity of JNK (Weber, Paricio, and Mlodzik 2000). JNK dominant negative completely rescues the premature lethality of DLK induction in both males and females. Showing that JNK is for sure downstream of this phenotype.

5.3.6 Loss of neurons after DLK/Wnd induction is caspase dependent apoptosis

To follow up on our eye screen and to assess whether caspase dependent apoptosis is involved in the neuronal loss we observe after inducing DLK in adults, P35 pan-caspase inhibitor was used. Strikingly, and in contrast to our findings in the eye, ectopic expression of P35 in adult brains lead to almost complete rescue of the lethality (Figure 5-8 A-B).

5.3.7 Sarm knockdown partially rescues lethality in a parallel pathway

To evaluate whether Sarm1 and DLK are in the same pathway leading to neuronal degeneration and death, we used the RNAi line that had rescued the eye phenotype along with UAS- *DLK/Wnd* and measured the survival of flies with Sarm knockdown. Interestingly, we observed a partial rescue of the lethality in males (Figure 5-9A). However, the female lifespan result was more complicated. Control flies on vehicle (ethanol) food showed a longer lifespan (Figure 5-9B). It has been previously proposed that there is a leaky expression of *Geneswitch elav* Gal4, especially in cases of expressing RNAi lines (Scialo et al. 2016) and this may be a reason the control flies are showing a difference in their lifespan. This also raises the question of whether knocking down Sarm can affect lifespan in a pathway parallel to DLK/Wnd induction of MAPK (JNK). This possibility is raised because the females and males that are on the drug and expressing DLK and Sarm RNAi are living half the controls on the vehicle. Deciphering these results needs

more experiments. It would be informative to perform whole brain dissection and see how Sarm knockdown affects the degeneration and cell death in the brain.

5.4 Discussion

In this study, we sought to characterize how DLK/Wnd activation leads to neuronal degeneration and cell death in the adult central nervous system. The fact that acute induction of DLK was sufficient to cause premature lethality after a few days of induction (Figure 5-2A-B) was striking and provided an avenue to study the effects of excess levels of activated DLK and better characterize the mechanism by which DLK contributes to neuronal loss and degeneration in the context of diseases.

DLK implication in neuronal death has been reported in mouse DRGs following NGF withdrawal (Ghosh et al. 2011; Larhammar, Huntwork-Rodriguez, Jiang, et al. 2017) and mouse retinal ganglion cells (RGCs) following optic nerve injury (Fernandes et al. 2014; Watkins et al. 2013; Welsbie et al. 2013). In both cases, DLK deletion is sufficient to rescue lethality. To find possible effectors of the DLK signaling pathway we turned to published sequencing data (Larhammar, Huntwork-Rodriguez, Jiang, et al. 2017) and after finding orthologs of some of the top hits from the sequencing data in *Drosophila*, we used the eye model to screen for genes responsible for the degeneration phenotype in the eye. One challenge in this method is the fact that we cannot separate the genes that are developmentally required for eye development from the genes that act downstream of DLK causing degeneration. Although knockdown of *PERK* and *GCN2* kinases from the ISR pathway did not rescue the eye phenotype, we cannot rule out the fact that they may be responsible for degeneration in mature neurons of the central nervous system. Moreover, the fact that the absence of ISR in a DLK overexpression background made the eye phenotype even worse, suggests that both ISR response and DLK signaling are working in parallel

and influence the formation of the eye. Although the absence of a severe eye phenotype when ISR kinases are knocked down individually raises the possibility of them working downstream of DLK activation but having a neuroprotective role.

The developmental paradigm of eye phenotype may not be the same as DLK activation in the CNS. From our data, we saw differences with dSarm and P35 in the fly eye model and adult induction of DLK. P35 is known to be an inhibitor of cleaved Dcp-1 and DrICE caspases (Hay, Wolff, and Rubin 1994) and therefore suppressor of apoptosis. We did not see suppression of the eye size and degeneration phenotype; however, we saw the complete rescue of premature lethality upon expression of P35 in adult neurons. This incongruence is possibly the result of activating two separate arms of JNK signaling. Li et al have previously shown that JNK signaling can lead to apoptotic and developmental apoptotic-independent defects in the fly eye (M. Li et al. 2019) and that the latter defects cannot be rescued by the expression of P35 or mutations in caspases such as Dronc (M. Li et al. 2019). The study suggested a new cell death paradigm via necrosis showing inhibition of apoptosis by P35 enhances necrosis dependent death in the fly eye (M. Li et al. 2019). Some follow-up experiments to confirm this hypothesis is to use heterozygous mutant of Dronc along with overexpression of DLK/Wnd and UAS- p35, if this rescues the eye phenotype, it will show that DLK/Wnd overexpression can activate both arms of JNK signaling.

One of our findings in this study was that Sarm1 knockdown can rescue the eye phenotype and enhance the survival of adult flies after DLK overexpression. However, we noticed that control flies carrying *dSarm* RNAi on the vehicle are living longer than the control RNAi on the vehicle. If the leaky expression of *Geneswitch* Gal4 is the reason we see this phenotype, then Sarm1 partial knockdown can extend the life span of the flies independently of DLK. The connection between DLK and Sarm1 has yet to be fully elucidated. Yang et al. observed that genetic inhibition of

MAPK signaling could blunt degeneration induced by ectopic activation of Sarm1 in DRG explants and proposed a role for MAPK in promoting degeneration downstream of Sarm1 (Yang et al. 2015). Walker et al. identified an upstream role for Sarm1 with the finding that MAPK signaling enhances the stability/turnover of NMNAT2 in both mouse DRG and fly motoneurons (Walker et al. 2017). Connections between DLK and NMNAT2 are also noted via their shared regulation by the PHR ubiquitin ligase (Babetto et al. 2013; Xiong and Collins 2012; Collins et al. 2006; Nakata et al. 2005). It is possible that Sarm1 and DLK can get activated in similar contexts and are both contributing to cell death and degeneration in parallel pathways.

We have considered thus far cell-autonomous mediators of lethality, but contributions of other cells to the lethality are worth considering since the RNA seq data has identified many secreted proteins as regulated by DLK. Then pro-degenerative roles of glial cells are a general point that can be made with references to mammalian literature as well. Eiger (Egr), the fly homolog of TNF-α is a good candidate to explore the non-cell-autonomous contributions of DLK activation to degeneration. The *Drosophila* system provides the genetic tools and simpler manipulation to study this non-cell-autonomous response and mechanisms of toxicity in the nervous system.

Table 5-1 RNAi lines used in our screen and later for testing suppression of lethality

Fly line	Reference
Wnd RNAi	VDRC - 26910
DGCN2 RNAi (II)	VDRC - 32664
DGCN2 RNAi (II)	VDRC - 103976
PEK RNAi (II)	VDRC- 16427
PEK RNAi (III)	Bloomington - 35162
Bsk RNAi	VDRC -
Dfos RNAi	
Jra(Jun) RNAi	VDRC
Jra RNAi	Bloomington - 31595
ATF3 RNAi	Bloomington - 26741
Crc (ATF4) RNAi	Bloomington 25085
Dsarm RNAi	VDRC – 104812/KK
Dsarm RNAi	VDRC – 102044/KK
Dsarm RNAi	VDRC – 105521/KK
Vrille RNAi	Bloomington - 25989
Vrille RNAi	Bloomington - 40862
Thor RNAi	Bloomington - 36815
Thor RNAi	Bloomington - 36667
Galectin RNAi	Bloomington - 34880
Pnt RNAi	Bloomington - 35038
SoxN RNAi	Bloomington - 25996
Rsp6 RNAi	Bloomington - 32418
UAS – *P35*	(Hay et al., 1994)
Aldh RNAi	Bloomington

Table 5-2 Groups of genes tested for their ability to rescue the eye phenotype

Group Name	Genes
JNK Signaling	*Fos* , *Bsk* (JNK), *Jra* (Jun)
Integrated Stress Response Pathway	*dGCN2* , *dPERK or PEK* , Crc
Transcription/ Translation Factors	*Fos* , *Jra* (Jun), *Vrille (Vri), Thor* , *SoxN* , *Pnt, Rps6*
Cell Death Pathway	*Sarm1* , P35

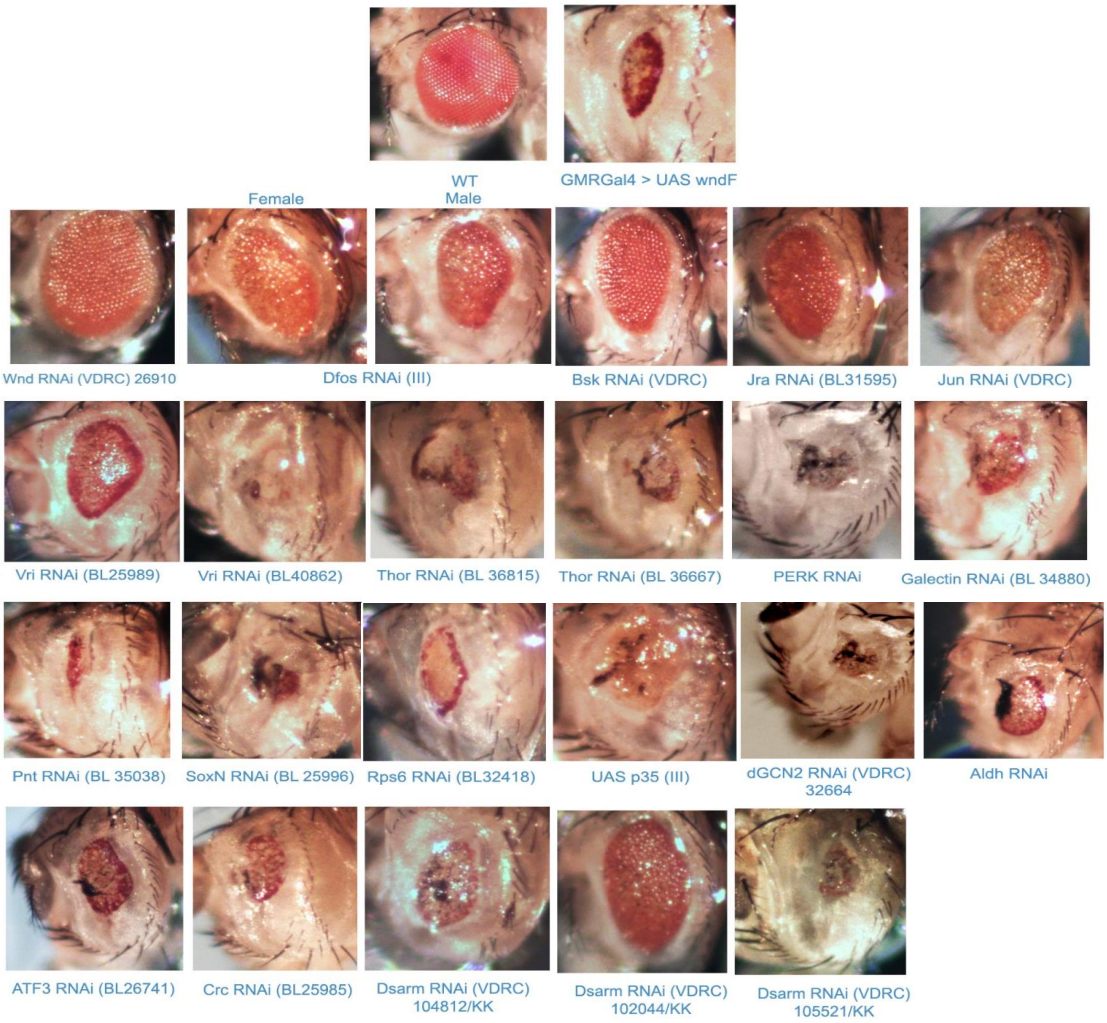

Figure 5-1 ***Biased screen in the fly eye, with the purpose of finding suppressors of the rough eye phenotype observed in overexpression of DLK/Wnd background.***

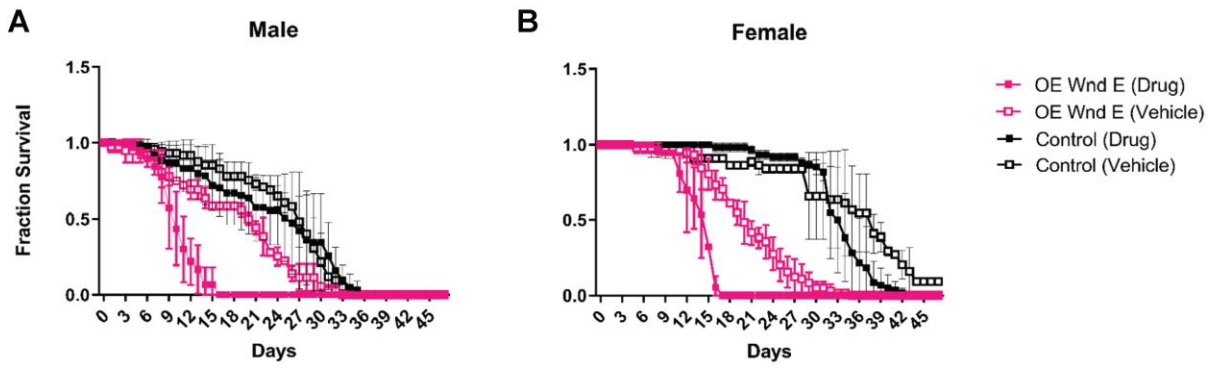

Figure 5-2 ***Acute induction of DLK/Wnd in adult brain leads to premature lethality.*** *15-20 males (A) or females (B) were collected 5 days post eclosion per genotype/treatment and were kept and assayed for survival every day. 3-4 vials for each genotype/treatment were used and each vial's fraction survival was considered as one n. Drug condition is food containing 200 µM of RU486 and vehicle food contained the equal volume of 80% ethanol.*

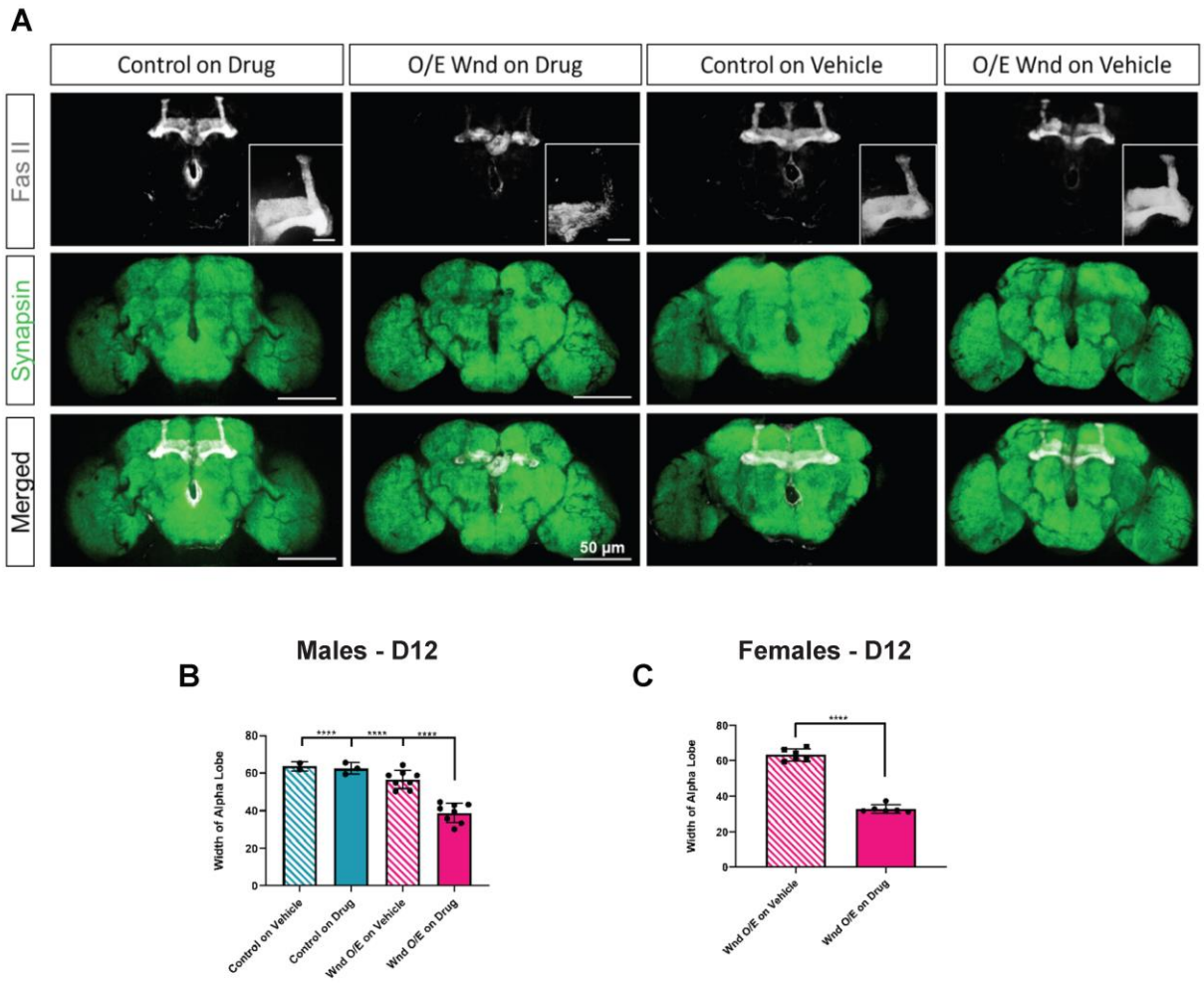

Figure 5-3 ***Neuronal overexpression of DLK/Wnd causes degeneration in the mushroom bodies lobes.*** *15-20 males/females (A) were collected 5 days post eclosion per genotype/treatment. Drug condition is food containing 200 µM of RU486 and vehicle food contained the equal volume of 80% ethanol. 12 days post shift on food containing drug/vehicle, flies were collected and their whole brain was dissected/washed and stained. 10X images were taken using a confocal microscope. Scale bar is 50 µm. N=6-8 for all conditions only control males on vehicle and drug has n=3. (B and C) quantification of alpha lobe width, average of 4 measurement (2 per alpha lobe when alpha lobe is still not completely degenerated) is used for each point.*

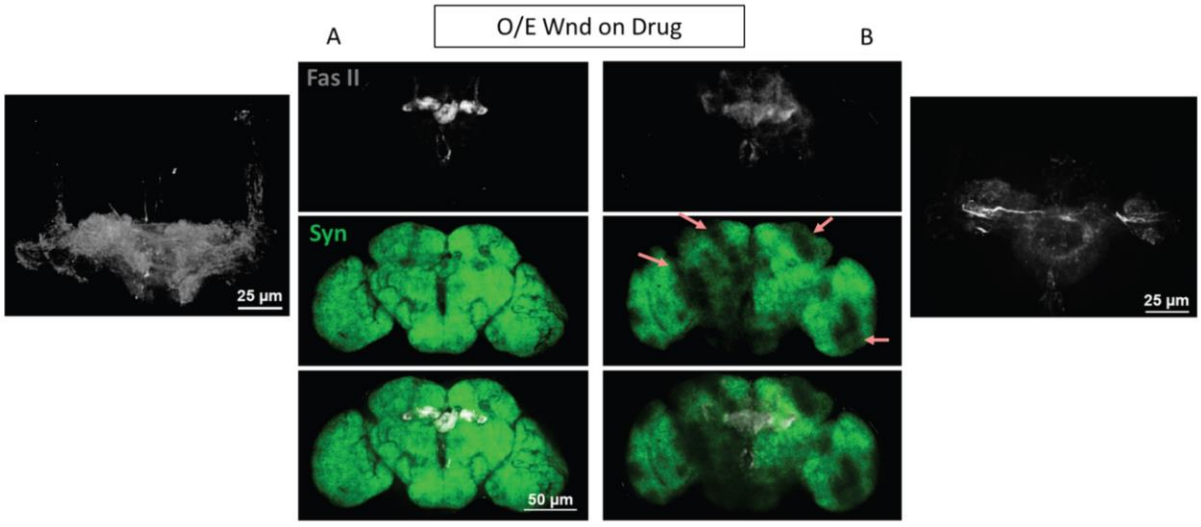

Figure 5-4 ***Synapsin loss in a male brain at Day 12 post DLK/Wnd induction.*** *(A) and (B) are two different brains at day 12 post shift on drug/vehicle containing food. 10X images were taken using spinning disk confocal. The insets are same brains imaged with 20X objective. Syn =synapsin, Fas II = Fasciculin.*

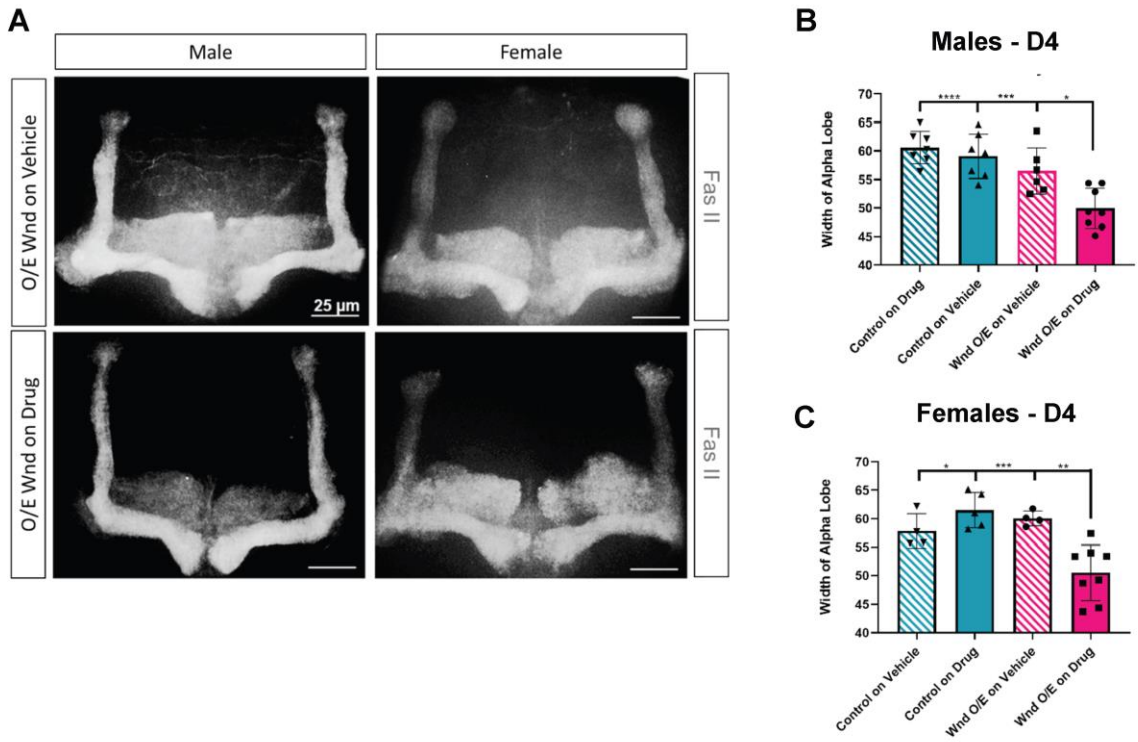

Figure 5-5 ***Axonal disintegration and loss is starting as early as 4 days after acute induction of DLK/Wnd.*** *15-20 males/females (A) were collected 5 days post eclosion per genotype/treatment and were transferred to the special food per condition. Drug condition is food containing 200 µM of RU486 and vehicle food contained the equal volume of 80% ethanol. 4 days post shift on food containing drug/vehicle, flies were collected and their whole brain was dissected/ washed and stained with fasiculin (Fas II). 40X images were taken using a confocal microscope. Scale bar is 25 µm. N=4-8 per condition. (B and C) Quantification of alpha lobe width. Each point is average of 4 measurements (2 per alpha lobe when alpha lobe if it is still not completely degenerated.*

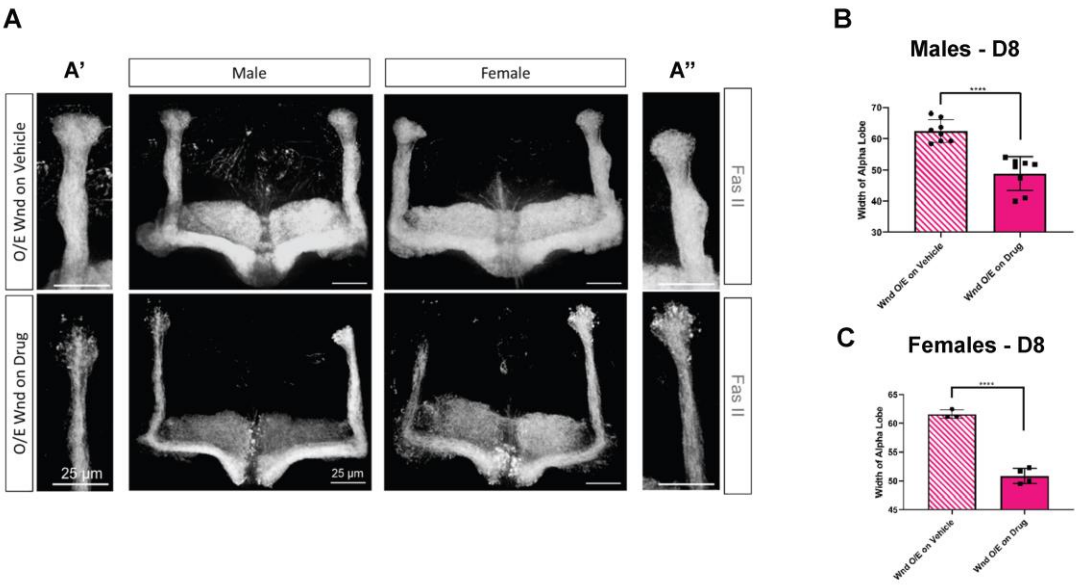

Figure 5-6 ***Axonal disintegration and loss has progressed drastically 8 days after acute induction of DLK/Wnd.*** *15-20 males/females (A) were collected 5 days post eclosion per genotype/treatment and were transferred to the special food per condition. Drug condition is food containing 200 µM of RU486 and vehicle food contained the equal volume of 80% ethanol. 8 days post shift on food containing drug/vehicle, flies were collected and their whole brain was dissected/ washed and stained with fasiculin (Fas II). 40X images were taken using a confocal microscope. Scale bar is 25 µm. N=4-8 per condition. A' and A'' are insets of male and female alpha lobe respectively (B and C) Quantification of alpha lobe width. Each point is average of 4 measurements (2 per alpha lobe when alpha lobe if it is still not completely degenerated.*

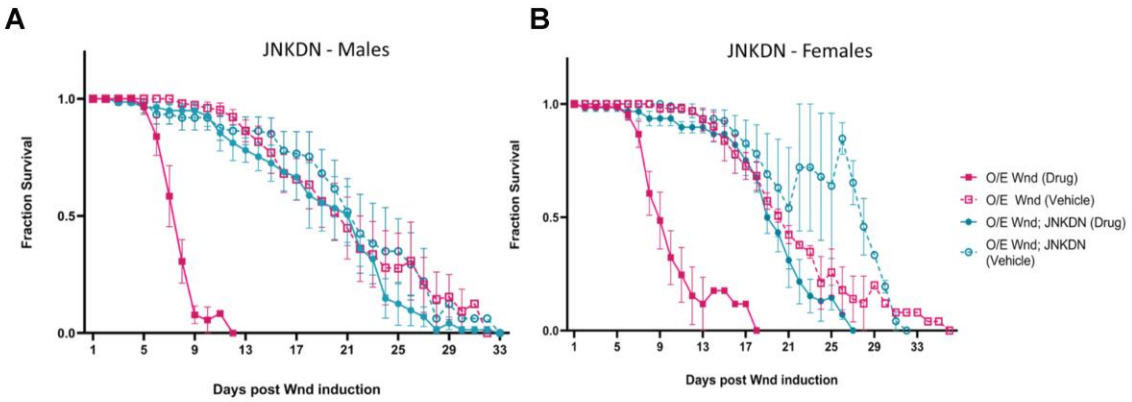

Figure 5-7 ***Premature lethality induced by DLK/Wnd overexpression is JNK dependent.*** *15-20 males (A) or females (B) were collected 5 days post eclosion per genotype/treatment and were kept and assayed for survival every day. 4 vials for each genotype/treatment were used and each vial's fraction survival was considered as one n. Drug condition is food containing 200 µM of RU486 and vehicle food contained the equal volume of 80% ethanol. JNK DN = Jun N terminal kinase Dominant negative is sufficient to rescue the lethality in both male and females.*

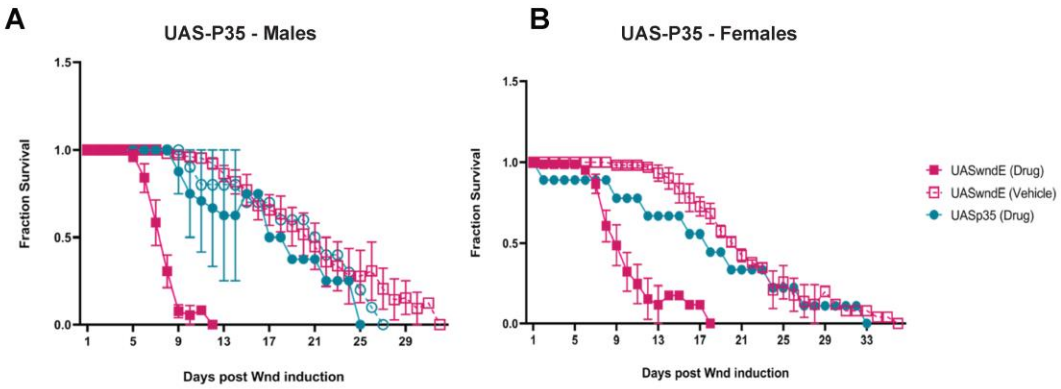

Figure 5-8 ***Apoptosis is involved in the lethality caused by DLK/Wnd induction.****15-20 males (A) or females (B) were collected 5 days post eclosion per genotype/treatment and were kept and assayed for survival every day. Three vials for each genotype/treatment were used and each vial's fraction survival was considered as one n. Drug condition is food containing 200 µM of RU486 and vehicle food contained the equal volume of 80% ethanol. Inhibiting apoptosis can rescue the premature lethality. N=3-6 after mixing males and females*

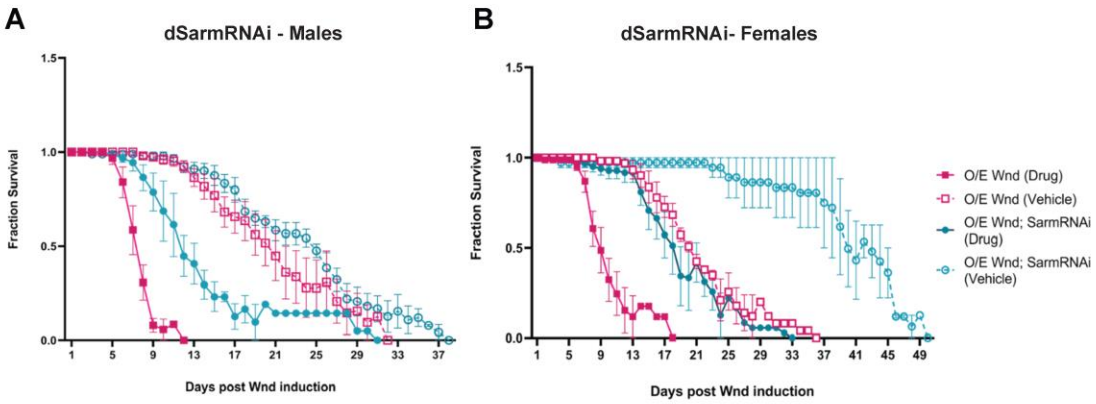

Figure 5-9 ***Knocking down Sarm partially rescues the lethality.*** *15-20 males (A) or females (B) were collected 5 days post eclosion per genotype/treatment and were kept and assayed for survival every day. 4-5 vials for each genotype/treatment were used and each vial's fraction survival was considered as one n. Drug condition is food containing 200 µM of RU486 and vehicle food contained the equal volume of 80% ethanol. Knocking down Sarm partially rescues the lethality but also extend the lifespan of female flies.*

Chapter 6 Concluding Remarks and Future Directions

The evolutionary conserved Dilucine Zipper Kinase (DLK) has been studied extensively in contexts of axonal injury, neuronal stress, and neurodegenerative diseases (Asghari Adib, Smithson, and Collins 2018; Tedeschi and Bradke 2013). To understand the contradictory nature of DLK responses, which range from degeneration and cell death to new axonal growth and circuit repair, my thesis aimed at identifying the molecular pathways that are regulated by DLK. I used two paradigms, a mouse model of peripheral nerve injury (PNI) and a fly model of neurodegeneration. This work led me to several new conclusions and ideas, which I would like to summarize here.

6.1 DLK is not essential for axonal regeneration

DLK has been reported to be necessary for axonal growth in invertebrates (Xiong et al. 2010; Hammarlund et al. 2009; Collins et al. 2006). However, recent studies in zebrafish have shown that DLK alone is not sufficient to stop functional regeneration (Adula et al. 2021). DLK and LZK (MAP3K13), a sister kinase with high similarity to DLK, are both required for regeneration post injury (Adula et al. 2021). We also saw that knocking out *Dlk* alone in motor neurons does not stop functional regeneration: apart from an initial delay, axons eventually reinnervate the muscles. This finding led us to hypothesize that DLK activation alone should gate other responses that are separate from regeneration and knowing the downstream targets of DLK activation which was the goal of our study can help establish what DLK activation alone does to neurons. It will be interesting in the future to look at individual knockout of *Lzk* and *Dlk/Lzk* double

knockout to find out which part of the responses to injury can be compensated by LZK in the absence of DLK.

6.2 DLK-regulated genes include many secreted proteins that may regulate responses by other cells to axonal injury

Our RiboTag profiling of DLK responses to axonal damage showed that most Regenerative Associative Genes (RAGs) become strongly upregulated in the *Dlk* KO MNs, hence can be induced independently of DLK function. However, we identified a distinct set of genes that strongly require DLK for their induction in injured MNs. These include neuropeptides, immune responses, and upstream regulators of complement, an arm of innate immunity. These DLK-regulated genes turned our attention to non-cell-autonomous responses gated by DLK activation.

6.3 The regulation of neuropeptides by DLK suggests a new candidate function in neuroprotection.

Neuropeptides in general are known for their neuroprotective effects, their role in learning and memory, and their normal neuromodulatory role in a healthy nervous system (D'Alessandro et al. 2014; Borbély, Scheich, and Helyes 2013; Cervia and Casini 2013; McCown 2009; Somogyvári-Vigh and Reglodi 2004). Previous work in the field has focused on the role of DLK in promoting neuronal death. However, our findings that DLK can induce neuropeptide expression suggest the possibility that it may also stimulate neuroprotective mechanisms. This means inhibiting DLK alone may have negative as well as positive effects, consistent with recent clinical trial data (Katz et al. 2022). Combining our understanding of neuropeptides and studying it in the context of DLK activation can help decipher the neuroprotective arms of DLK activation from its deleterious aspects. This can lead to the design/ discovery of better therapeutics as well.

6.4 DLK directs the activation of complement

We also found members of the complement cascade such as all subunits of C1q and MASP1 regulated by DLK signaling in neurons. MASP1 can activate a complement cascade independent of C1q. This can be why knocking out C1q is not enough to rescue synapse loss. Changes in the transcriptional levels of C1q and MASP1 is not enough to explain how they become activated. The absence of an actual damage in the spinal cord in the PNI model, suggests that there should be another mechanism to induce complement cascade. Another interesting question to address is whether known complement activation in other contexts such as developmental pruning or neurodegenerative diseases require DLK. Our comparison of our DLK-gated DEGs with other paradigms of DLK activation revealed that in sensory and cortical neurons, activation of DLK can lead to increased expression of all C1q subunits in neurons. Induction of complement in early symptomatic and symptomatic stages of ALS in motoneurons can be due to DLK activation and is worth exploring.

6.5 DLK is required for synapse loss and inflammation in axotomized motor neurons

Synapse loss post PNI is an old but still poorly understood phenomenon (Alvarez et al. 2020; Blinzinger and Kreutzberg 1968) and the role of microglia in this type of synapse loss is debated. Termed “synaptic stripping,” this phenomenon has multiple steps from intrinsic changes to gliosis. We found that the DLK signaling pathway within neurons is required for the removal of upstream inputs onto these axotomized cells. Although DLK has been shown to affect synaptic levels in kinesin-3 mutants’ models and has also been shown to affect synaptic levels in cultured cortical neurons (Verschuuren et al. 2019; J. Li et al. 2017), this is the first study to link it to synaptic stripping. Although the contribution of innate immunity and microglia have been observed in developmental pruning and some models of neurodegenerative disease, The

mechanism by which these responses are controlled are not fully understood (Gomez-Arboledas, Acharya, and Tenner 2021; Schartz and Tenner 2020; Carpanini, Torvell, and Morgan 2019). In future studies, it is important to look at the mechanism by which complement activation in axotomized neurons can help remove synaptic inputs. Another interesting question is whether DLK activation can contribute to synapse loss in ischemic models or traumatic brain injuries and if it does, is it through a similar pathway/mechanism, or can DLK activation affect synapses in a context-dependent manner?

6.6 DLK regulates neuropeptide signaling in multiple paradigms, cell types, and organisms

The expression of neuropeptides, immune response, and inflammation in our injury model posit the question of whether DLK regulates common target genes in other paradigms of activation. Our analysis comparing our dataset with other existing datasets showed that neuropeptide signaling is gated by DLK in multiple paradigms of injury (MN and sensory), disease model (ALS), and fly model of DLK overexpression. We have also shown that cultured embryonic neurons have the least similarity in their DLK activated genes with other datasets, suggesting different roles for DLK signaling pre and post development.

DLK is well known for its cell-autonomous phenotypes in injured/stressed neurons. My thesis work has proposed a new role for DLK in triggering non-cell-autonomous responses following axonal damage. Whether DLK activation leads to inflammation and synapse loss or axon degeneration and neuronal death, there seems to be an overarching theme of neuronal plasticity at play. These DLK gated forms of structural plasticity equips the nervous system with a broad spectrum of mechanisms to adapt to damage.

Appendices

Appendix 1 Unique Gene Sets in Sensory and MNs post Injury

Gene set enrichment analysis for the unique differentially expressed genes (DEGs) 3 days post sciatic nerve crush (SNC).

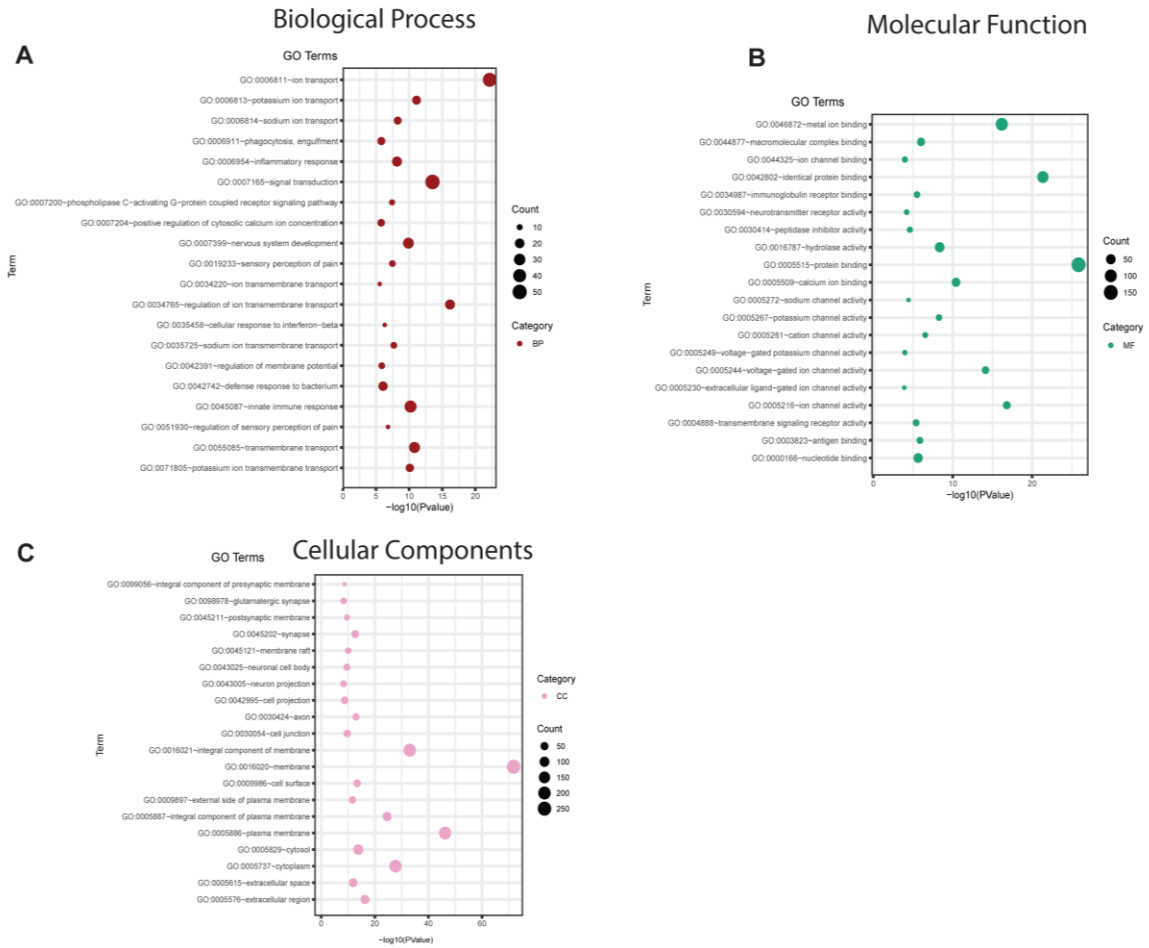

Figure 0-1 ***bubble plots of GO Terms with sensory neuron specific DEGs.*** *(A) Ion transport and signal transduction are among the overrepresented biological processes Terms. (B) Ion Channel and receptor activity MF Terms are highly enriched in sensory neurons post injury. (C) There are glutamatergic and synaptic associated Terms in the cellular component category.*

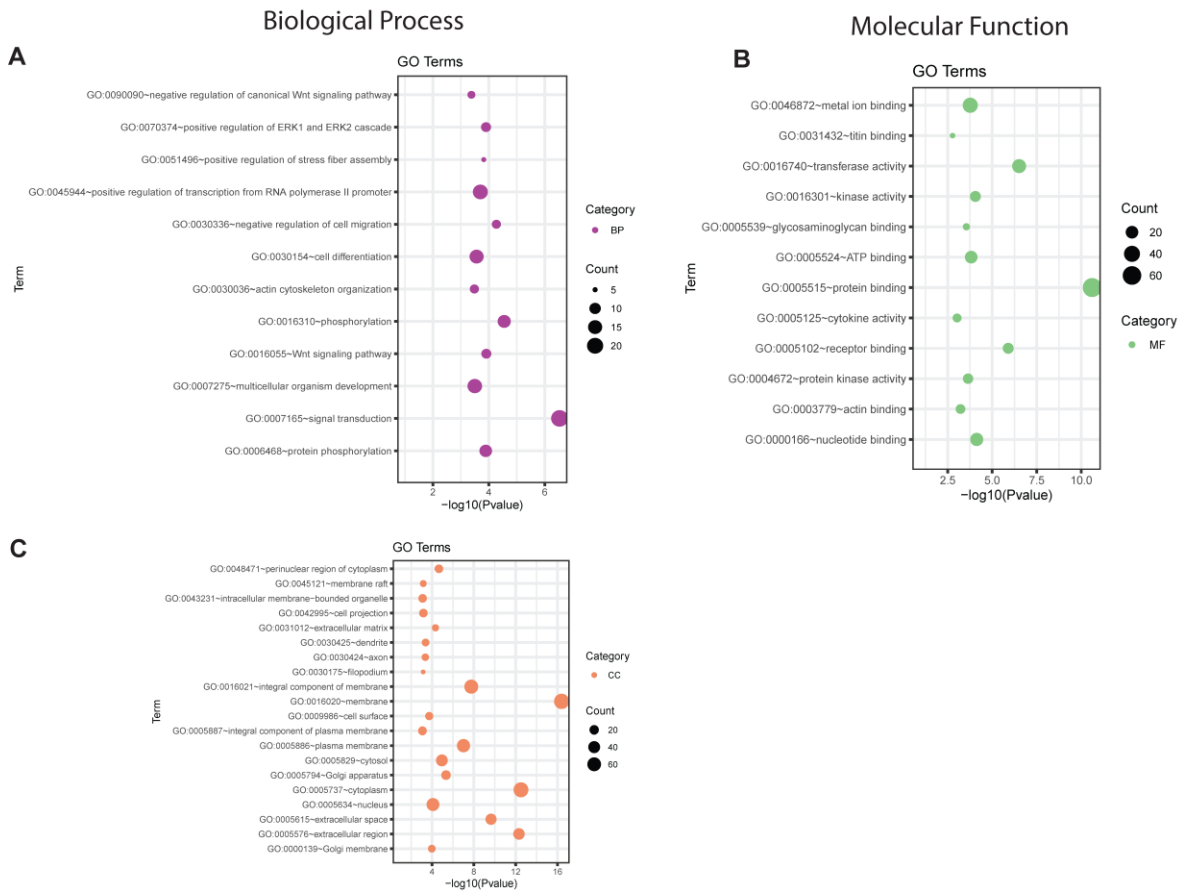

Figure 0-2 ***bubble plots of GO Terms with motoneurons neuron specific DEGs****. (A) Regulation of ERK and Wnt signaling along with cytoskeletal organization Terms are the unique overrepresented Biological Process Terms in axotomized MNs. (B) Kinase and cytokine activity and multiple Terms associated with binding to actin, proteins and nucleotides are highly enriched Molecular Function Terms in MNs post injury. (C) Membrane rafts, Golgi, axon, and dendrites are enriched in the cellular Component category.*

Appendix 2 Profiling Analysis Script

This appendix contains the codes used for the analysis of the profiling dataset. We analyzed the data when the University was using the Flux system and therefore the jobs were submitted based on the requirements of the Flux system. The followings are the Bash script used to submit jobs using ubuntu on my laptop.

Adaptor Trimming, mapping, and sorting step:

```
cd /scratch/lsa_flux/ unique name /RNA_seq/Fastq/Sample_1211${PBS_ARRAYID}
mkdir star_output

echo Begin adaptor_quality_trimming_bbduk
date +"%T"

# A loop to go through all the lanes

for i in {4..8};
do
        #echo ${PBS_ARRAYID}*${i}_R1_001.fastq.gz
        bbduk.sh -Xmx1g in1=1211${PBS_ARRAYID}_L00${i}_R1_001.fastq.gz
in2=1211${PBS_ARRAYID}_L00${i}_R2_001.fastq.gz
out1=1211${PBS_ARRAYID}_L00${i}_R1_001.trimmed.fastq.gz
out2=1211${PBS_ARRAYID}_L00${i}_R2_001.trimmed.fastq.gz minlen=25 qtrim=rl
trimq=10 ktrim=r k=25 mink=11
literal='AGATCGGAAGAGCACACGTCTGAACTCCAGTCA,AGATCGGAAGAGCGTCGT
GTAGGGAAAGAGTGT' ktrim=r k=23 mink=11 hdist=1
done

echo adaptor_quality_trimming_bbduk Finished
date +"%T"

echo Begin Gunzip
gunzip *.trimmed.fastq.gz

echo unzipping Finished
date +"%T"

echo Star alignment begun
###Note - using star/2.5.2a
date +"%T"
```

```
# A loop to go through all the lanes while mapping to the genome

for i in {4..8};
do
        STAR --runThreadN 3 --genomeDir /scratch/lsa_flux/adibe/RNA_seq/Ref --readFilesIn
1211${PBS_ARRAYID}_L00${i}_R1_001.trimmed.fastq
1211${PBS_ARRAYID}_L00${i}_R2_001.trimmed.fastq --quantMode TranscriptomeSAM
GeneCounts --outSAMtype BAM SortedByCoordinate --outBAMsortingThreadN 3 --
outFileNamePrefix
/scratch/lsa_flux/adibe/RNA_seq/Fastq/Sample_1211${PBS_ARRAYID}/star_output/1211${P
BS_ARRAYID}_L00${i}_
done

echo Star alignment Finished


cd /scratch/lsa_flux/unique name/RNA_seq/AllBam/


echo Begin merging
date +"%T"

# Merging the Lanes

samtools merge 1211${PBS_ARRAYID}.merged.bam
1211${PBS_ARRAYID}_L004_Aligned.sortedByCoord.out.bam
1211${PBS_ARRAYID}_L005_Aligned.sortedByCoord.out.bam
1211${PBS_ARRAYID}_L006_Aligned.sortedByCoord.out.bam
1211${PBS_ARRAYID}_L007_Aligned.sortedByCoord.out.bam
1211${PBS_ARRAYID}_L008_Aligned.sortedByCoord.out.bam

echo merging Finished
date +"%T"

# Post mapping quality Control
cd /scratch/lsa_flux/unique name/RNA_seq/AllBam/

echo QoRTs QC
date +"%T"

Alighned_DIR='/scratch/lsa_flux/adibe/RNA_seq/AllBam/'
for f in ${Alighned_DIR}/*.bam
do
        base=`basename ${f} .merged.bam`
```

```
        echo currently running ${base}...
QoRTs QC --generatePlots --maxReadLength 100 ${f}
/scratch/lsa_flux/adibe/RNA_seq/Ref/gencode.vM21.chr_patch_hapl_scaff.annotation.gtf
/scratch/lsa_flux/adibe/RNA_seq/QoRTs/${base}
done

echo QoRTs QC Finished
date +"%T"
```

The Deseq2 generated tables from QoRTs are used for the rest of the analysis. The rest of the analysis is performed in R language using the Rstudio interface.

```
library(DESeq2)


setwd("C:/~/RNA-seq (Hiseq)")
decoder_UnjCtl <- read.table("C:/~/RNA-seq Experiment/RNA-seq
(Hiseq)/Allcomparison.txt",header=T,stringsAsFactors=F)
directory <- "C:/~/RNA-seq Experiment/RNA-seq (Hiseq)/Tables"
sampleFiles <- paste0(decoder_UnjCtl$unique.ID,".dat")
sampleCondition <- decoder_UnjCtl$group.ID
sampleName <- decoder_UnjCtl$sample.ID
sampleTable <- data.frame(sampleName = sampleName,fileName = sampleFiles,condition =
sampleCondition)


dds <- DESeqDataSetFromHTSeqCount(sampleTable = sampleTable,directory =
directory,design = ~ condition)
dds$condition <- relevel(dds$condition, 'Control_N')

# any condition that is going to be used as a base for comparison should be used with relevel
function

dds.N <- DESeq(dds)
resultsNames(dds.N)

######## Prefiltering DESeq Object ########
# Only keep genes that have non-zero counts
keep <- rowSums(counts(dds.N)) >= 10
dds.N <- dds.N[keep,]


######### Rename rownames from ENSEMBL IDs to remove isoform number (decimal point)
########
# this will allow us to find the gene ids in ENSEMBL
geneid = rownames(dds.N)
```

```
geneid = unlist(lapply(geneid, function(x) {
  x <- strsplit(x,split='.',fixed=TRUE)[[1]][1]
  return(x)
}))
length(unique(geneid))==length(rownames(dds.N)) # making sure that we're not losing any
genes
rownames(dds.N) = geneid
head(rownames(dds.N))

resN <- results(dds.N)
resN <- resN[order(resN$padj), ]


# MA plots:
library("genefilter")
library("pheatmap")

resLFC_condition_Control_Inj_vs_Control_N = lfcShrink(dds.N,
coef="condition_Control_Inj_vs_Control_N", type="apeglm")
plotMA(resLFC_condition_Control_Inj_vs_Control_N, alpha = 0.05, main = "Control Injured vs
Naive", ylim = c(-3,3))

resLFC_condition_Control_Unj_vs_Control_N = lfcShrink(dds.N,
coef="condition_Control_Unj_vs_Control_N", type="apeglm")
plotMA(resLFC_condition_Control_Unj_vs_Control_N, alpha = 0.05, main = "Control
Uninjured vs Naive", ylim = c(-3,3))

resLFC_condition_DLKKO_Inj_vs_Control_N = lfcShrink(dds.N,
coef="condition_DLKKO_Inj_vs_Control_N", type="apeglm")
plotMA(resLFC_condition_DLKKO_Inj_vs_Control_N, alpha = 0.05, main = "DLK Inj vs
Control Naive", ylim = c(-3,3))

resLFC_condition_DLKKO_N_vs_Control_N = lfcShrink(dds.N,
coef="condition_DLKKO_N_vs_Control_N", type="apeglm")
plotMA(resLFC_condition_DLKKO_N_vs_Control_N, alpha = 0.05, main = "DLK Naive vs
Control Naive", ylim = c(-3,3))

resLFC_condition_DLKKO_Unj_vs_Control_N = lfcShrink(dds.N,
coef="condition_DLKKO_Unj_vs_Control_N", type="apeglm")
plotMA(resLFC_condition_DLKKO_Unj_vs_Control_N, alpha = 0.05, main = "DLK Uninjured
vs Control Naive", ylim = c(-3,3))


### heatmap
vsd <- vst(dds.N, blind = FALSE)
colnames(sampleTable)
```

```
colnames(dds.N)
plotPCA(vsd, "condition")

topVarGenes <- head(order(rowVars(assay(vsd)), decreasing = TRUE), 100)
mat  <- assay(vsd)[topVarGenes, ]
gns <- select(org.Mm.eg.db, row.names(mat), "SYMBOL", "ENSEMBL")
row.names(mat)[match(gns[,1], row.names(mat))] <- gns[,2]
mat  <- mat - rowMeans(mat)

anno <- as.data.frame(colData(vsd)[,"condition"])
rownames(anno) <- colnames(vsd)
cols = colorRampPalette(c("#FFFFCC", "#300033"))(30)
cols = colorRampPalette(c("blue", "white", "darkorange"))(30)
pheatmap(mat, annotation_col = anno, color = cols) #, border_color= 'black'

#anno <- as.data.frame(colData(vsd)[,"condition"])
#rownames(anno) <- colnames(vsd)
#pheatmap(mat, annotation_col = anno)


################### Annotate ENSEMBL IDs to gene symbols #################
# add 2 columns to results table: gene symbol and entrez ID
library("AnnotationDbi")
library("org.Mm.eg.db")

columns(org.Mm.eg.db)
resN$symbol = mapIds(org.Mm.eg.db,
                     keys=rownames(resN),
                     column="SYMBOL",
                     keytype="ENSEMBL",
                     multiVals="first")
resN$entrez <- mapIds(org.Mm.eg.db,
                      keys=row.names(resN),
                      column="ENTREZID",
                      keytype="ENSEMBL",
                      multiVals="first")


resN <- resN[order(resN$padj), ]
resdataN <- merge(as.data.frame(resN), as.data.frame(counts(dds.N, normalized=TRUE)),
by="row.names", sort=FALSE)

####### Now for each condition, depending on what is the comparison the following codes are
used
# DLKKO_Inj_vs_Control_N
```

```
res_DLKKOINJ_ControlN <- results(dds.N, contrast = c("condition", "DLKKO_Inj",
"Control_N"))
columns(org.Mm.eg.db)
res_DLKKOINJ_ControlN$symbol = mapIds(org.Mm.eg.db,
                    keys=rownames(res_DLKKOINJ_ControlN),
                    column="SYMBOL",
                    keytype="ENSEMBL",
                    multiVals="first")
res_DLKKOINJ_ControlN$entrez <- mapIds(org.Mm.eg.db,
                     keys=row.names(res_DLKKOINJ_ControlN),
                     column="ENTREZID",
                     keytype="ENSEMBL",
                     multiVals="first")


res_DLKKOINJ_ControlN <-
res_DLKKOINJ_ControlN[order(res_DLKKOINJ_ControlN$padj), ]

res_DLKKOINJ_ControlN <- merge(as.data.frame(res_DLKKOINJ_ControlN),
as.data.frame(counts(dds.N, normalized=TRUE)), by="row.names", sort=FALSE)


library(dplyr)
sig = 0.05
res_DLKKOINJ_ControlN_mutated <- res_DLKKOINJ_ControlN %>%
  mutate(padj_manual = p.adjust(pvalue, method = 'BH')) %>%
  mutate(significant.Up = log2FoldChange > 0 & padj <= sig) %>%
  mutate(significant.Down = log2FoldChange < 0 & padj <= sig) %>%
  mutate(type = case_when(log2FoldChange < 0 & padj <= sig ~ 'Down-regulated',
                      log2FoldChange > 0 & padj <= sig ~ 'Up-regulated',
                      TRUE ~ 'Unchanged'),
         expression_quantile = ntile(baseMean, 5))

Down_DLKKOINJ_ControlN <- filter(res_DLKKOINJ_ControlN_mutated, significant.Down
== "TRUE")
Up_DLKKOINJ_ControlN <- filter(res_DLKKOINJ_ControlN_mutated, significant.Up ==
"TRUE")


hist(res_DLKKOINJ_ControlN_mutated $log2FoldChange, main = "Log2 Fold Change
DLK_KO Injured vs Control Naive", xlab = "Log2 Fold Change", col = "green")
hist(res_DLKKOINJ_ControlN_mutated $pvalue, main = "Histograms of P-values DLK_KO
Injured vs Control Naive", xlab = "P-values", col = "green")
hist(res_DLKKOINJ_ControlN_mutated $padj_manual, main = "Histogram of Adjusted P-
values DLK_KO Injured vs Control Naive", xlab = "Adjusted P-values", col = "green")
```

```
write.csv(res_DLKKOINJ_ControlN_mutated,file="All_DLK_KO_Injured_vs_Control_Naive.csv")
write.csv(Up_DLKKOINJ_ControlN,file="Up_DLK_KO_Injured_vs_Control_Naive.csv")
write.csv(Down_DLKKOINJ_ControlN,file="Down_DLK_KO Injured vs Control Naive.csv")
```

Volcano Plot

```
DLKKOINJ_ControlN <- na.omit(res_DLKKOINJ_ControlN_mutated)

indicesLookup <- match(rownames(DLKKOINJ_ControlN),
DLKKOINJ_ControlN$Row.names)
head(DLKKOINJ_ControlN[indicesLookup, "symbol"])
dftmp <- data.frame(rownames(DLKKOINJ_ControlN), DLKKOINJ_ControlN[indicesLookup,
c("Row.names", "symbol")])
head(dftmp, 20)
table(dftmp[,1] == dftmp[,2])
rownames(DLKKOINJ_ControlN) <- paste(DLKKOINJ_ControlN[indicesLookup, "symbol"],
c(1:length(indicesLookup)), sep="_")
head(rownames(DLKKOINJ_ControlN),20)

library(EnhancedVolcano)

EnhancedVolcano(DLKKOINJ_ControlN,
        lab = gsub("_[0-9]*$", "", rownames(DLKKOINJ_ControlN)),
        x = 'log2FoldChange',
        y = 'padj',
        xlim = c(-5, 12),
        ylim=c(-1, 300),
        title = 'DLKKO Inj vs Control Naive',
        pCutoff = 10e-16,
        FCcutoff = 1.5,
        transcriptPointSize = 1.5,
        transcriptLabSize = 3.0)
ggsave("Volcano plot DLK_KO_Inj_vs_Control_Naive.png")
```

#To make bubble plots for our gene set enrichment analysis

```
All_MF <- read.csv("C:/~/RNA-seq Experiment/RNA-seq (Hiseq)/David/ ALLMF.csv",header
= TRUE, sep=",")
All_MF <- All_MF[c(1:7), c(1:6)]
colnames(All_MF)[1] <- "Category"
colnames(All_MF)[6] <- "PValue"
RGPalette <- c("#990000", "#CC00CC")

Godifferent <- ggplot(All_MF,aes (x = -log10(PValue), y = Term, size=Count, color=Category
))+#, color=Category )) +  ### this plots the data
```

```
  ggtitle ("GO Terms") +
  geom_point() +
  #scale_y_discrete(limits = rev(unique(sort(All_SUbsetChart$Term))))+   # in alphabetical order
  #scale_colour_brewer(palette = 'Accent') +   # Accent and Dark2 and Paired are all good
  scale_colour_manual(values=RGPalette) +
  xlim(1, 7) +
  #theme_classic()
  expand_limits(x = 1, y = 0) + ## this makes the graph start at 0
  theme_bw()
Godifferent

ggsave('Godifferent.png', width=4.65, height=2.25, units='in', limitsize = FALSE)
```

#The same is applied for BP and CC bubble plot

#To make the bubble plots of all categories side by side using Go Plot

```
gene_list <- read.csv("C:/~David/DLKDEG.csv",header = TRUE, sep=",")

All_Chart <-  read.csv("C:/~/RNA-seq (Hiseq)/David/All_Chart.csv",header = TRUE, sep=",")


colnames(All_Chart)[1] <- "Category"
colnames(gene_list)[1] <- "ID"

circ <- circle_dat(All_Chart, gene_list)
reduced_Circ <- reduce_overlap(circ, overlap = 0.75)
GOBubble(reduced_Circ, labels = 3)

# Add a title, change the colour of the circles, facet the plot according to the categories and
change the label threshold
GOBubble(circ, title = 'Bubble plot', colour = c('orange', 'darkred', 'darkblue'), display =
'multiple', labels = 3, ID = FALSE)

# Colour the background according to the category
GOBubble(circ, title = 'Bubble plot with background colour', display = 'multiple', bg.col = T,
labels = 3)
```

GeneSCF is a command line tool and it is not run in R:

```
./geneSCF -m=normal -i=../DEG.txt -o=./ -t=sym -db=GO_MF -bg=20000 --plot=yes -org=mgi

./geneSCF -m=normal -i=../DEG.txt -o=./ -t=sym -db=GO -bg=20000 --plot=yes -org=mgi
```

Bibliography

Adula, Kadidia Pemba, Mathew Shorey, Vasudha Chauhan, Khaled Nassman, Shu-Fan Chen, Melissa M. Rolls, and Alvaro Sagasti. 2021. "The MAP3Ks DLK and LZK Direct Diverse Responses to Axon Damage in Zebrafish Peripheral Neurons." *BioRxiv*. https://doi.org/10.1101/2021.07.03.450951.

Aldskogius, Hakan. 2011. "Mechanisms and Consequences of Microglial Responses to Peripheral Axotomy." *Frontiers in Bioscience* 3 (3): 857–68.

Ali, Yousuf O., Kai Ruan, and R. Grace Zhai. 2012. "NMNAT Suppresses Tau-Induced Neurodegeneration by Promoting Clearance of Hyperphosphorylated Tau Oligomers in a Drosophila Model of Tauopathy." *Human Molecular Genetics* 21 (2): 237–50.

Alvarez, Francisco J., Travis M. Rotterman, Erica T. Akhter, Alicia R. Lane, Arthur W. English, and Timothy C. Cope. 2020. "Synaptic Plasticity on Motoneurons After Axotomy: A Necessary Change in Paradigm." *Frontiers in Molecular Neuroscience* 13 (April): 68.

Andrews, Simon, and Others. 2010. "FastQC: A Quality Control Tool for High Throughput Sequence Data." Babraham Bioinformatics, Babraham Institute, Cambridge, United Kingdom.

Asghari Adib, Elham, Laura J. Smithson, and Catherine A. Collins. 2018. "An Axonal Stress Response Pathway: Degenerative and Regenerative Signaling by DLK." *Current Opinion in Neurobiology* 53 (July): 110–19.

Babetto, Elisabetta, Bogdan Beirowski, Emilie V. Russler, Jeffrey Milbrandt, and Aaron DiAntonio. 2013. "The Phr1 Ubiquitin Ligase Promotes Injury-Induced Axon Self-Destruction." *Cell Reports* 3 (5): 1422–29.

Backhaus, B., E. Sulkowski, and F. W. Schlote. 1984. "A Semi-Synthetic, General-Purpose Medium for Drosophila Melanogaster." *Drosophila Information Service* 60: 210–12.

Baker, Scott T., Karla J. Opperman, Erik D. Tulgren, Shane M. Turgeon, Willy Bienvenut, and Brock Grill. 2014. "RPM-1 Uses Both Ubiquitin Ligase and Phosphatase-Based Mechanisms to Regulate DLK-1 during Neuronal Development." *PLoS Genetics* 10 (5): e1004297.

"BBMap." n.d. SourceForge. Accessed April 5, 2022. https://sourceforge.net/projects/bbmap/.

Berg, Alexander, Johan Zelano, Alexander Stephan, Sebastian Thams, Ben A. Barres, Milos Pekny, Marcela Pekna, and Staffan Cullheim. 2012. "Reduced Removal of Synaptic Terminals from Axotomized Spinal Motoneurons in the Absence of Complement C3." *Experimental Neurology* 237 (1): 8–17.

Bhattacharya, Martha R. C., Josiah Gerdts, Sarah A. Naylor, Emily X. Royse, Sarah Y. Ebstein, Yo Sasaki, Jeffrey Milbrandt, and Aaron DiAntonio. 2012. "A Model of Toxic Neuropathy in Drosophila Reveals a Role for MORN4 in Promoting Axonal Degeneration." *The Journal of Neuroscience: The Official Journal of the Society for Neuroscience* 32 (15): 5054–61.

Blighe, Kevin, Sharmila Rana, and Myles Lewis. 2019. "EnhancedVolcano: Publication-Ready Volcano Plots with Enhanced Colouring and Labeling." *R Package Version* 1 (0).

Blinzinger, K., and G. Kreutzberg. 1968. “Displacement of Synaptic Terminals from Regenerating Motoneurons by Microglial Cells.” *Zeitschrift Fur Zellforschung Und Mikroskopische Anatomie* 85 (2): 145–57.

Bloom, A. Joseph, Bradley R. Miller, Joshua R. Sanes, and Aaron DiAntonio. 2007. “The Requirement for Phr1 in CNS Axon Tract Formation Reveals the Corticostriatal Boundary as a Choice Point for Cortical Axons.” *Genes & Development* 21 (20): 2593–2606.

Bolus, Harris, Kassi Crocker, Grace Boekhoff-Falk, and Stanislava Chtarbanova. 2020. “Modeling Neurodegenerative Disorders in Drosophila Melanogaster.” *International Journal of Molecular Sciences* 21 (9). https://doi.org/10.3390/ijms21093055.

Borbély, Eva, Bálint Scheich, and Zsuzsanna Helyes. 2013. “Neuropeptides in Learning and Memory.” *Neuropeptides* 47 (6): 439–50.

Börchers, Svenja, Rohollah Babaei, Catarina Klimpel, Jorge Duque Escobar, Sabine Schröder, Roland Blume, Muhammad Nasir Hayat Malik, and Elke Oetjen. 2017. “TNFα-Induced DLK Activation Contributes to Apoptosis in the Beta-Cell Line HIT.” *Naunyn-Schmiedeberg’s Archives of Pharmacology* 390 (8): 813–25.

Borgen, Melissa A., Dandan Wang, and Brock Grill. 2017. “RPM-1 Regulates Axon Termination by Affecting Growth Cone Collapse and Microtubule Stability.” *Development* 144 (24): 4658–72.

Borgen, Melissa, Kimberly Rowland, Jana Boerner, Brandon Lloyd, Aruna Khan, and Rodney Murphey. 2017. “Axon Termination, Pruning, and Synaptogenesis in the Giant Fiber System of Drosophila Melanogaster Is Promoted by Highwire.” *Genetics* 205 (3): 1229–45.

Bounoutas, Alexander, John Kratz, Lesley Emtage, Charles Ma, Ken C. Nguyen, and Martin Chalfie. 2011. “Microtubule Depolymerization in Caenorhabditis Elegans Touch Receptor Neurons Reduces Gene Expression through a P38 MAPK Pathway.” *Proceedings of the National Academy of Sciences of the United States of America* 108 (10): 3982–87.

Brace, E. J., Chunlai Wu, Vera Valakh, and Aaron DiAntonio. 2014. “SkpA Restrains Synaptic Terminal Growth during Development and Promotes Axonal Degeneration Following Injury.” *The Journal of Neuroscience: The Official Journal of the Society for Neuroscience* 34 (25): 8398–8410.

Brand, A. H., and N. Perrimon. 1993. “Targeted Gene Expression as a Means of Altering Cell Fates and Generating Dominant Phenotypes.” *Development* 118 (2): 401–15.

Brown, A. G., and R. E. Fyffe. 1981. “Direct Observations on the Contacts Made between Ia Afferent Fibres and Alpha-Motoneurones in the Cat’s Lumbosacral Spinal Cord.” *The Journal of Physiology* 313: 121–40.

Burke, R. E., B. Walmsley, and J. A. Hodgson. 1979. “HRP Anatomy of Group La Afferent Contacts on Alpha Motoneurones.” *Brain Research* 160 (2): 347–52.

Byrne, Alexandra B., Rebecca D. McWhirter, Yuichi Sekine, Stephen M. Strittmatter, David M. Miller III, and Marc Hammarlund. 2016a. “Inhibiting Poly(ADP-Ribosylation) Improves Axon Regeneration.” *ELife* 5 (October): e12734.

Campenot, Robert B. 2009. “NGF Uptake and Retrograde Signaling Mechanisms in Sympathetic Neurons in Compartmented Cultures.” In *Cell Biology of the Axon*, edited by Edward Koenig, 141–58. Berlin, Heidelberg: Springer Berlin Heidelberg.

Campos, Raquel M. P., Maria Carolina Barbosa-Silva, and Victor T. Ribeiro-Resende. 2021. "Comparison of Effect of Crush or Transection Peripheral Nerve Lesion on Lumbar Spinal Cord Synaptic Plasticity and Microglial Dynamics." *IBRO Neuroscience Reports* 10 (June): 225–35.

Carpanini, Sarah M., Megan Torvell, and Bryan Paul Morgan. 2019. "Therapeutic Inhibition of the Complement System in Diseases of the Central Nervous System." *Frontiers in Immunology* 10 (March): 362.

Cervia, D., and G. Casini. 2013. "The Neuropeptide Systems and Their Potential Role in the Treatment of Mammalian Retinal Ischemia: A Developing Story." *Current Neuropharmacology* 11 (1): 95–101.

Chen, Chun-Hao, Albert Lee, Chien-Po Liao, Ya-Wen Liu, and Chun-Liang Pan. 2014. "RHGF-1/PDZ-RhoGEF and Retrograde DLK-1 Signaling Drive Neuronal Remodeling on Microtubule Disassembly." *Proceedings of the National Academy of Sciences of the United States of America* 111 (46): 16568–73.

Chen, Li, Michelle C. Stone, Juan Tao, and Melissa M. Rolls. 2012. "Axon Injury and Stress Trigger a Microtubule-Based Neuroprotective Pathway." *Proceedings of the National Academy of Sciences of the United States of America* 109 (29): 11842–47.

Chen, Lizhen, Zhiping Wang, Anindya Ghosh-Roy, Thomas Hubert, Dong Yan, Sean O'Rourke, Bruce Bowerman, Zilu Wu, Yishi Jin, and Andrew D. Chisholm. 2011. "Axon Regeneration Pathways Identified by Systematic Genetic Screening in C. Elegans." *Neuron* 71 (6): 1043–57.

Chen, Meifan, Cédric G. Geoffroy, Hetty N. Wong, Oliver Tress, Mallorie T. Nguyen, Lawrence B. Holzman, Yishi Jin, and Binhai Zheng. 2016. "Leucine Zipper-Bearing Kinase Promotes Axon Growth in Mammalian Central Nervous System Neurons." *Scientific Reports* 6 (August): 31482.

Chen, Xiqun, Margarita Rzhetskaya, Tatyana Kareva, Ross Bland, Matthew J. During, A. William Tank, Nikolai Kholodilov, and Robert E. Burke. 2008. "Antiapoptotic and Trophic Effects of Dominant-Negative Forms of Dual Leucine Zipper Kinase in Dopamine Neurons of the Substantia Nigra in Vivo." *The Journal of Neuroscience: The Official Journal of the Society for Neuroscience* 28 (3): 672–80.

Chistiakov, Dimitry A., Murry C. Killingsworth, Veronika A. Myasoedova, Alexander N. Orekhov, and Yuri V. Bobryshev. 2017. "CD68/Macrosialin: Not Just a Histochemical Marker." *Laboratory Investigation; a Journal of Technical Methods and Pathology* 97 (1): 4–13.

Chung, Samuel H., Mehraj R. Awal, James Shay, Melissa M. McLoed, Eric Mazur, and Christopher V. Gabel. 2016. "Novel DLK-Independent Neuronal Regeneration in Caenorhabditis Elegans Shares Links with Activity-Dependent Ectopic Outgrowth." *Proceedings of the National Academy of Sciences of the United States of America*.

Collins, Catherine A., Yogesh P. Wairkar, Sylvia L. Johnson, and Aaron DiAntonio. 2006. "Highwire Restrains Synaptic Growth by Attenuating a MAP Kinase Signal." *Neuron* 51 (1): 57–69.

Conforti, Laura, Jonathan Gilley, and Michael P. Coleman. 2014. "Wallerian Degeneration: An Emerging Axon Death Pathway Linking Injury and Disease." *Nature Reviews. Neuroscience* 15 (6): 394–409.

D'Alessandro, Angelo, Davide Cervia, Elisabetta Catalani, Federica Gevi, Lello Zolla, and Giovanni Casini. 2014. "Protective Effects of the Neuropeptides PACAP, Substance P

and the Somatostatin Analogue Octreotide in Retinal Ischemia: A Metabolomic Analysis." *Molecular BioSystems* 10 (6): 1290–1304.
Daviau, Alex, Marco Di Fruscio, and Richard Blouin. 2009. "The Mixed-Lineage Kinase DLK Undergoes Src-Dependent Tyrosine Phosphorylation and Activation in Cells Exposed to Vanadate or Platelet-Derived Growth Factor (PDGF)." *Cellular Signalling* 21 (4): 577–87.
"DAVID Functional Annotation Bioinformatics Microarray Analysis." n.d. Accessed April 19, 2018. https://david.ncifcrf.gov/.
Dobin, Alexander, Carrie A. Davis, Felix Schlesinger, Jorg Drenkow, Chris Zaleski, Sonali Jha, Philippe Batut, Mark Chaisson, and Thomas R. Gingeras. 2013. "STAR: Ultrafast Universal RNA-Seq Aligner." *Bioinformatics* 29 (1): 15–21.
Druart, Mélanie, and Corentin Le Magueresse. 2019. "Emerging Roles of Complement in Psychiatric Disorders." *Frontiers in Psychiatry / Frontiers Research Foundation* 10 (August): 573.
Essuman, Kow, Daniel W. Summers, Yo Sasaki, Xianrong Mao, Aaron DiAntonio, and Jeffrey Milbrandt. 2017. "The SARM1 Toll/Interleukin-1 Receptor Domain Possesses Intrinsic NAD+ Cleavage Activity That Promotes Pathological Axonal Degeneration." *Neuron* 93 (6): 1334-1343.e5.
Eto, Kaoru, Takeshi Kawauchi, Makiko Osawa, Hidenori Tabata, and Kazunori Nakajima. 2010. "Role of Dual Leucine Zipper-Bearing Kinase (DLK/MUK/ZPK) in Axonal Growth." *Neuroscience Research* 66 (1): 37–45.
Fan, G., S. E. Merritt, M. Kortenjann, P. E. Shaw, and L. B. Holzman. 1996. "Dual Leucine Zipper-Bearing Kinase (DLK) Activates P46SAPK and P38mapk but Not ERK2." *The Journal of Biological Chemistry* 271 (40): 24788–93.
Farley, Madeline M., and Trent A. Watkins. 2018. "Intrinsic Neuronal Stress Response Pathways in Injury and Disease." *Annual Review of Pathology* 13 (January): 93–116.
Feoktistov, Alexander I., and Tory G. Herman. 2016. "Wallenda/DLK Protein Levels Are Temporally Downregulated by Tramtrack69 to Allow R7 Growth Cones to Become Stationary Boutons." *Development* 143 (16): 2983–93.
Fernandes, Kimberly A., Jeffrey M. Harder, Simon W. John, Peter Shrager, and Richard T. Libby. 2014. "DLK-Dependent Signaling Is Important for Somal but Not Axonal Degeneration of Retinal Ganglion Cells Following Axonal Injury." *Neurobiology of Disease* 69 (September): 108–16.
Fribley, Andrew, Kezhong Zhang, and Randal J. Kaufman. 2009. "Regulation of Apoptosis by the Unfolded Protein Response." *Methods in Molecular Biology* 559: 191–204.
Fukuyama, K., M. Yoshida, A. Yamashita, T. Deyama, M. Baba, A. Suzuki, H. Mohri, et al. 2000. "MAPK Upstream Kinase (MUK)-Binding Inhibitory Protein, a Negative Regulator of MUK/Dual Leucine Zipper-Bearing Kinase/Leucine Zipper Protein Kinase." *The Journal of Biological Chemistry* 275 (28): 21247–54.
Geden, Matthew J., and Mohanish Deshmukh. 2016. "Axon Degeneration: Context Defines Distinct Pathways." *Current Opinion in Neurobiology* 39 (August): 108–15.
Gerdts, Josiah, E. J. Brace, Yo Sasaki, Aaron DiAntonio, and Jeffrey Milbrandt. 2015. "SARM1 Activation Triggers Axon Degeneration Locally via NAD Destruction." *Science*. https://doi.org/10.1126/science.1258366.

Gerdts, Josiah, Daniel W. Summers, Jeffrey Milbrandt, and Aaron DiAntonio. 2016. “Axon Self-Destruction: New Links among SARM1, MAPKs, and NAD+ Metabolism.” *Neuron* 89 (3): 449–60.

Ghosh, Arundhati Sengupta, Bei Wang, Christine D. Pozniak, Mark Chen, Ryan J. Watts, and Joseph W. Lewcock. 2011. “DLK Induces Developmental Neuronal Degeneration via Selective Regulation of Proapoptotic JNK Activity.” *The Journal of Cell Biology* 194 (5): 751–64.

Gilley, Jonathan, Giuseppe Orsomando, Isabel Nascimento-Ferreira, and Michael P. Coleman. 2015. “Absence of SARM1 Rescues Development and Survival of NMNAT2-Deficient Axons.” *Cell Reports* 10 (12): 1975–82.

Goel, Pragya, and Dion Dickman. 2018a. “Distinct Homeostatic Modulations Stabilize Reduced Postsynaptic Receptivity in Response to Presynaptic DLK Signaling.” *Nature Communications* 9 (1): 1856.

Gomez-Arboledas, Angela, Munjal M. Acharya, and Andrea J. Tenner. 2021. “The Role of Complement in Synaptic Pruning and Neurodegeneration.” *ImmunoTargets and Therapy* 10 (September): 373–86.

Guan, Zhonghui, Julia A. Kuhn, Xidao Wang, Bradley Colquitt, Carlos Solorzano, Smitha Vaman, Andrew K. Guan, et al. 2016. “Injured Sensory Neuron-Derived CSF1 Induces Microglial Proliferation and DAP12-Dependent Pain.” *Nature Neuroscience* 19 (1): 94–101.

Hammarlund, Marc, Paola Nix, Linda Hauth, Erik M. Jorgensen, and Michael Bastiani. 2009. “Axon Regeneration Requires a Conserved MAP Kinase Pathway.” *Science* 323 (5915): 802–6.

Han, Sung Min, Huma S. Baig, and Marc Hammarlund. 2016a. “Mitochondria Localize to Injured Axons to Support Regeneration.” *Neuron* 92 (6): 1308–23.

Hao, Yan, and Catherine Collins. 2017. “Intrinsic Mechanisms for Axon Regeneration: Insights from Injured Axons in Drosophila.” *Current Opinion in Genetics & Development* 44 (June): 84–91.

Hao, Yan, Erin Frey, Choya Yoon, Hetty Wong, Douglas Nestorovski, Lawrence B. Holzman, Roman J. Giger, Aaron DiAntonio, and Catherine Collins. 2016. “An Evolutionarily Conserved Mechanism for CAMP Elicited Axonal Regeneration Involves Direct Activation of the Dual Leucine Zipper Kinase DLK.” *ELife* 5: 1–19.

Hartley, Stephen W., and James C. Mullikin. 2015. “QoRTs: A Comprehensive Toolset for Quality Control and Data Processing of RNA-Seq Experiments.” *BMC Bioinformatics* 16 (July): 224.

Hay, B. A., T. Wolff, and G. M. Rubin. 1994. “Expression of Baculovirus P35 Prevents Cell Death in Drosophila.” *Development* 120 (8): 2121–29.

Herdegen, T., F. X. Claret, T. Kallunki, A. Martin-Villalba, C. Winter, T. Hunter, and M. Karin. 1998. “Lasting N-Terminal Phosphorylation of c-Jun and Activation of c-Jun N-Terminal Kinases after Neuronal Injury.” *The Journal of Neuroscience: The Official Journal of the Society for Neuroscience* 18 (14): 5124–35.

Hirai, Syu-Ichi, Yumi Banba, Tomoko Satake, and Shigeo Ohno. 2011. “Axon Formation in Neocortical Neurons Depends on Stage-Specific Regulation of Microtubule Stability by the Dual Leucine Zipper Kinase-c-Jun N-Terminal Kinase Pathway.” *The Journal of Neuroscience: The Official Journal of the Society for Neuroscience* 31 (17): 6468–80.

Hirai, Syu-Ichi, De Feng Cui, Takaki Miyata, Masaharu Ogawa, Hiroshi Kiyonari, Yoko Suda, Shinichi Aizawa, Yumi Banba, and Shigeo Ohno. 2006. “The C-Jun N-Terminal Kinase Activator Dual Leucine Zipper Kinase Regulates Axon Growth and Neuronal Migration in the Developing Cerebral Cortex.” *The Journal of Neuroscience: The Official Journal of the Society for Neuroscience* 26 (46): 11992–2.

Hirth, Frank. 2010. “Drosophila Melanogaster in the Study of Human Neurodegeneration.” *CNS & Neurological Disorders Drug Targets* 9 (4): 504–23.

Hoang, Thao X., Jaime H. Nieto, Niranjala J. K. Tillakaratne, and Leif A. Havton. 2003. “Autonomic and Motor Neuron Death Is Progressive and Parallel in a Lumbosacral Ventral Root Avulsion Model of Cauda Equina Injury.” *The Journal of Comparative Neurology* 467 (4): 477–86.

Holland, Sabrina M., Kaitlin M. Collura, Andrea Ketschek, Kentaro Noma, Toby A. Ferguson, Yishi Jin, Gianluca Gallo, and Gareth M. Thomas. 2016. “Palmitoylation Controls DLK Localization, Interactions and Activity to Ensure Effective Axonal Injury Signaling.” *Proceedings of the National Academy of Sciences of the United States of America* 113 (3). https://doi.org/10.1073/pnas.1514123113.

Holmes, F. E., S. Mahoney, V. R. King, A. Bacon, N. C. Kerr, V. Pachnis, R. Curtis, J. V. Priestley, and D. Wynick. 2000. “Targeted Disruption of the Galanin Gene Reduces the Number of Sensory Neurons and Their Regenerative Capacity.” *Proceedings of the National Academy of Sciences of the United States of America* 97 (21): 11563–68.

Hu, Zhongsheng, Nan Deng, Kaili Liu, and Wenwen Zeng. 2019a. “DLK Mediates the Neuronal Intrinsic Immune Response and Regulates Glial Reaction and Neuropathic Pain.” *Experimental Neurology* 322 (December): 113056.

Huang, Yu-Wen Alvin, Bo Zhou, Marius Wernig, and Thomas C. Südhof. 2017. “ApoE2, ApoE3, and ApoE4 Differentially Stimulate APP Transcription and Aβ Secretion.” *Cell* 168 (3): 427-441.e21.

Huntwork-Rodriguez, Sarah, Bei Wang, Trent Watkins, Arundhati Sengupta Ghosh, Christine D. Pozniak, Daisy Bustos, Kim Newton, Donald S. Kirkpatrick, and Joseph W. Lewcock. 2013. “JNK-Mediated Phosphorylation of DLK Suppresses Its Ubiquitination to Promote Neuronal Apoptosis.” *The Journal of Cell Biology* 202 (5). https://doi.org/10.1083/jcb.201303066.

Itoh, Aki, Makoto Horiuchi, Peter Bannerman, David Pleasure, and Takayuki Itoh. 2009. “Impaired Regenerative Response of Primary Sensory Neurons in ZPK/DLK Gene-Trap Mice.” *Biochemical and Biophysical Research Communications* 383 (2): 258–62.

Itoh, Aki, Makoto Horiuchi, Kouji Wakayama, Jie Xu, Peter Bannerman, David Pleasure, and Takayuki Itoh. 2011. “ZPK/DLK, a Mitogen-Activated Protein Kinase Kinase Kinase, Is a Critical Mediator of Programmed Cell Death of Motoneurons.” *The Journal of Neuroscience: The Official Journal of the Society for Neuroscience* 31 (20): 7223–28.

Janda, Elzbieta, Laura Boi, and Anna R. Carta. 2018. “Microglial Phagocytosis and Its Regulation: A Therapeutic Target in Parkinson’s Disease?” *Frontiers in Molecular Neuroscience* 11 (April): 144.

Jessen, Kristjan R., and Rhona Mirsky. 2019. “The Success and Failure of the Schwann Cell Response to Nerve Injury.” *Frontiers in Cellular Neuroscience* 13 (February): 33.

Kalla, R., Z. Liu, S. Xu, A. Koppius, Y. Imai, C. U. Kloss, S. Kohsaka, et al. 2001. “Microglia and the Early Phase of Immune Surveillance in the Axotomized Facial Motor Nucleus: Impaired Microglial Activation and Lymphocyte Recruitment but No Effect on Neuronal

Survival or Axonal Regeneration in Macrophage-Colony Stimulating Factor-Deficient Mice." *The Journal of Comparative Neurology* 436 (2): 182–201.
Katz, Jonathan S., Jeffrey D. Rothstein, Merit E. Cudkowicz, Angela Genge, Björn Oskarsson, Avis B. Hains, Chen Chen, et al. 2022. "A Phase 1 Study of GDC-0134, a Dual Leucine Zipper Kinase Inhibitor, in ALS." *Annals of Clinical and Translational Neurology* 9 (1): 50–66.
Kelly, Seth M., Alexandra Elchert, and Michael Kahl. 2017. "Dissection and Immunofluorescent Staining of Mushroom Body and Photoreceptor Neurons in Adult Drosophila Melanogaster Brains." *Journal of Visualized Experiments: JoVE*, no. 129 (November). https://doi.org/10.3791/56174.
Kenney, A. M., and J. D. Kocsis. 1998. "Peripheral Axotomy Induces Long-Term c-Jun Amino-Terminal Kinase-1 Activation and Activator Protein-1 Binding Activity by c-Jun and JunD in Adult Rat Dorsal Root Ganglia In Vivo." *The Journal of Neuroscience: The Official Journal of the Society for Neuroscience* 18 (4): 1318–28.
Kettenmann, Helmut, Frank Kirchhoff, and Alexei Verkhratsky. 2013. "Microglia: New Roles for the Synaptic Stripper." *Neuron* 77 (1): 10–18.
Kim, Inhyeok, Yonjae Kim, Daewoong Kang, Junyang Jung, Sungsoo Kim, Hwasung Rim, Sanghoon Kim, and Seung-Geun Yeo. 2021. "Neuropeptides Involved in Facial Nerve Regeneration." *Biomedicines* 9 (11). https://doi.org/10.3390/biomedicines9111575.
Kim, Jung Hwan, Xin Wang, Rosemary Coolon, and Bing Ye. 2013. "Dscam Expression Levels Determine Presynaptic Arbor Sizes in Drosophila Sensory Neurons." *Neuron* 78 (5): 827–38.
Klinedinst, Susan, Xin Wang, Xin Xiong, Jill M. Haenfler, and Catherine A. Collins. 2013. "Independent Pathways Downstream of the Wnd/DLK MAPKKK Regulate Synaptic Structure, Axonal Transport, and Injury Signaling." *The Journal of Neuroscience: The Official Journal of the Society for Neuroscience* 33 (31): 12764–78.
Koller, Andreas, Susanne Maria Brunner, Rodolfo Bianchini, Andrea Ramspacher, Michael Emberger, Felix Locker, Sandra Schlager, and Barbara Kofler. 2019. "Galanin Is a Potent Modulator of Cytokine and Chemokine Expression in Human Macrophages." *Scientific Reports* 9 (1): 7237.
Kurup, Naina, Dong Yan, Alexandr Goncharov, and Yishi Jin. 2015. "Dynamic Microtubules Drive Circuit Rewiring in the Absence of Neurite Remodeling." *Current Biology: CB* 25 (12): 1594–1605.
LaCount, D. J., S. F. Hanson, C. L. Schneider, and P. D. Friesen. 2000. "Caspase Inhibitor P35 and Inhibitor of Apoptosis Op-IAP Block in Vivo Proteolytic Activation of an Effector Caspase at Different Steps." *The Journal of Biological Chemistry* 275 (21): 15657–64.
Larhammar, Martin, Sarah Huntwork-Rodriguez, Zhiyu Jiang, Hilda Solanoy, Arundhati Sengupta Ghosh, Bei Wang, Joshua S. Kaminker, et al. 2017. "Dual Leucine Zipper Kinase-Dependent PERK Activation Contributes to Neuronal Degeneration Following Insult." *ELife* 6 (April). https://doi.org/10.7554/eLife.20725.
Larhammar, Martin, Sarah Huntwork-Rodriguez, York Rudhard, Arundhati Sengupta-Ghosh, and Joseph W. Lewcock. 2017. "The Ste20 Family Kinases MAP4K4, MINK1, and TNIK Converge to Regulate Stress-Induced JNK Signaling in Neurons." *The Journal of Neuroscience: The Official Journal of the Society for Neuroscience* 37 (46): 11074–84.
Le Pichon, Claire E., William J. Meilandt, Sara Dominguez, Hilda Solanoy, Han Lin, Hai Ngu, Alvin Gogineni, et al. 2017. "Loss of Dual Leucine Zipper Kinase Signaling Is Protective

in Animal Models of Neurodegenerative Disease." *Science Translational Medicine* 9 (403). https://doi.org/10.1126/scitranslmed.aag0394.
Lee, Ji Eun, Mckenna Oney, Kimberly Frizzell, Nitin Phadnis, and Julie Hollien. 2015. "Drosophila Melanogaster Activating Transcription Factor 4 Regulates Glycolysis during Endoplasmic Reticulum Stress." *G3* 5 (4): 667–75.
Lesiak, Adam J., Matthew Brodsky, and John F. Neumaier. 2015. "RiboTag Is a Flexible Tool for Measuring the Translational State of Targeted Cells in Heterogeneous Cell Cultures." *BioTechniques* 58 (6): 308–17.
Lewcock, Joseph W., Nicolas Genoud, Karen Lettieri, and Samuel L. Pfaff. 2007. "The Ubiquitin Ligase Phr1 Regulates Axon Outgrowth through Modulation of Microtubule Dynamics." *Neuron* 56 (4): 604–20.
Li, Jiaxing, Yao V. Zhang, Elham Asghari Adib, Doychin T. Stanchev, Xin Xiong, Susan Klinedinst, Pushpanjali Soppina, et al. 2017. "Restraint of Presynaptic Protein Levels by Wnd / DLK Signaling Mediates Synaptic Defects Associated with the Kinesin-3 Motor Unc-104." *ELife*, e24271–e24271.
Li, Mingli, Shiyao Sun, Jessica Priest, Xiaolin Bi, and Yun Fan. 2019. "Characterization of TNF-Induced Cell Death in Drosophila Reveals Caspase- and JNK-Dependent Necrosis and Its Role in Tumor Suppression." *Cell Death & Disease* 10 (8): 613.
Liu, Jia-Jia. 2017. "Regulation of Dynein-Dynactin-Driven Vesicular Transport." *Traffic* 18 (6): 336–47.
Liu, Yan, and Huan Wang. 2020. "Peripheral Nerve Injury Induced Changes in the Spinal Cord and Strategies to Counteract/Enhance the Changes to Promote Nerve Regeneration." *Neural Regeneration Research* 15 (2): 189–98.
Love, Michael, Simon Anders, and Wolfgang Huber. 2014. "Differential Analysis of Count Data--the DESeq2 Package." *Genome Biology* 15 (550): 10–1186.
Luo, Xin, and W. Lee Kraus. 2012. "On PAR with PARP: Cellular Stress Signaling through Poly(ADP-Ribose) and PARP-1." *Genes & Development* 26 (5): 417–32.
Ma, J., L. N. Novikov, M. Wiberg, and J. O. Kellerth. 2001. "Delayed Loss of Spinal Motoneurons after Peripheral Nerve Injury in Adult Rats: A Quantitative Morphological Study." *Experimental Brain Research. Experimentelle Hirnforschung. Experimentation Cerebrale* 139 (2): 216–23.
MacGillavry, Harold D., Floor J. Stam, Marion M. Sassen, Linde Kegel, William T. J. Hendriks, Joost Verhaagen, August B. Smit, and Ronald E. van Kesteren. 2009. "NFIL3 and CAMP Response Element-Binding Protein Form a Transcriptional Feedforward Loop That Controls Neuronal Regeneration-Associated Gene Expression." *The Journal of Neuroscience: The Official Journal of the Society for Neuroscience* 29 (49): 15542–50.
Magill, Christina K., Alice Tong, David Kawamura, Ayato Hayashi, Daniel A. Hunter, Alexander Parsadanian, Susan E. Mackinnon, and Terence M. Myckatyn. 2007. "Reinnervation of the Tibialis Anterior Following Sciatic Nerve Crush Injury: A Confocal Microscopic Study in Transgenic Mice." *Experimental Neurology* 207 (1): 64–74.
Mahoney, Sally-Ann, Richard Hosking, Sarah Farrant, Fiona E. Holmes, Arie S. Jacoby, John Shine, Tiina P. Iismaa, Malcolm K. Scott, Ralf Schmidt, and David Wynick. 2003. "The Second Galanin Receptor GalR2 Plays a Key Role in Neurite Outgrowth from Adult Sensory Neurons." *The Journal of Neuroscience: The Official Journal of the Society for Neuroscience* 23 (2): 416–21.

Marcette, Jana Dorfman, Jessica Jie Chen, and Michael L. Nonet. 2014. “The Caenorhabditis Elegans Microtubule Minus-End Binding Homolog PTRN-1 Stabilizes Synapses and Neurites.” *ELife* 3 (February): e01637.

Martin, Sarah L., Adam J. Reid, Alexei Verkhratsky, Valerio Magnaghi, and Alessandro Faroni. 2019. “Gene Expression Changes in Dorsal Root Ganglia Following Peripheral Nerve Injury: Roles in Inflammation, Cell Death and Nociception.” *Neural Regeneration Research* 14 (6): 939–47.

Martín-Blanco, E., A. Gampel, J. Ring, K. Virdee, N. Kirov, A. M. Tolkovsky, and A. Martinez-Arias. 1998. “Puckered Encodes a Phosphatase That Mediates a Feedback Loop Regulating JNK Activity during Dorsal Closure in Drosophila.” *Genes & Development* 12 (4): 557–70.

Martini, Rudolf, Stefan Fischer, Rubèn López-Vales, and Samuel David. 2008. “Interactions between Schwann Cells and Macrophages in Injury and Inherited Demyelinating Disease.” *Glia* 56 (14): 1566–77.

Mason, Matthew R. J., Susan Erp, Kim Wolzak, Axel Behrens, Gennadij Raivich, and Joost Verhaagen. 2021. “The Jun-Dependent Axon Regeneration Gene Program: Jun Promotes Regeneration over Plasticity.” *Human Molecular Genetics*, October. https://doi.org/10.1093/hmg/ddab315.

Massaro, Catherine M., Jan Pielage, and Graeme W. Davis. 2009. “Molecular Mechanisms That Enhance Synapse Stability despite Persistent Disruption of the Spectrin/Ankyrin/Microtubule Cytoskeleton.” *The Journal of Cell Biology* 187 (1): 101–17.

Matsuda, Wakoto, Takahiro Furuta, Kouichi C. Nakamura, Hiroyuki Hioki, Fumino Fujiyama, Ryohachi Arai, and Takeshi Kaneko. 2009. “Single Nigrostriatal Dopaminergic Neurons Form Widely Spread and Highly Dense Axonal Arborizations in the Neostriatum.” *The Journal of Neuroscience: The Official Journal of the Society for Neuroscience* 29 (2): 444–53.

McCown, Thomas J. 2009. “Adeno-Associated Virus Vector-Mediated Expression and Constitutive Secretion of Galanin Suppresses Limbic Seizure Activity.” *Neurotherapeutics: The Journal of the American Society for Experimental NeuroTherapeutics* 6 (2): 307–11.

McGurk, Leeanne, Amit Berson, and Nancy M. Bonini. 2015. “Drosophila as an In Vivo Model for Human Neurodegenerative Disease.” *Genetics* 201 (2): 377–402.

Mecklenburg, Kirk L., Forrest P. Weghorst, Stephanie A. Freed, and Joseph E. O’Tousa. 2018. “Discordant Responses to MAPK Pathway Stimulation Include Axonal Growths in Adult Drosophila Photoreceptors.” *Frontiers in Molecular Neuroscience* 11 (December): 441.

Milde, Stefan, Jonathan Gilley, and Michael P. Coleman. 2013. “Axonal Trafficking of NMNAT2 and Its Roles in Axon Growth and Survival in Vivo.” *In Vivo. Sci Ep* 3: 2567.

Millecamps, Stéphanie, and Jean-Pierre Julien. 2013. “Axonal Transport Deficits and Neurodegenerative Diseases.” *Nature Reviews. Neuroscience* 14 (3): 161–76.

Miller, Bradley R., Craig Press, Richard W. Daniels, Yo Sasaki, Jeffrey Milbrandt, and Aaron DiAntonio. 2009. “A DLK-Dependent Axon Self-Destruction Program Promotes Wallerian Degeneration.” *Nature Neuroscience* 12 (4): 387–89.

Mishra, Bibhudatta, Ross Carson, Richard I. Hume, and Catherine A. Collins. 2013. “Sodium and Potassium Currents Influence Wallerian Degeneration of Injured Drosophila Axons.”

The Journal of Neuroscience: The Official Journal of the Society for Neuroscience 33 (48): 18728–39.
Mok, Sue-Ann, Karen Lund, and Robert B. Campenot. 2009. "A Retrograde Apoptotic Signal Originating in NGF-Deprived Distal Axons of Rat Sympathetic Neurons in Compartmented Cultures." *Cell Research* 19 (5): 546–60.
Moreno, Julie A., Helois Radford, Diego Peretti, Joern R. Steinert, Nicholas Verity, Maria Guerra Martin, Mark Halliday, et al. 2012. "Sustained Translational Repression by EIF2α-P Mediates Prion Neurodegeneration." *Nature* 485 (7399): 507–11.
Nakata, Katsunori, Benjamin Abrams, Brock Grill, Alexandr Goncharov, Xun Huang, Andrew D. Chisholm, and Yishi Jin. 2005. "Regulation of a DLK-1 and P38 MAP Kinase Pathway by the Ubiquitin Ligase RPM-1 Is Required for Presynaptic Development." *Cell* 120 (3): 407–20.
Navarro, X., Meritxell Vivó, and Antoni Valero-Cabré. 2007. "Neural Plasticity after Peripheral Nerve Injury and Regeneration." *Progress in Neurobiology* 82 (4): 163–201.
Nicolini, Gabriella, Marianna Monfrini, and Arianna Scuteri. 2015. "Axonal Transport Impairment in Chemotherapy-Induced Peripheral Neuropathy." *Toxics* 3 (3): 322–41.
Nihalani, D., S. Merritt, and L. B. Holzman. 2000. "Identification of Structural and Functional Domains in Mixed Lineage Kinase Dual Leucine Zipper-Bearing Kinase Required for Complex Formation and Stress-Activated Protein Kinase Activation." *The Journal of Biological Chemistry* 275 (10): 7273–79.
Oliveira, Alexandre L. R., Sebastian Thams, Olle Lidman, Fredrik Piehl, Tomas Hökfelt, Klas Kärre, Hans Lindå, and Staffan Cullheim. 2004. "A Role for MHC Class I Molecules in Synaptic Plasticity and Regeneration of Neurons after Axotomy." *Proceedings of the National Academy of Sciences of the United States of America* 101 (51): 17843–48.
Olsen, D. S., B. Jordan, D. Chen, R. C. Wek, and D. R. Cavener. 1998. "Isolation of the Gene Encoding the Drosophila Melanogaster Homolog of the Saccharomyces Cerevisiae GCN2 EIF-2alpha Kinase." *Genetics* 149 (3): 1495–1509.
Owens, D. M., and S. M. Keyse. 2007. "Differential Regulation of MAP Kinase Signalling by Dual-Specificity Protein Phosphatases." *Oncogene* 26 (22): 3203–13.
Page, G., A. Rioux Bilan, S. Ingrand, C. Lafay-Chebassier, S. Pain, M. C. Perault Pochat, C. Bouras, T. Bayer, and J. Hugon. 2006. "Activated Double-Stranded RNA-Dependent Protein Kinase and Neuronal Death in Models of Alzheimer's Disease." *Neuroscience* 139 (4): 1343–54.
Pakos-Zebrucka, Karolina, Izabela Koryga, Katarzyna Mnich, Mila Ljujic, Afshin Samali, and Adrienne M. Gorman. 2016. "The Integrated Stress Response." *EMBO Reports* 17 (10): 1374–95.
Patel, Snahel, William J. Meilandt, Rebecca I. Erickson, Jinhua Chen, Gauri Deshmukh, Anthony A. Estrada, Reina N. Fuji, et al. 2017. "Selective Inhibitors of Dual Leucine Zipper Kinase (DLK, MAP3K12) with Activity in a Model of Alzheimer's Disease." *Journal of Medicinal Chemistry* 60 (19): 8083–8102.
Perego, Carlo, Stefano Fumagalli, and Maria-Grazia De Simoni. 2011. "Temporal Pattern of Expression and Colocalization of Microglia/Macrophage Phenotype Markers Following Brain Ischemic Injury in Mice." *Journal of Neuroinflammation* 8 (December): 174.
Perry, V. Hugh, and Vincent O'Connor. 2010. "The Role of Microglia in Synaptic Stripping and Synaptic Degeneration: A Revised Perspective." *ASN Neuro* 2 (5): e00047.

Pomar, Natalia, Juan J. Berlanga, Sonsoles Campuzano, Greco Hernandez, Monica Elias, and Cesar de Haro. 2003. “Functional Characterization of Drosophila Melanogaster PERK Eukaryotic Initiation Factor 2alpha (EIF2alpha) Kinase.” *European Journal of Biochemistry / FEBS* 270 (2): 293–306.

Pozniak, Christine D., Arundhati Sengupta Ghosh, Alvin Gogineni, Jesse E. Hanson, Seung-Hye Lee, Jessica L. Larson, Hilda Solanoy, et al. 2013. “Dual Leucine Zipper Kinase Is Required for Excitotoxicity-Induced Neuronal Degeneration.” *The Journal of Experimental Medicine* 210 (12): 2553–67.

Presumey, Jessy, Allison R. Bialas, and Michael C. Carroll. 2017. “Chapter Two - Complement System in Neural Synapse Elimination in Development and Disease.” In *Advances in Immunology*, edited by Frederick W. Alt, 135:53–79. Academic Press.

Purves, D. 1975. “Functional and Structural Changes in Mammalian Sympathetic Neurones Following Interruption of Their Axons.” *The Journal of Physiology* 252 (2): 429–63.

Qian, Changhui, Dandan Tan, Xianghai Wang, Lixia Li, Jinkun Wen, Mengjie Pan, Yuanyuan Li, Wutian Wu, and Jiasong Guo. 2018. “Peripheral Nerve Injury-Induced Astrocyte Activation in Spinal Ventral Horn Contributes to Nerve Regeneration.” *Neural Plasticity* 2018 (April): 8561704.

Richardson, Claire E., Kerri A. Spilker, Juan G. Cueva, John Perrino, Miriam B. Goodman, and Kang Shen. 2014. “PTRN-1, a Microtubule Minus End-Binding CAMSAP Homolog, Promotes Microtubule Function in Caenorhabditis Elegans Neurons.” *ELife* 3 (February): e01498.

Robitaille, K., A. Daviau, G. Lachance, J-P Couture, and R. Blouin. 2008. “Calphostin C-Induced Apoptosis Is Mediated by a Tissue Transglutaminase-Dependent Mechanism Involving the DLK/JNK Signaling Pathway.” *Cell Death and Differentiation* 15 (9): 1522–31.

Roman, G., K. Endo, L. Zong, and R. L. Davis. 2001. “P[Switch], a System for Spatial and Temporal Control of Gene Expression in Drosophila Melanogaster.” *Proceedings of the National Academy of Sciences of the United States of America* 98 (22): 12602–7.

Rotterman, Travis M., Erica T. Akhter, Alicia R. Lane, Kathryn P. MacPherson, Violet V. García, Malú G. Tansey, and Francisco J. Alvarez. 2019. “Spinal Motor Circuit Synaptic Plasticity after Peripheral Nerve Injury Depends on Microglia Activation and a CCR2 Mechanism.” *The Journal of Neuroscience: The Official Journal of the Society for Neuroscience* 39 (18): 3412–33.

Sang, Tzu-Kang, and George R. Jackson. 2005. “Drosophila Models of Neurodegenerative Disease.” *NeuroRx: The Journal of the American Society for Experimental NeuroTherapeutics* 2 (3): 438–46.

Santoyo, J., J. Alcalde, R. Méndez, D. Pulido, and C. de Haro. 1997. “Cloning and Characterization of a cDNA Encoding a Protein Synthesis Initiation Factor-2alpha (EIF-2alpha) Kinase from Drosophila Melanogaster. Homology To Yeast GCN2 Protein Kinase.” *The Journal of Biological Chemistry* 272 (19): 12544–50.

Schaefer, A. M., G. D. Hadwiger, and M. L. Nonet. 2000. “Rpm-1, a Conserved Neuronal Gene That Regulates Targeting and Synaptogenesis in C. Elegans.” *Neuron* 26 (2): 345–56.

Schartz, Nicole D., and Andrea J. Tenner. 2020. “The Good, the Bad, and the Opportunities of the Complement System in Neurodegenerative Disease.” *Journal of Neuroinflammation* 17 (1): 1–25.

Scialo, Filippo, Ashwin Sriram, Rhoda Stefanatos, and Alberto Sanz. 2016. “Practical Recommendations for the Use of the GeneSwitch Gal4 System to Knock-Down Genes in Drosophila Melanogaster.” *PloS One* 11 (8): e0161817.

Shadrach, Jennifer L., Wesley M. Stansberry, Allison M. Milen, Rachel E. Ives, Elizabeth A. Fogarty, Anthony Antonellis, and Brian A. Pierchala. 2021. “Translatomic Analysis of Regenerating and Degenerating Spinal Motor Neurons in Injury and ALS.” *IScience* 24 (7): 102700.

Shen, Wei, and Barry Ganetzky. 2009. “Autophagy Promotes Synapse Development in Drosophila.” *The Journal of Cell Biology* 187 (1): 71–79.

Shin, Jung Eun, Yongcheol Cho, Bogdan Beirowski, Jeffrey Milbrandt, Valeria Cavalli, and Aaron DiAntonio. 2012. “Dual Leucine Zipper Kinase Is Required for Retrograde Injury Signaling and Axonal Regeneration.” *Neuron* 74 (6): 1015–22.

Shin, Jung Eun, and Aaron DiAntonio. 2011. “Highwire Regulates Guidance of Sister Axons in the Drosophila Mushroom Body.” *The Journal of Neuroscience: The Official Journal of the Society for Neuroscience* 31 (48): 17689–700.

Shin, Jung Eun, Hongseok Ha, Yoon Ki Kim, Yongcheol Cho, and Aaron DiAntonio. 2019a. “DLK Regulates a Distinctive Transcriptional Regeneration Program after Peripheral Nerve Injury.” *Neurobiology of Disease* 127 (July): 178–92.

Simon, David J., Jason Pitts, Nicholas T. Hertz, Jing Yang, Yuya Yamagishi, Olav Olsen, Milica Tešić Mark, Henrik Molina, and Marc Tessier-Lavigne. 2016. “Axon Degeneration Gated by Retrograde Activation of Somatic Pro-Apoptotic Signaling.” *Cell* 164 (5): 1031–45.

Somogyvári-Vigh, Anikó, and Dóra Reglodi. 2004. “Pituitary Adenylate Cyclase Activating Polypeptide: A Potential Neuroprotective Peptide.” *Current Pharmaceutical Design* 10 (23): 2861–89.

Spejo, Aline Barroso, and Alexandre L. R. Oliveira. 2015. “Synaptic Rearrangement Following Axonal Injury: Old and New Players.” *Neuropharmacology* 96 (Pt A): 113–23.

Stephan, Alexander H., Ben A. Barres, and Beth Stevens. 2012. “The Complement System: An Unexpected Role in Synaptic Pruning during Development and Disease.” *Annual Review of Neuroscience* 35: 369–89.

Stevens, Beth, Nicola J. Allen, Luis E. Vazquez, Gareth R. Howell, Karen S. Christopherson, Navid Nouri, Kristina D. Micheva, et al. 2007. “The Classical Complement Cascade Mediates CNS Synapse Elimination.” *Cell* 131 (6): 1164–78.

Stone, Michelle C., Richard M. Albertson, Li Chen, and Melissa M. Rolls. 2014. “Dendrite Injury Triggers DLK-Independent Regeneration.” *Cell Reports* 6 (2): 247–53.

Stone, Michelle C., Michelle M. Nguyen, Juan Tao, Dana L. Allender, and Melissa M. Rolls. 2010. “Global Up-Regulation of Microtubule Dynamics and Polarity Reversal during Regeneration of an Axon from a Dendrite.” *Molecular Biology of the Cell* 21 (5): 767–77.

Subhash, Santhilal, and Chandrasekhar Kanduri. 2016. “GeneSCF: A Real-Time Based Functional Enrichment Tool with Support for Multiple Organisms.” *BMC Bioinformatics* 17 (1): 365.

Svensson, M., and H. Aldskogius. 1993. “Synaptic Density of Axotomized Hypoglossal Motorneurons Following Pharmacological Blockade of the Microglial Cell Proliferation.” *Experimental Neurology* 120 (1): 123–31.

Tamai, So-Ichi, Keisuke Imaizumi, Nobuhiro Kurabayashi, Minh Dang Nguyen, Takaya Abe, Masatoshi Inoue, Yoshitaka Fukada, and Kamon Sanada. 2014. “Neuroprotective Role of

the Basic Leucine Zipper Transcription Factor NFIL3 in Models of Amyotrophic Lateral Sclerosis." *The Journal of Biological Chemistry* 289 (3): 1629–38.
Tedeschi, Andrea, and Frank Bradke. 2013. "The DLK Signalling Pathway--a Double-Edged Sword in Neural Development and Regeneration." *EMBO Reports* 14 (7): 605–14.
Tian, Ruilin, Mariam A. Gachechiladze, Connor H. Ludwig, Matthew T. Laurie, Jason Y. Hong, Diane Nathaniel, Anika V. Prabhu, et al. 2019. "CRISPR Interference-Based Platform for Multimodal Genetic Screens in Human IPSC-Derived Neurons." *Neuron* 104 (2): 239-255.e12.
Tsujino, H., E. Kondo, T. Fukuoka, Y. Dai, A. Tokunaga, K. Miki, K. Yonenobu, T. Ochi, and K. Noguchi. 2000. "Activating Transcription Factor 3 (ATF3) Induction by Axotomy in Sensory and Motoneurons: A Novel Neuronal Marker of Nerve Injury." *Molecular and Cellular Neurosciences* 15 (2): 170–82.
Valakh, Vera, Erin Frey, Elisabetta Babetto, Lauren J. Walker, and Aaron DiAntonio. 2015. "Cytoskeletal Disruption Activates the DLK/JNK Pathway, Which Promotes Axonal Regeneration and Mimics a Preconditioning Injury." *Neurobiology of Disease* 77: 13–25.
Valakh, Vera, Lauren J. Walker, James B. Skeath, and Aaron DiAntonio. 2013. "Loss of the Spectraplakin Short Stop Activates the DLK Injury Response Pathway in Drosophila." *The Journal of Neuroscience: The Official Journal of the Society for Neuroscience* 33 (45): 17863–73.
Valero-Cabré, A., and X. Navarro. 2001. "H Reflex Restitution and Facilitation after Different Types of Peripheral Nerve Injury and Repair." *Brain Research* 919 (2): 302–12.
Valero-Cabré, Antoni, Konstantin Tsironis, Emmanouil Skouras, Xavier Navarro, and Wolfram F. Neiss. 2004. "Peripheral and Spinal Motor Reorganization after Nerve Injury and Repair." *Journal of Neurotrauma* 21 (1): 95–108.
Verhey, Kristen J. 2007. "Motor Proteins: Trafficking and Signaling Collide." *Current Biology: CB*.
Verschuuren, Marlies, Peter Verstraelen, Gerardo García-Díaz Barriga, Ines Cilissen, Emma Coninx, Mieke Verslegers, Peter H. Larsen, Rony Nuydens, and Winnok H. De Vos. 2019. "High-Throughput Microscopy Exposes a Pharmacological Window in Which Dual Leucine Zipper Kinase Inhibition Preserves Neuronal Network Connectivity." *Acta Neuropathologica Communications* 7 (1): 93.
Voelzmann, Andre, Pilar Okenve-Ramos, Yue Qu, Monika Chojnowska-Monga, Manuela Del Caño-Espinel, Andreas Prokop, and Natalia Sanchez-Soriano. 2016. "Tau and Spectraplakins Promote Synapse Formation and Maintenance through Jun Kinase and Neuronal Trafficking." *ELife* 5 (August). https://doi.org/10.7554/eLife.14694.
Walker, Lauren J., Daniel W. Summers, Yo Sasaki, E. J. Brace, Jeffrey Milbrandt, and Aaron DiAntonio. 2017. "MAPK Signaling Promotes Axonal Degeneration by Speeding the Turnover of the Axonal Maintenance Factor NMNAT2." *ELife* 6 (January). https://doi.org/10.7554/eLife.22540.
Walter, Wencke, Fátima Sánchez-Cabo, and Mercedes Ricote. 2015. "GOplot: An R Package for Visually Combining Expression Data with Functional Analysis." *Bioinformatics* 31 (17): 2912–14.
Wang, Xin, Jung Hwan Kim, Mouna Bazzi, Sara Robinson, Catherine A. Collins, and Bing Ye. 2013. "Bimodal Control of Dendritic and Axonal Growth by the Dual Leucine Zipper Kinase Pathway." *PLoS Biology* 11 (6): e1001572.

Warren, Nicola, Cullen O'Gorman, Alexander Lehn, and Dan Siskind. 2017. "Dopamine Dysregulation Syndrome in Parkinson's Disease: A Systematic Review of Published Cases." *Journal of Neurology, Neurosurgery, and Psychiatry* 88 (12): 1060–64.

Watkins, Trent a., Bei Wang, Sarah Huntwork-Rodriguez, Jing Yang, Zhiyu Jiang, Jeffrey Eastham-Anderson, Zora Modrusan, Joshua S. Kaminker, Marc Tessier-Lavigne, and Joseph W. Lewcock. 2013. "DLK Initiates a Transcriptional Program That Couples Apoptotic and Regenerative Responses to Axonal Injury." *Proceedings of the National Academy of Sciences of the United States of America* 110 (10). https://doi.org/10.1073/pnas.1211074110.

Watkins, Trent A., Bei Wang, Sarah Huntwork-Rodriguez, Jing Yang, Zhiyu Jiang, Jeffrey Eastham-Anderson, Zora Modrusan, Joshua S. Kaminker, Marc Tessier-Lavigne, and Joseph W. Lewcock. 2013. "DLK Initiates a Transcriptional Program That Couples Apoptotic and Regenerative Responses to Axonal Injury." *Proceedings of the National Academy of Sciences of the United States of America* 110 (10): 4039–44.

Weber, U., N. Paricio, and M. Mlodzik. 2000. "Jun Mediates Frizzled-Induced R3/R4 Cell Fate Distinction and Planar Polarity Determination in the Drosophila Eye." *Development* 127 (16): 3619–29.

Welsbie, Derek S., Katherine L. Mitchell, Vinod Jaskula-Ranga, Valentin M. Sluch, Zhiyong Yang, Jessica Kim, Eugen Buehler, et al. 2017. "Enhanced Functional Genomic Screening Identifies Novel Mediators of Dual Leucine Zipper Kinase-Dependent Injury Signaling in Neurons." *Neuron* 94 (6): 1142-1154.e6.

Welsbie, Derek S., Zhiyong Yang, Yan Ge, Katherine L. Mitchell, Xinrong Zhou, Scott E. Martin, Cynthia A. Berlinicke, et al. 2013. "Functional Genomic Screening Identifies Dual Leucine Zipper Kinase as a Key Mediator of Retinal Ganglion Cell Death." *Proceedings of the National Academy of Sciences of the United States of America* 110 (10): 4045–50.

Werneburg, Sebastian, Jonathan Jung, Rejani B. Kunjamma, Seung-Kwon Ha, Nicholas J. Luciano, Cory M. Willis, Guangping Gao, et al. 2020. "Targeted Complement Inhibition at Synapses Prevents Microglial Synaptic Engulfment and Synapse Loss in Demyelinating Disease." *Immunity* 52 (1): 167-182.e7.

Wickham, Hadley. 2011. "Ggplot2." *WIREs Computational Statistics* 3 (2): 180–85.

Wiesenfeld-Hallin, Z., T. Bartfai, and T. Hökfelt. 1992. "Galanin in Sensory Neurons in the Spinal Cord." *Frontiers in Neuroendocrinology* 13 (4): 319–43.

Wlaschin, Josette J., Jacob M. Gluski, Eileen Nguyen, Hanna Silberberg, James H. Thompson, Alexander T. Chesler, and Claire E. Le Pichon. 2018. "Dual Leucine Zipper Kinase Is Required for Mechanical Allodynia and Microgliosis after Nerve Injury." *ELife* 7 (July). https://doi.org/10.7554/eLife.33910.

Wong, Ching-On, Michela Palmieri, Jiaxing Li, Dmitry Akhmedov, Yufang Chao, Geoffrey T. Broadhead, Michael X. Zhu, et al. 2015. "Diminished MTORC1-Dependent JNK Activation Underlies the Neurodevelopmental Defects Associated with Lysosomal Dysfunction." *Cell Reports* 12 (12): 2009–20.

Wu, Cheng-Chung, Hong-Jin Wu, Chia-Hui Wang, Chia-Hua Lin, Shu-Ching Hsu, Yi-Rong Chen, Michael Hsiao, et al. 2015. "Akt Suppresses DLK for Maintaining Self-Renewal of Mouse Embryonic Stem Cells." *Cell Cycle* 14 (8): 1207–17.

Wu, Chunlai, Yogesh P. Wairkar, Catherine A. Collins, and Aaron DiAntonio. 2005. "Highwire Function at the Drosophila Neuromuscular Junction: Spatial, Structural, and Temporal

Requirements." *The Journal of Neuroscience: The Official Journal of the Society for Neuroscience* 25 (42): 9557–66.
Xiong, Xin, and Catherine A. Collins. 2012. "A Conditioning Lesion Protects Axons from Degeneration via the Wallenda/DLK MAP Kinase Signaling Cascade." *The Journal of Neuroscience: The Official Journal of the Society for Neuroscience* 32 (2): 610–15.
Xiong, Xin, Yan Hao, Kan Sun, Jiaxing Li, Xia Li, Bibhudatta Mishra, Pushpanjali Soppina, Chunlai Wu, Richard I. Hume, and Catherine A. Collins. 2012. "The Highwire Ubiquitin Ligase Promotes Axonal Degeneration by Tuning Levels of Nmnat Protein." *PLoS Biology* 10 (12): e1001440.
Xiong, Xin, Xin Wang, Ronny Ewanek, Pavan Bhat, Aaron DiAntonio, and Catherine A. Collins. 2010. "Protein Turnover of the Wallenda/DLK Kinase Regulates a Retrograde Response to Axonal Injury." *The Journal of Cell Biology* 191 (1): 211–23.
Yan, Dong, and Yishi Jin. 2012. "Regulation of DLK-1 Kinase Activity by Calcium-Mediated Dissociation from an Inhibitory Isoform." *Neuron* 76 (3): 534–48.
Yan, Dong, Zilu Wu, Andrew D. Chisholm, and Yishi Jin. 2009. "The DLK-1 Kinase Promotes mRNA Stability and Local Translation in C. Elegans Synapses and Axon Regeneration." *Cell* 138 (5): 1005–18.
Yang, Jing, Zhuhao Wu, Nicolas Renier, David J. Simon, Kunihiro Uryu, David S. Park, Peter A. Greer, Cathy Tournier, Roger J. Davis, and Marc Tessier-Lavigne. 2015. "Pathological Axonal Death through a MAPK Cascade That Triggers a Local Energy Deficit." *Cell* 160 (1–2): 161–76.
Yin, Cheng, Guang-Fu Huang, Xiao-Chuan Sun, Zongduo Guo, and John H. Zhang. 2017. "DLK Silencing Attenuated Neuron Apoptosis through JIP3/MA2K7/JNK Pathway in Early Brain Injury after SAH in Rats." *Neurobiology of Disease* 103 (July): 133–43.
Zhan, Lihong, Qijing Xie, and Randal S. Tibbetts. 2015. "Opposing Roles of P38 and JNK in a Drosophila Model of TDP-43 Proteinopathy Reveal Oxidative Stress and Innate Immunity as Pathogenic Components of Neurodegeneration." *Human Molecular Genetics* 24 (3): 757–72.
Zhang, Kelvin Xi, Liming Tan, Matteo Pellegrini, S. Lawrence Zipursky, and Jason M. McEwen. 2016. "Rapid Changes in the Translatome during the Conversion of Growth Cones to Synaptic Terminals." *Cell Reports* 14 (5): 1258–71.
Zhen, M., X. Huang, B. Bamber, and Y. Jin. 2000. "Regulation of Presynaptic Terminal Organization by C. Elegans RPM-1, a Putative Guanine Nucleotide Exchanger with a RING-H2 Finger Domain." *Neuron* 26 (2): 331–43.